Synthesis and Property of an Alkyl-Substituted Alumanyl Anion

炭素置換アルマニルアニオンの合成と性質の解明

Satoshi Kurumada

車田 怜史

Department of Molecular and Macromolecular Chemistry, Graduate School of Engineering, Nagoya University

List of Abbreviations

DFT	density functional theory
TD-DFT	time dependent-density functional theory
AIM	atoms in molecules
NBO	natural bond orbital
NPA	natural population analysis
HOMO	highest occupied molecular orbital
LUMO	lowest unoccupied molecular orbital
NMR	nuclear magnetic resonance
UV-vis	unvisible-visible
KIE	kinetic isotope effect
EWG	electron withdrawing group
NHC	N-hetero cyclic carbene
cAAC	cyclic alkyl amino carbene
THF	tetrahydrofuran
DME	dimethoxyethylene
tol	toluene
DMAP	N,N-dimethyl amino pyridine
Me	methyl
Et	ethyl
Ad	adamantyl
Ph	phenyl
Mes	mesityl
Dip	diisopropylphenyl
Pin	pinacorato
nacnac	1,3-diketiminate

Chapter 1:
General Introduction

1-1. Singlet carbene

Singlet carbenes, which have an electronic structure as six-electron species possessing two substituents, one lone-pair, and one vacant 2p-orbital on sp^2-hybridized carbon atom, represent one of the most important classes of reactive molecules in organic chemistry (Figure 1-1-1a). They exhibit both Lewis basicity and Lewis acidity on the carbon atom due to their characteristic coexistence of filled and vacant orbitals. The history of singlet carbenes was remarkably developed by reports of isolable carbene species (Figure 1-1-1b). In 1988, Bertrand *et al.* reported isolable (phosphino)(silyl)carbene **I** as the first example.[1] Although no structural analysis of **I** has been performed, it was expected to have an allene-type resonance structure due to push-pull orbital interactions resulting from the presence of electron-donating phosphino group and electron-withdrawing silyl group. Subsequently, N-heterocyclic carbene (NHC) **II** having a cyclic structure with diamino ligand was synthesized by Arduengo *et al*.[2] Furthermore, cyclic (alkyl)(amino)carbene (cAAC) **III**, in which one of the amino groups stabilizing the singlet carbene in NHC is replaced by a carbon substituent, has also been reported by Bertrand *et al*.[3] As another significant stabilizing effect for carbene, introducing bulky substituent(s) to sterically protect the reactive center is utilized in **II** and **III (**adamantyl, 2,6-*i*$Pr_2C_6H_3$ on N atom).

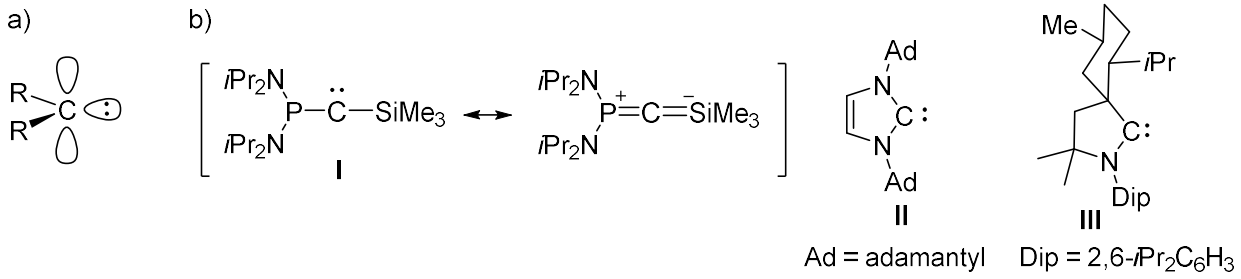

Figure 1-1-1. a) Structure of singlet-carbene possessing lone-pair and vacant 2p-orbital on sp^2 carbon center. b) Isolable carbenes **I**-**III**.

As observed in isolable carbenes **II** and **III**, the nitrogen substituent could stabilize the singlet carbene (Figure 1-1-2a). That is, characteristic Lewis acidity and Lewis basicity of singlet carbene are weakened through π-donating resonance effect and the electron-withdrawing inductive effect of nitrogen atom(s), respectively. In contrast, carbon substituents are regarded as electronically non-stabilizing substituents toward carbene because they have no lone-pair and lower electronegativity than nitrogen atom. In fact, (alkyl)(amino)carbene has a higher energy level of HOMO, which is corresponding to the lone-pair, and lower LUMO, which is corresponding to the vacant 2p-orbital, than those of NHC.[4] In contrast to that NHC **V** does not react with H_2, (alkyl)(amino)carbene **III** undergoes cleavage of H-H σ-bond in H_2 (Figure 1-1-2b).[5] This is caused by the highly reactive lone-pair and vacant 2p-orbitals which simultaneously interact with the $\sigma^*_{H\text{-}H}$ and $\sigma_{H\text{-}H}$ orbitals of H_2, respectively.

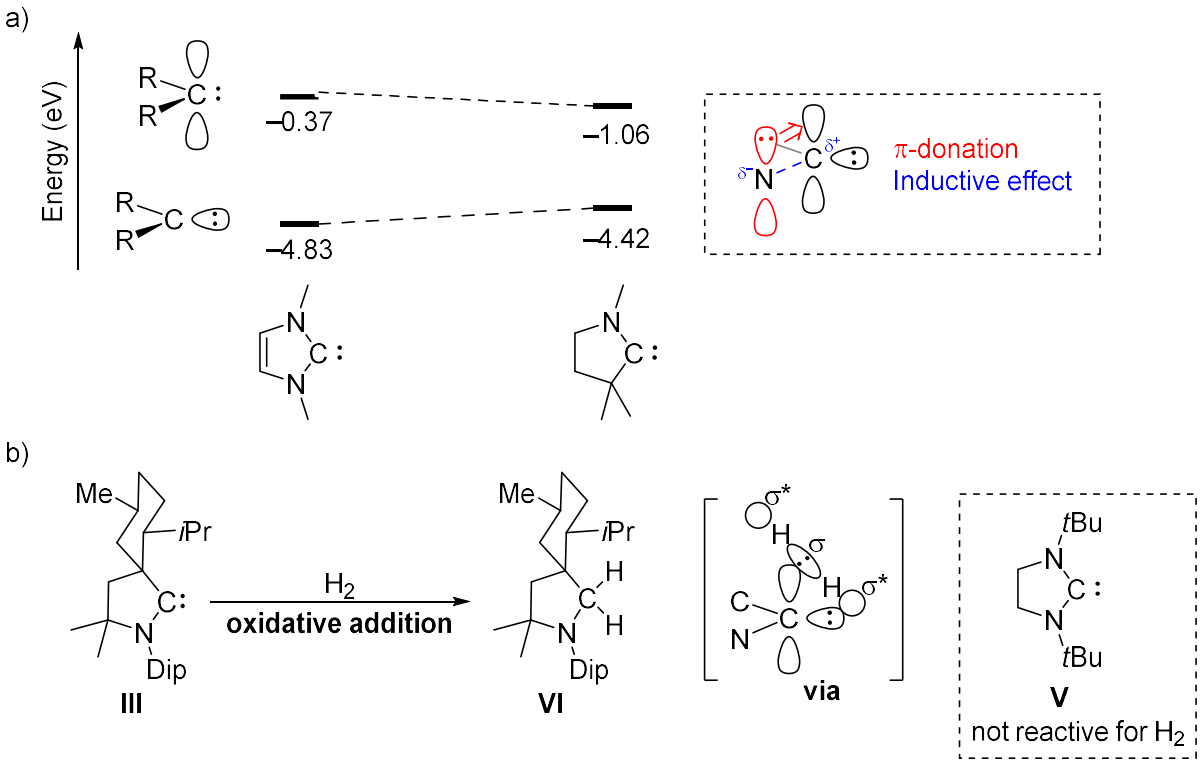

Figure 1-1-2. (a) Electronically stabilizing effect of nitrogen substituents for carbene, and (b) H-H bond cleavage in dihydrogen by higher reactive (alkyl)(amino)carbene than NHC.

Carbenes have been widely used in organic synthesis (Figure 1-1-3). For example, Rovis *et al.* achieved to form a chiral quaternary carbon through an intramolecular asymmetric Stetter reaction by using *in situ* generated carbene **IV** as a catalyst.[6] Another example is the use of NHC ligands in Ru complex **V**, which is known as a highly practical olefin metathesis catalyst reported by Grubbs *et al.*[7]

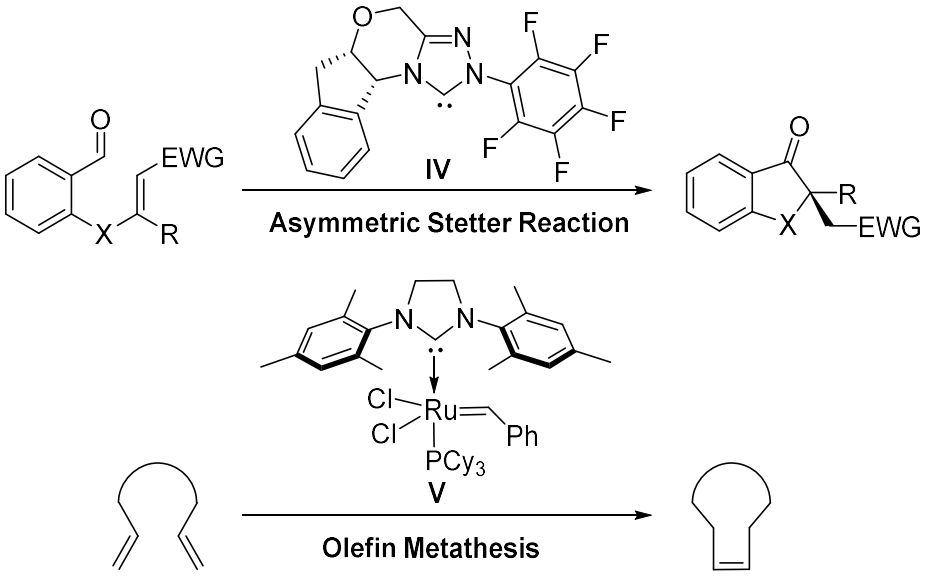

Figure 1-1-3. Example of carbenes for organic synthesis; Asymmetric Stetter reaction by **IV**, and NHC in Ru complex **V** for practical olefin metathesis catalyst.

1-2. Carbene analogues

Replacement of the carbon atom in carbenes with other main-group elements generates a series of carbene analogues (Figure 1-2-1). Group 14 elements such as carbon and silicon, which have four valence electrons, form a neutral six-electron system possessing two substituents and a lone pair of electrons. In case of that group 13 elements such as boron and aluminum, which have three valence electrons, form isoelectronic six-electron system, it should have an anionic charge on the central group 13 element, whereas replacement with a group 15 element should produce a positively charged compound. Since boron and aluminum have lower electronegativity[8] than those of the corresponding group 14 elements, anionic group 13 element compounds should be stronger bases.[9]

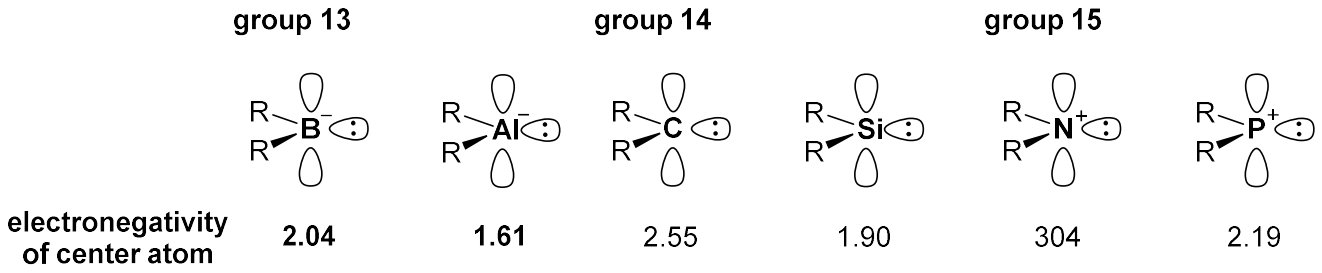

Figure 1-2-1. Electronic structure of carbene analogues of group 14 and 13 elements.

In the last fifteen years, they have seen a remarkable development of isolable boryl anion (Figure 1-2-2). In 2006, the first isolable boryl anion **VII** possessing cyclic-diamino ligand similar to NHC was reported as lithium salt. DFT calculations revealed the lone-pair on the boron atom mainly contributed to the highest occupied molecular orbital (HOMO).[10] Similarly, a dimeric potassium salt **VIII** of boryl anion having two B-K-B three-center-two-electron bonds and a potassium salt of diboryllithate **IX** have also been reported.[11-12] As another method for stabilizing boryl anions is introducing a coordination of Lewis bases to vacant 2p-orbitals as utilized in the firstly observed phosphine coordinated boryllithim.[13] Moreover, isolable eight-electron boryl anions **X-XIII** emerged later.[14] In the case of them, there is also the stabilization of lone-pair on the boron atom by electron accepting substituents.

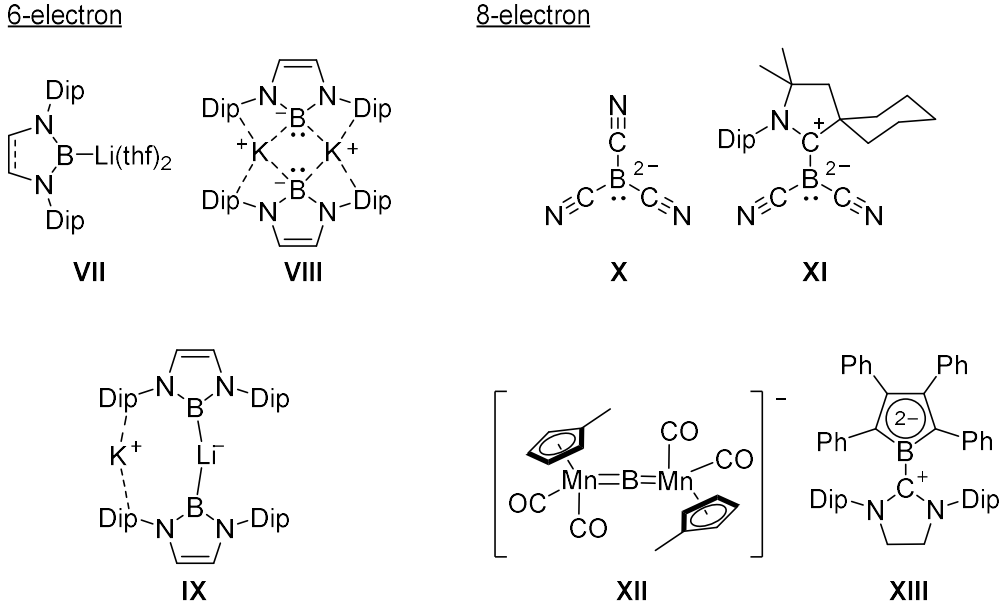

Figure 1-2-2. Structure of Isolated (a) 6-electron (b) 8-electron boryl anions **VII-XIII**.

The characteristic strong basicity of the boryl anion is evident from the reaction of **IX** with benzene (Scheme 1-2-1). Although benzene has a very low acidity with a pK_a of 43,[15] **IX** deprotonates benzene at room temperature to generate the corresponding hydroborane and phenyl-lithium/potassium.[12] The mechanism of this deprotonation is supported by kinetic analysis and DFT calculations. **VIII** was also reported to decompose in benzene, but the product was **XV**, which would form through intramolecular C-H cleavage at the benzylic position of the Dip substituent, instead of a deprotonated product of benzene.[11] This reaction was proposed to proceed via deprotonation of the C-H bond, reflecting the strong basicity of the boryl anion.[16]

Scheme 1-2-1. Transformations of boryl anions **IX** and **VIII** in a benzene solution to afford (a) hydroborane and phenyllithium/potassium, and (b) a polymeric borate **XV**.

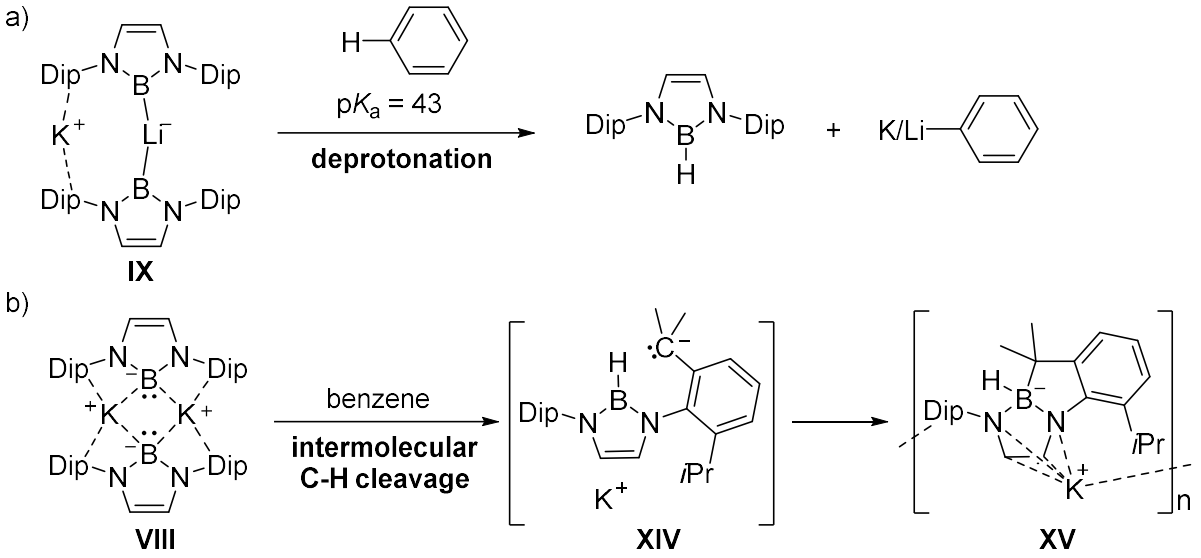

Boryl anions are known to behave as a nucleophile (Scheme 1-2-2). Reactions of boryl anion **VII** toward alkyl electrophiles or fluorobenzenes proceeds through S_N2 or S_NAr reactions, respectively, while the reaction toward carbonyls afforded nucleophilically borylated adducts **XVII**. [16] Furthermore, **VII** easily undergoes transmetalation with s-, p-, d-, and f-block metals and electrophiles to form B-**M** or B-**E** bonds (**M**, **E** = various s-, p-, d-, and f-block metals and elements).[17-18] It should be noted that the most of these newly formed bonds are the first examples of the B-**M** or B-**E** bonds (**M** = Sc, Ti, Y, Cd, Hf, Hg, Er, Lu, **E** = Be). This is because the boron compounds normally behave as an electrophile and the synthetic methods to prepare boron compounds had been limited until boryl anions were discovered. In other words, the appearance of boryl anions, which are boron nucleophiles, was a breakthrough in the synthesis of boron-containing compounds.

4

Scheme 1-2-2. Direct borylation by **VII** via nucleophilic substitution, addition, or transmetalation.

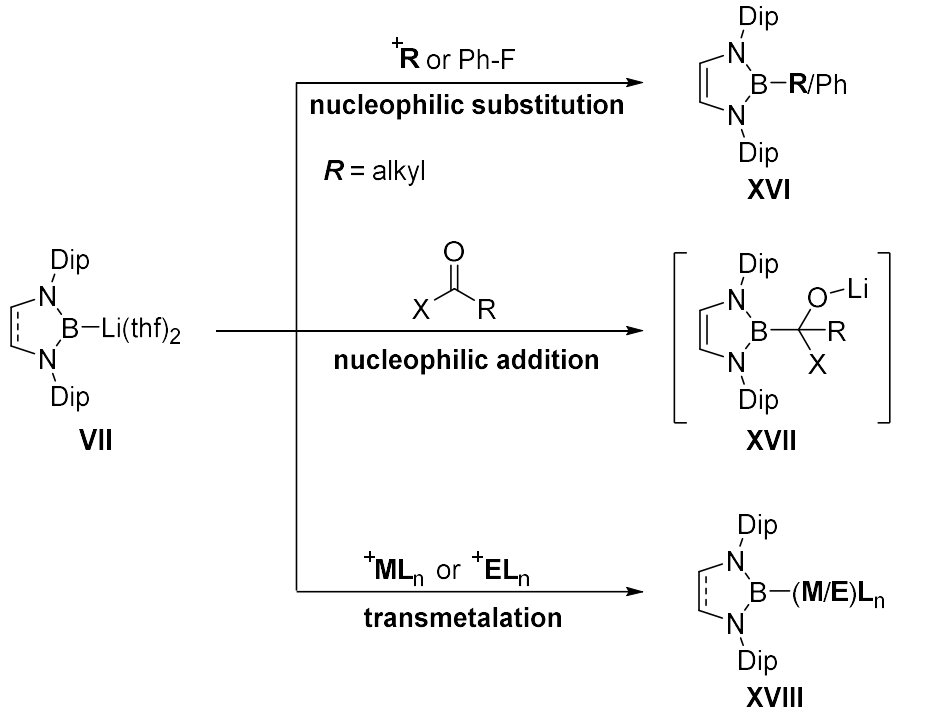

M = Sc, Ti, Mn, Fe, Co, Cu, Zn, Y, Ag, Cd, Hf, Re, Au, Hg, Er, Lu
E = Be, Mg, Al, Si, Ga, Ge, In, Sn, Sb, Tl, Pb, Bi
L = Ligand

Similar to singlet carbenes, the effect of replacing nitrogen substituents with carbon substituents was investigated in the chemistry of boryl anion (Figure 1-2-3). The two-electron reduction of cyclic (alkyl)(amino)(bromo)borane **XIX** with Li to give the corresponding boryl anion **XX** as confirmed by ^{1}H, ^{11}B and ^{7}Li NMR spectroscopy.[19] In contrast to that the (diamino)boryl anion **VII** could be crystallized from THF solution, **XX** was highly unstable and decomposed above −35°C to give the hydroborane **XXI**. The proton source was considered to be THF based on the deuterium labeling experiment, suggesting that (alkyl)(amino)boryl anion is stronger base than the (diamino)boryl anion, which is confirmed by DFT calculations showing the increase of HOMO energy level. These results suggest that alkyl substituents are responsible for destabilization of the boryl anion as well as the singlet carbene. Furthermore, a slight decrease of the LUMO energy level, which is partially contributed by the vacant 2p-orbital on the boron atom, was also reported.

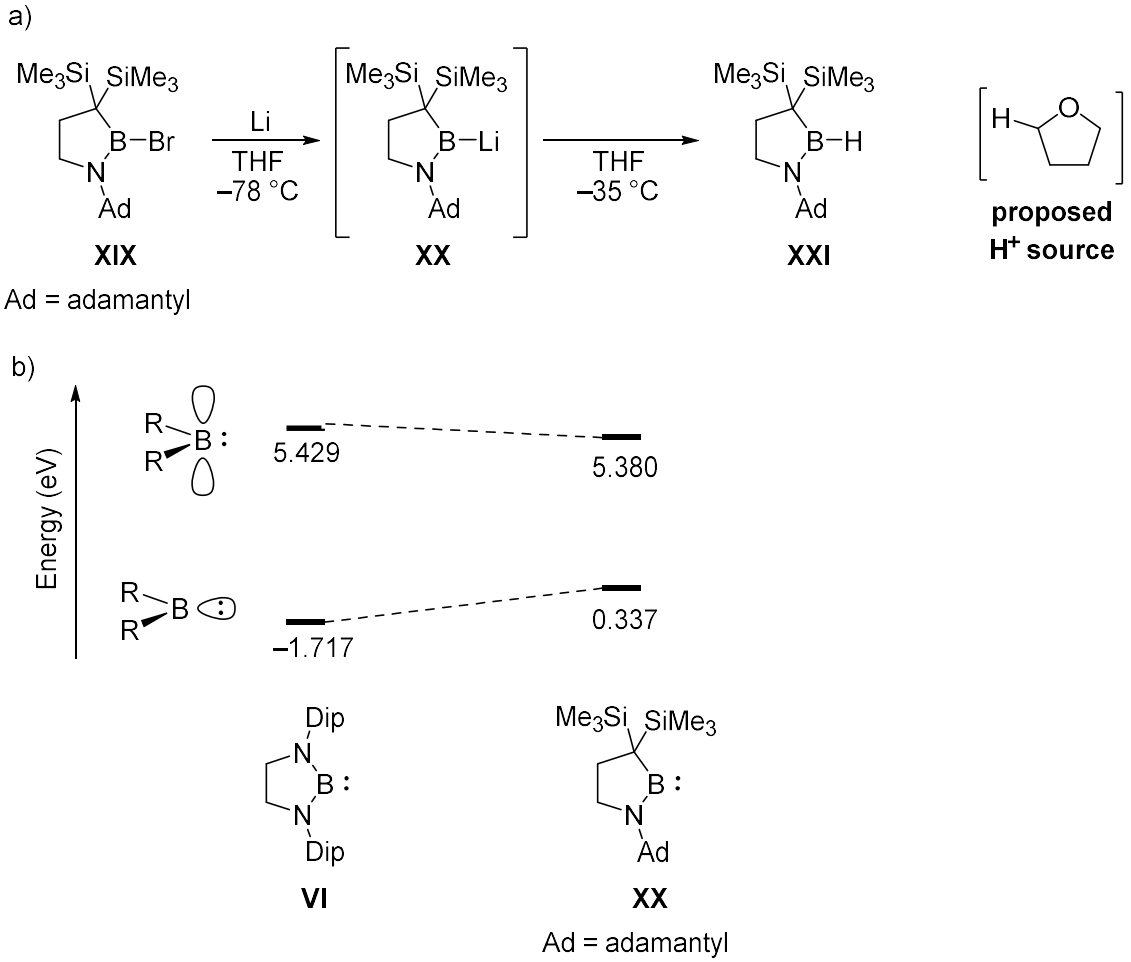

Figure 1-2-3. (a) Decomposition of (alkyl)(amino)boryl anion undergoing deprotonation of THF, which is the possible proton source, and (b) narrowered its HOMO-LUMO enery gap (calculated at the B3LYP/6-31+G(d) level of theory) of bory anion by installing alkyl subdtituent.

Substituent effects for silylene, a heavy analog of carbene, has also been extensively investigated. Kira *et al.* reported that (dialkyl)silylene **XXII** is thermally unstable and decomposes at room temperature in solution to afford **XXIII** via a 1,2-shift of the silyl group. While (alkyl)(amino)silylene **XXIV** reported by Iwamoto is more thermally stable than **XXV** and does not undergo 1,2-silyl shift even under reflux conditions in toluene, and alternatively reacts with toluene solvent to cleave benzylic C-H bond.[20-21] It was mentioned that this difference in stability between silylenes **XXII** and **XXIV** is due to the difference in the energy gap between their characteristic lone-pair orbital (HOMO) and vacant 3p-orbital (LUMO). In fact, DFT calculations showed that **XXII** has a higher HOMO and a lower LUMO energy level. It was also mentioned that (diamino)silylene **XXVI** has further lower HOMO and further higher LUMO energy level.[22] In other words, stabilization by namino groups is also effective for silylenes.

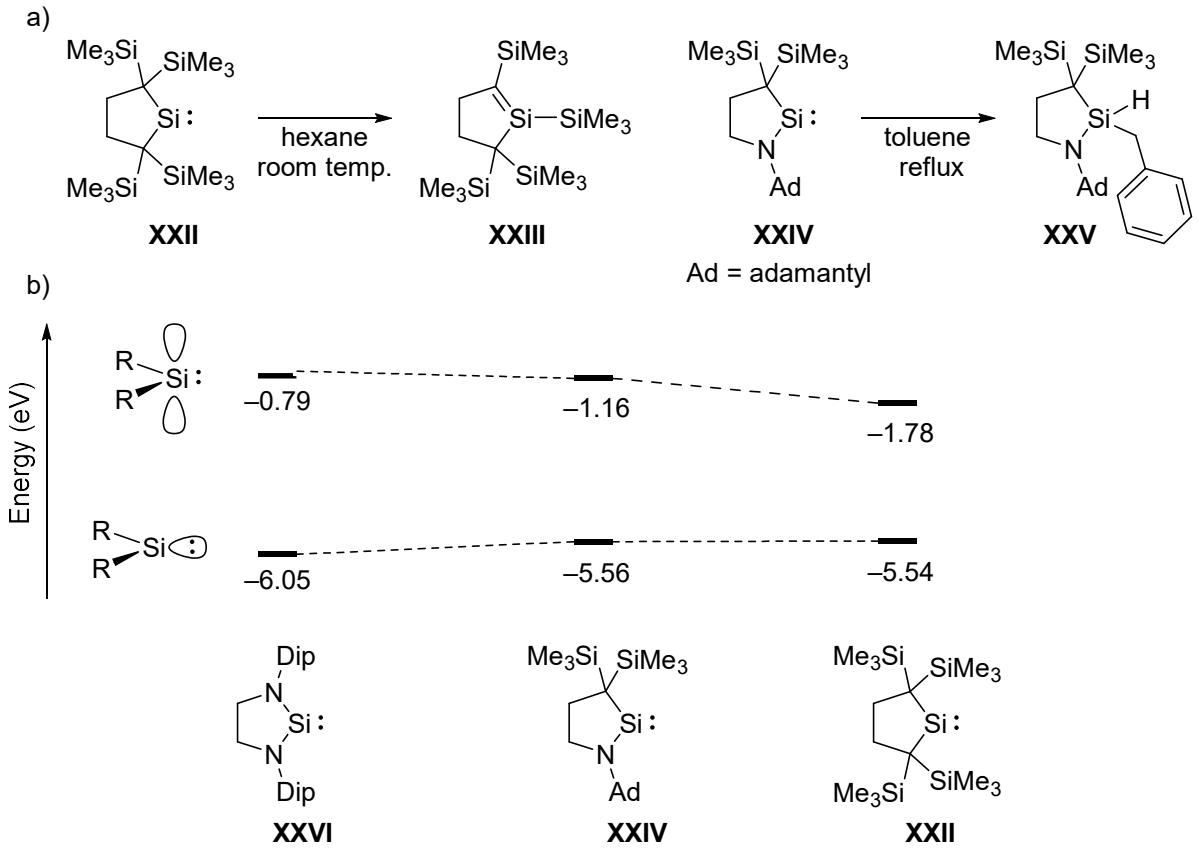

Figure 1-2-3. Alkyl substituents (a) to led silylene be higher reactive than diaminosilylene, and (b) its effect to narrower HOMO-LUMO gap, calculated at the B3PW91-D3/6-31G(d)level theory.

The carbene analogue of aluminum, alumanyl anion, is a highly reactive species because the most electropositive aluminum in the p-block elements has a negative charge. The nature of alumanyl anion had not been clarified until the recent report of the first alumanyl anion. The first Al(I) anion **A** has been isolated as a potassium salt, with a xanthene-based tridentate ligand by Aldridge and Goicoechea *et al*.[23] Afterward, diamino-substituted Al(I) anions **A-G,** and (alkyl)(amino)-substituted Al(I) anion **H,** which is a separated ion pair of potassium salt, were reported.[24-26] I will discuss the alumanyl anion in detail in Chapter 2 and later.

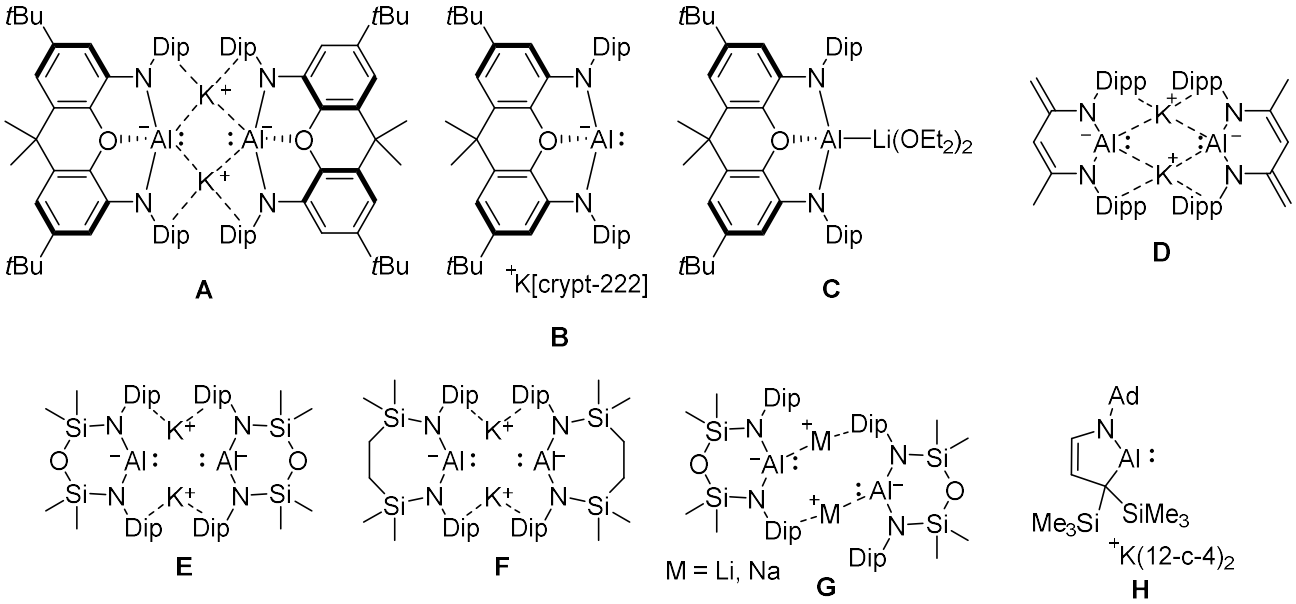

Dip = 2,6-(iPr)$_2$C$_6$H$_3$ Ad = adamanthyl

Figure 1-2-4. Reported anionic Al(I) species **A-H.**

1-3. Outline of this thesis

In this doctoral thesis, the properties of an alkyl-substituted alumanyl anion is revealed. Chapter 2 describes the synthesis of alkyl-substituted alumanyl anion **8** from bis(silyl)ethylene **3** in four steps and the detailed electronic property of 8. Chapter 3 describes the reactivity of **8** including nucleophilic substitution and oxidative addition. Chapter 4 describes the synthesis and properties of alumaboranes **21**. Chapter 5 summarizes this doctoral thesis.

Chapter 2

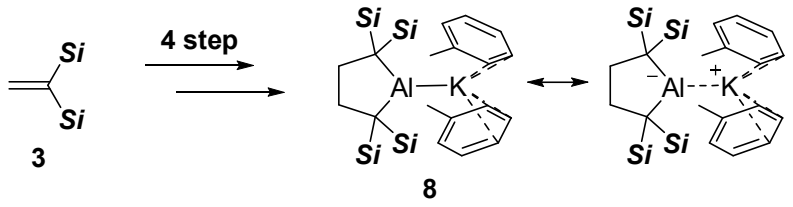

Chapter 3

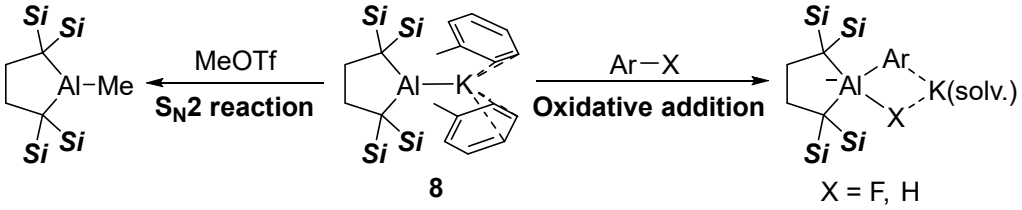

Chapter 4

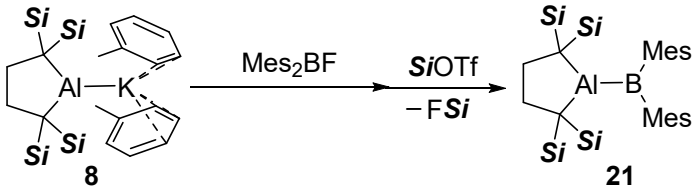

Chapter 5: Conclusion

Chapter 6: Acknowledgement

Figure 1-3-1. Outline of this thesis.

1-4. References

1. Igau, A.; Grutzmacher, H.; Baceiredo, A.; Bertrand, G. *J. Am. Chem. Soc.* **1988**, *110*, 6463–6466.
2. Arduengo III, J. A.; Harlow, L. R.; Kline, M. *J. Am. Chem. Soc.* **1991**, *113*, 361–363.
3. Lavallo,V.; Canac, Y.; Präsang, C.; Donnadieu, B.; Bertrand, G. *Angew. Chem. Int. Ed.* **2005**, *4*, 5705-5709.
4. Andrada1, M. D.; Holzmann, N.; Hamadi, T.; Frenking, G. *Beilstein J. Org. Chem.* **2015**, *11*, 2727–2736.
5. Frey, G. D.; Lavallo, V.; Donnadieu, B.; Schoeller, W. W.; Bertrand, G. *Science* **2007**, *316*, 439.
6. Kerr, S. M.; Rovis, T., *J. Am. Chem. Soc.* **2004**, *126*, 8876–8877.
7. Scholl, M.; Ding, S.; Lee, W. C.; Grubbs, H. R. *Org. Lett.* **1999**, *1*, 953–956.
8. Emsley, J. Te Elements 3rd edn (Oxford Univ. Press, 1998).
9. Laidig, E. K.; Streitwieser, A. *J. Comput. Chem.***1996**,*17*,1771–1781.
10. Segawa, Y.; Yamashita, M.; Nozaki, K. *Science* **2006,** *314*, 113-115.
11. Protchenko, V. A.; Vasko, P.; Fuentes, M.; Hicks, J.; Vidovic, D.; Aldridge, S. *Angew. Chem. Int. Ed.* **2021**, *60*, 2064–2068
12. Ohsato, T.; Okuno, Y.; Ishida, S.; Iwamoto, T.; Lee, K.-H.; Lin, Z.; Yamashita, M.; Nozaki, K. *Angew. Chem. Int. Ed.* **2016**, *55*, 11426-11430.
13. Imamoto, T.; Hikosaka, T. *J. Org. Chem.* **1994**, *59*, 6753–6759
14. (a) Bernhardt, E.; Bernhardt-Pitchougina, V.; Willner, H.; Ignatiev, N. *Angew. Chem. Int. Ed.* **2011,** *50*, 12085–12088. (b) Ruiz, D. A.; Ung, G.; Melaimi; M. Bertrand, G. *Angew. Chem. Int. Ed.* **2013**, *52*, 7590–7592. (c) Braunschweig, H.; Burzler, M.; Dewhurst, R. D.; Radacki, K. *Angew. Chem. Int. Ed.* **2008**, 47, 5650–5653. (d) Braunschweig, H.; Chiu, C.-W.: Radacki, K.; Kupfer, T. *Angew. Chem. Int. Ed.* **2010**, *49*, 2041–2044.
15. CarbonAcids, D.J.Cram, *in Fundamentals of Carbanion Chemistry, Academic* Press, San Diego,**1965**.
16. Segawa, Y.; Suzuki, Y.; Yamashita, M.; Nozaki, K. *J. Am. Chem. Soc.* **2008**, *130*, 16069-16079.
17. (a) Terabayashi, T.; Kajiwara, T.; Yamashita, M.; Nozaki, K. *J. Am. Chem. Soc.* **2009**, *131*, 14162–14163. (b) Saleh, L. M. A.; Birjkumar, K. H.; Protchenko, A. V.; Schwarz, A. D.; Aldridge, S.; Jones, C.; Kaltsoyannis, N.; Mountford, P. *J. Am. Chem. Soc.* **2011**, *133*, 3836–3839. (c) Protchenko, A. V.; Dange, D.; Schwarz, A. D.; Tang, C. Y.; Phillips, N.; Mountford, P.; Jones, C.; Aldridge, S. *Chem. Commun.* **2014**, *50*, 3841–3844. (d) Wang, B.; Nishiura, M.; Cheng, J.; Hou, Z. *Dalton Trans.* **2014**, *43*, 14215–14218. (e) Frank, R.; Howell, J.; Tirfoin, R.; Dange, D.; Jones, C.; Mingos, D. M. P.; Aldridge, S. *J. Am. Chem. Soc.* **2014**, *136*, 15730–15741. (f) Campos, J.; Aldridge, S. *Angew. Chem. Int. Ed.* **2015**, *54*, 14159–14163. (g) Frank, R.; Howell, J.; Campos, J.; Tirfoin, R.; Phillips, N.; Zahn, S.; Mingos, D. M. P.; Aldridge, S. *Angew. Chem. Int. Ed.* **2015**, *54*, 9586–9590. (h) Segawa, Y.; Yamashita, M.; Nozaki, K. *Angew. Chem. Int. Ed.* **2007**, *46*, 6710-6713. (i) Kajiwara, T.; Terabayashi, T.; Yamashita, M.; Nozaki, K. *Angew. Chem. Int. Ed.* **2008**, *47*, 6606-6610. (k) Yamashita, M.; Suzuki, Y.; Segawa, Y.; Nozaki, K. *J. Am. Chem. Soc.* **2007**, *129*, 9570-9571.
18. (a) Protchenko, A. V.; Birjkumar, K. H.; Dange, D.; Schwarz, A. D.; Vidovic, D.; Jones, C.; Kaltsoyannis, N.; Mountford, P.; Aldridge, S. *J. Am. Chem. Soc.* **2012**, *134*, 6500–6503. (b) Kaaz, M.; Bender, J.; Förster, D.; Frey, W.; Nieger, M.; Gudat, D. *Dalton Trans.* **2013**, *43* , 680–689. (c) Protchenko, A. V.; Dange, D.; Harmer, J. R.; Tang, C. Y.; Schwarz, A. D.; Kelly, M. J.; Phillips, N.; Tirfoin, R.; Birjkumar, K. H.; Jones, C.; Kaltsoyannis, N.; Mountford, P.; Aldridge, S. *Nature Chem* **2014**, *6*, 315–319. (d) Braunschweig, H.; Ewing,

W. C.; Kramer, T.; Mies, J.; Schuster, J. K. *Chem. Commun.* **2014**, *51*, 737–740. (e) Dange, D.; Davey, A.; Abdalla, J. A. B.; Aldridge, S.; Jones, C. *Chem. Commun.* **2015**, *51*, 7128–7131. (f) Rit, A.; Campos, J.; Niu, H.; Aldridge, S. *Nature Chem* **2016**, *8*, 1022–1026. (g) Mangan, R. J.; Rit, A.; Sindlinger, C. P.; Tirfoin, R.; Campos, J.; Hicks, J.; Christensen, K. E.; Niu, H.; Aldridge, S. *Chem. Eur. J.* **2020**, *26*, 306–315.

19. Kisu, H.; Kosai, T.; Iwamoto, T.; Yamashita, M. *Chem. Lett.* **2021,** *50,* 293-296.
20. Kira, M.; Ishida, S.; Iwamoto, T.; Kabuto, C., *J. Am. Chem. Soc.* **1999,** *121*, 9722-9723.
21. Kosaim T.; Ishida, S.; Iwamoto, T., *Angew.Chem.Int.Ed.* **2016**, *55*,15554–15558.
22. Denk, M.; Lennon, R.; Hayashi, R.; West, R.; Belyakov, V. A.; Verne, P. H; Haaland, A.; Wagner, M.; Metzler. N., *J. Am. Chem. Soc.* **1994**, *116*, 2691–2692.
23. (a) Hicks, J.; Vasko, P.; Goicoechea, J. M.; Aldridge, S., *Nature* **2018**, *557*, 92-95; (b) Hicks, J.; Vasko, P.; Goicoechea, J. M.; Aldridge, S., *J. Am. Chem. Soc.* **2019**, *141*, 11000-1100.
24. (a) Schwamm, R. J.; Anker, M. D.; Lein, M.; Coles, M. P. *Angew. Chem. Int. Ed.* **2019**, *58*, 1489-1493. (b) Evans J. M., Anker, M. D., McMullin, L. C., Neale, E. S., Coles, M. P. *Angew. Chem. Int. Ed.* **2021**, *60*, 22289-22292.
25. Harder, S.; Grams, S.; Eyselein, J.; Langer, J.; Färber, C. *Angew. Chem. Int. Ed.* **2020**, *59*, 15982-15986.
26. Koshino, K.; Kinjo, R. *J. Am. Chem. Soc.* **2020**, *142*, 9057-9062.

Chapter 2:
Synthesis and Properties of Dialkyl-Substituted Aluminum Anion

2-1. Introduction

Considering similarity between carbene and silylene and that between boron and aluminum, alumanyl anion would have similar substituent effect to those for the boryl anion (group 13 element) and silylene (3rd period element) (Figure 2-1-1). In other words, the energy gap between the lone-pair and the vacant orbital becomes larger due to stabilization of the amino group, and the reactivity decreases accordingly, and it is expected that dialkyl-alumanyl anion will be more reactive than amino-subatituted alumanyl anions.

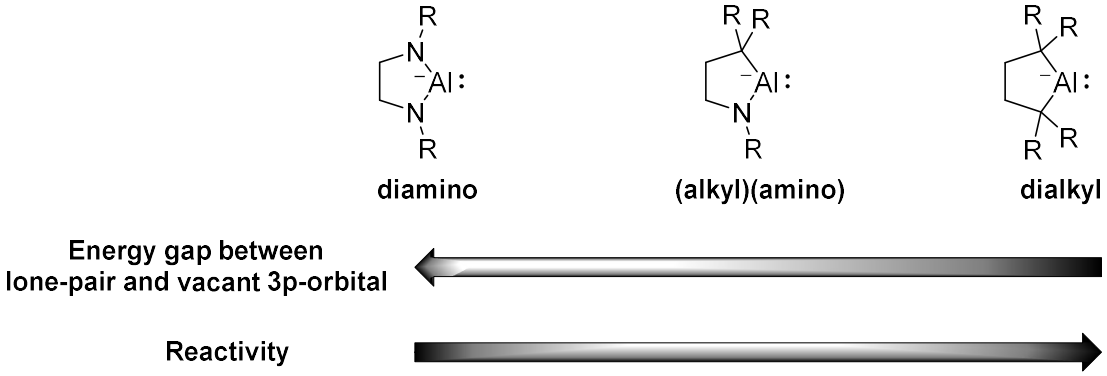

Figure 1-2-4. Anticipated effects of substituents for alumanyl anion.

On the other hand, silylene **I** and phosphimyl radical **J** have been reported by means of a tetrasilylalkylene ligand (Figure 2-1-2).[1,2] In these cases, bulkiness of silyl groups, and a regulation for the C-E-C bond angle (E = Si, P) by the cyclic alkylene ligand stabilize them. Moreover, hyperconjugation of Si-C σ-bond toward vacant orbital located on the β-position of silyl group also stabilize the species. Inspired by the effective method for synthesizing period 3 compounds with low oxidative number, I aimed to synthesize dialkyl-substituted Al(I) anion, which is electronically non-stabilized Al(I) anion, by using tetrasilyl-alkylene ligand.

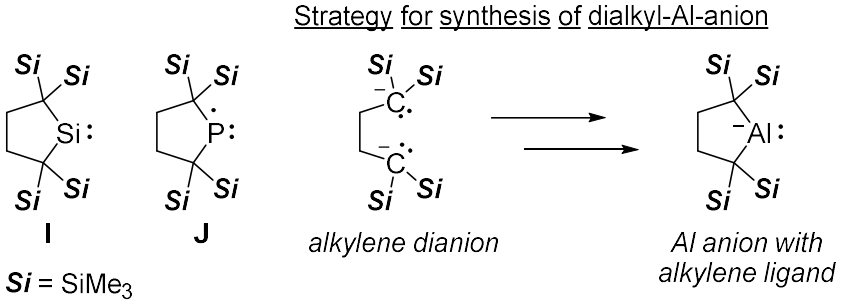

Figure 2-1-2. Reported silylene **I** and group 15 species **J** having a bulky alkylene ligand, and a strategy for electronically non-stabilized Al(I) anion by using the ligand.

2-2. Synthesis of dialkyl-alumanyl anion

The reaction of dialkyllithate[7] **1**, having tetrasilylalkylene ligand and THF-coordinated Li^+ as a counter cation, with AlX_3 (X = Cl, Br, I) was performed to obtain dialkyl-aluminum halide by referring to the synthesis of dialkyl-silicon and phosphorus species (Scheme 2-2-1).[1-1-2] However, tetrasilylbutane **2**, which is doubly protonated alkylene dianion, was obtained quantitatively in all cases. One could expect that the α-hydrogen of THF, dissociated from Li atom in **1**, was activated by Lewis acidic AlX_3, and became a proton source.

Scheme 2-2-1. Reaction of dialkyllithate **1** with AlX_3 (X = Cl, Br, I).

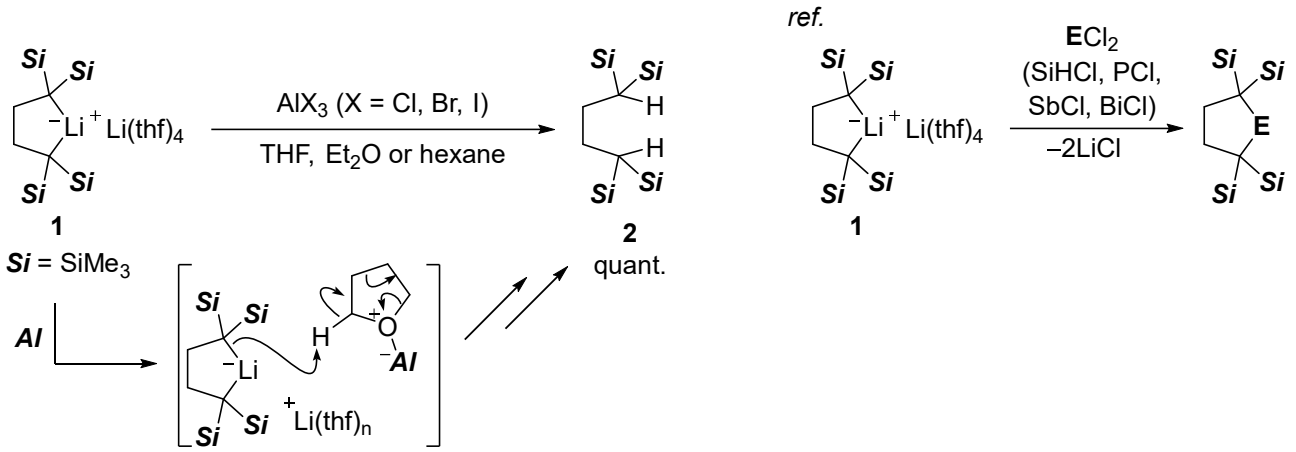

To avoid using THF as a coordinating solvent to Li^+ cation, a new synthetic equivalent of alkylene dianion was prepared in the absence of THF. The reaction of 1,1-bis(trimethylsilyl)ethylene **3** with Li powder in ether afforded ether-solvated 1,4-dilithiobutane **4** as a crystalline material (Scheme 2-2-2). The linear structure of **4** was revealed by a single-crystal X-ray diffraction analysis. ^1H NMR spectrum in C_6D_6 shows the signals of slightly downfield shifted Et_2O moiety, which indicates the existence of coordination of oxygen atom in Et_2O toward Li^+ as observed in the solid state.

Scheme 2-2-2. Syntheis of dilithiobutane **4**.

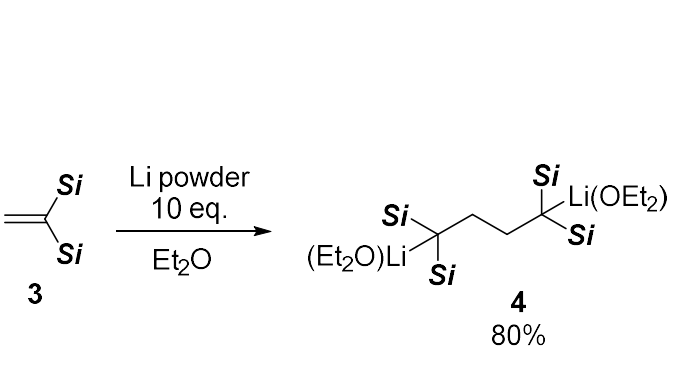

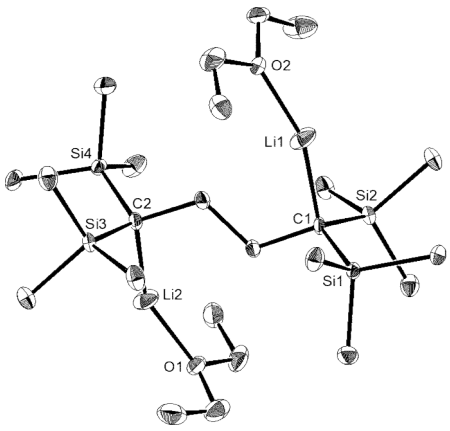

Subsequently, the addition of AlI_3 to **4** furnished cyclic five-membered aluminum iodide **5** in 56% isolated

yield without the formation of **2** (Scheme 2-2-3). The upfield shifted signals of the silyl group and methylene moiety compared to those of **4** (Me_3Si: 0.40 to 0.24, methylene: 1.97 to 1.92) reflected the formation of C-Al bond. The single crystal X-ray structural analysis shows the trigonal planar structure around the Al atom with the angle sum of 360°.

Scheme 2-2-3. Reaction of **4** with AlI_3 to afford five-membered aluminium iodide **5**.

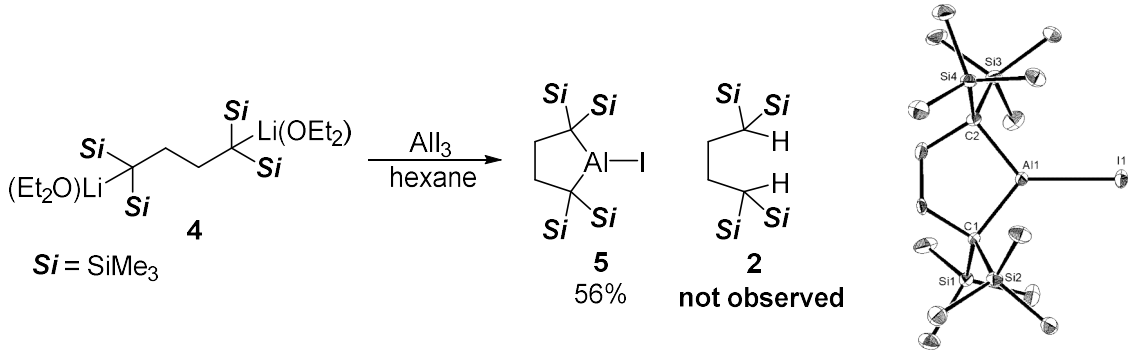

To obtain Al(I) anion, reduction of **5** was performed (Scheme 2-2-4). Fixing elemental Li as a reductant, various solvents were examined to reduce **5**. Using THF solvent gave a complex mixture, whereases the dialumane **6**, which is the dimer of Al(II) radical generated by the one-electron reduction of **5**, was obtained under the condition using hexane as a solvent. The downfielded shifted protons of silyl groups and methylene compare to those of **5** in ^{1}H NMR spectra were arisen by the low oxidation numbered aluminum species. The single crystal x-ray structural analysis revealed the structure of aluminum(II) including an Al-Al single bond. The two cyclic-dialkylaluminum planes were in an orthogonal position to avoid the steric hindrance of bulky silyl groups. On the other hand, using only 3 equivalents of THF in hexane led to afford bicyclic aluminate **7**.

Scheme 2-2-4. Reduction of **5**.

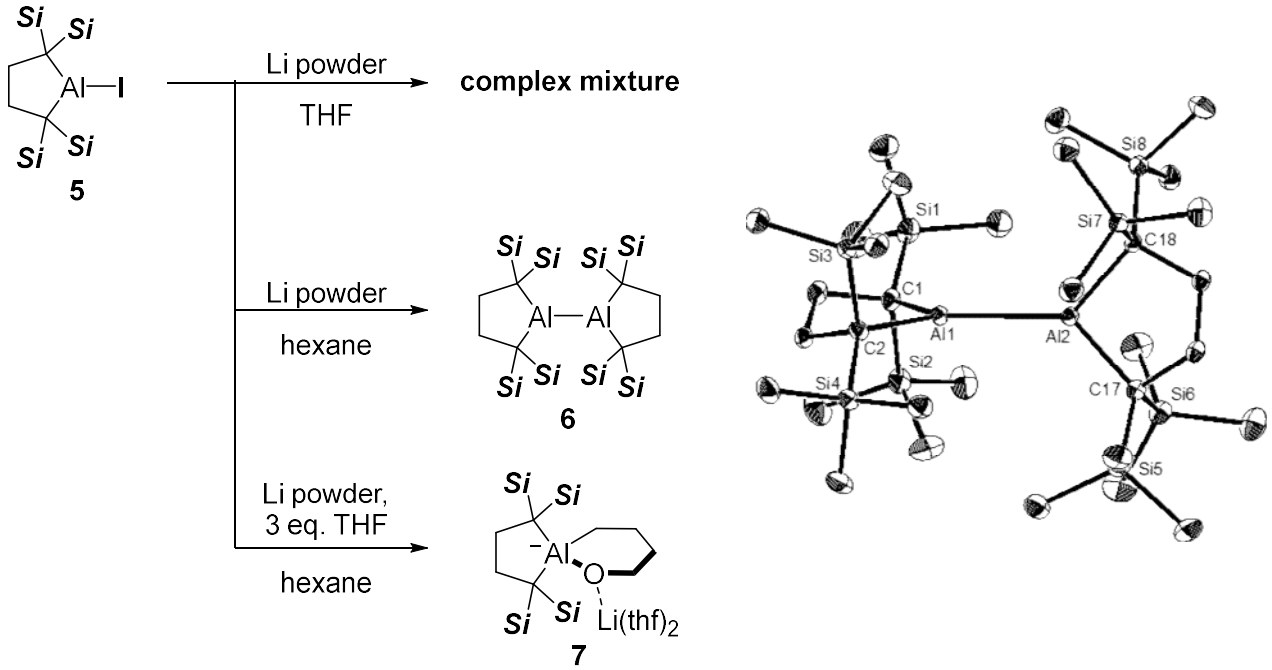

The mechanism for the generation of **7** is proposed as follows (Scheme 2-2-5). There are several possible pathways. The first is through the decomposition of anionic Al(I) anion. That is, the reduction of Al(II) radical **I** or its dimer **6** gave anionic Al(I) **II** and subsequent aluminum insertion toward C-O bond affords **7**. The latter is through the reductive C-O cleavage of THF.[4] The C-O cleaved intermediate **V** generates by reduction of the combination of **I** and Li, or two Li and **IV**, which is generated through the coordination of THF for Lewis acidic aluminum center in **5**. Subsequent intermolecular nucleophilic addition affords **7**. As alternative process to let C-O bond in THF cleaved, intermolecular ring-opening reaction would be considered, and following two-electron reduction gave same intermediate **V**. Based on the above considerations, I considered that the reduction of isolated **6** in presence of THF would give the target Al(I) anion with less side reactions (via **I** or **IV**). It should be noted that the reductive Al–Al bond cleavage of tetraalkyldialumane **6** has been reported, where the dialkyl-Al(I) anion was proposed as an intermediate (Scheme 2-2-6).[5] The Al(I) anion intermediate spontaneously reacted with DME solvent to form C-O cleaved product **7**.

Scheme 2-2-5. Proposed mechanism for the reduction of **5** with Li affording **7**.

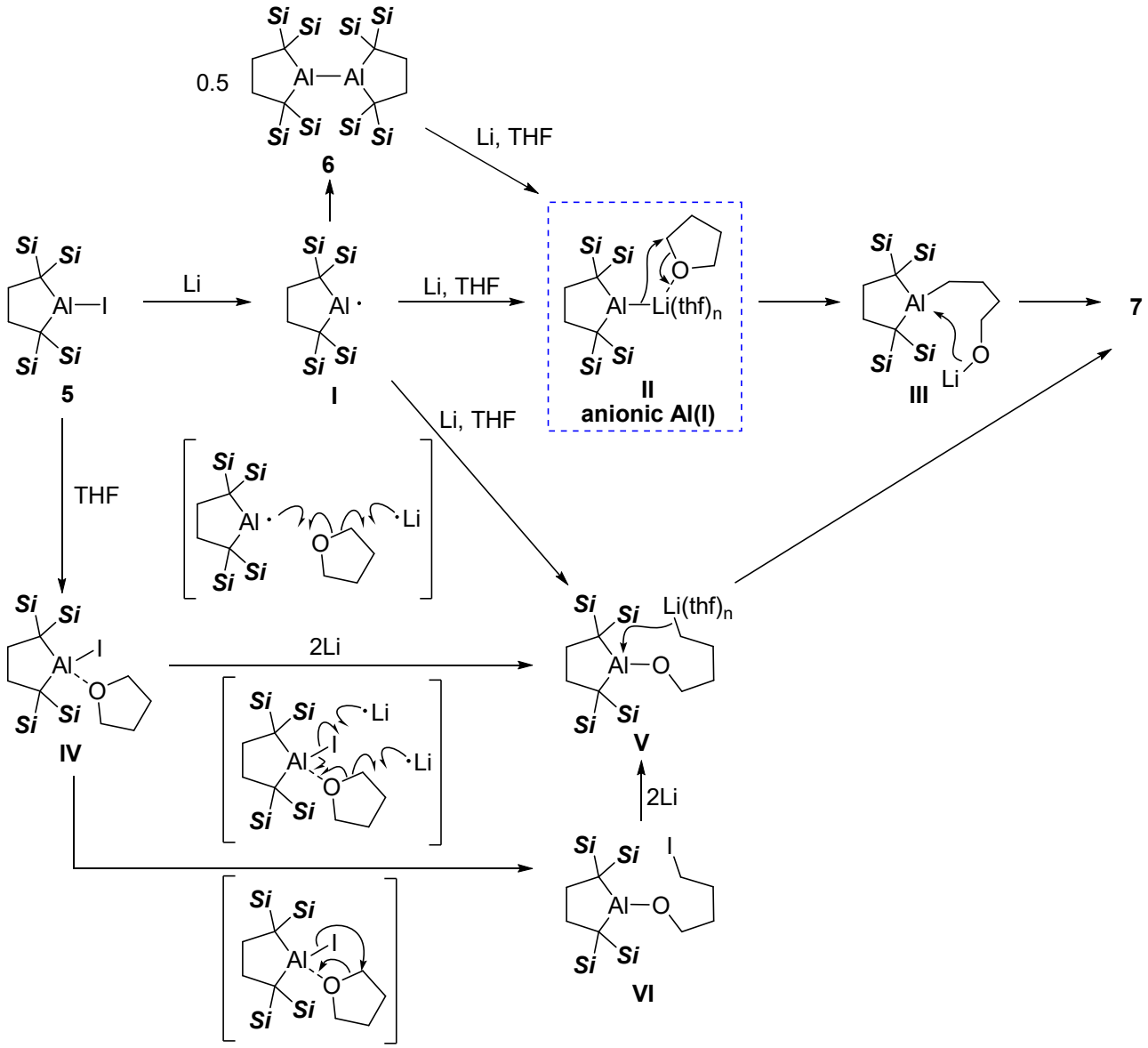

Scheme 2-2-6. Reported reduction of tetraalkyl-dialumane **I**.

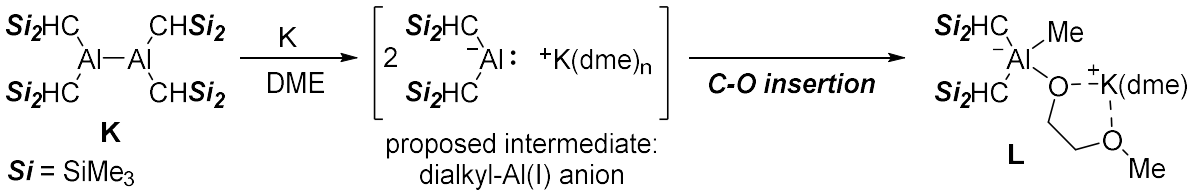

Treatment of **6** with a Na/K alloy in a THF/toluene (1/100) mixed solvent induced the cleavage of the Al–Al bond to give toluene-solvated alumanylpotassium **8** as a red crystalline solid. The reaction in toluene did not proceed, whereas the reaction in THF afforded a complex mixture of products (Scheme 2-2-7).

Scheme 2-2-7. Reductive Al-Al cleavage of dialumane **6**, and crystal structure of **8**.

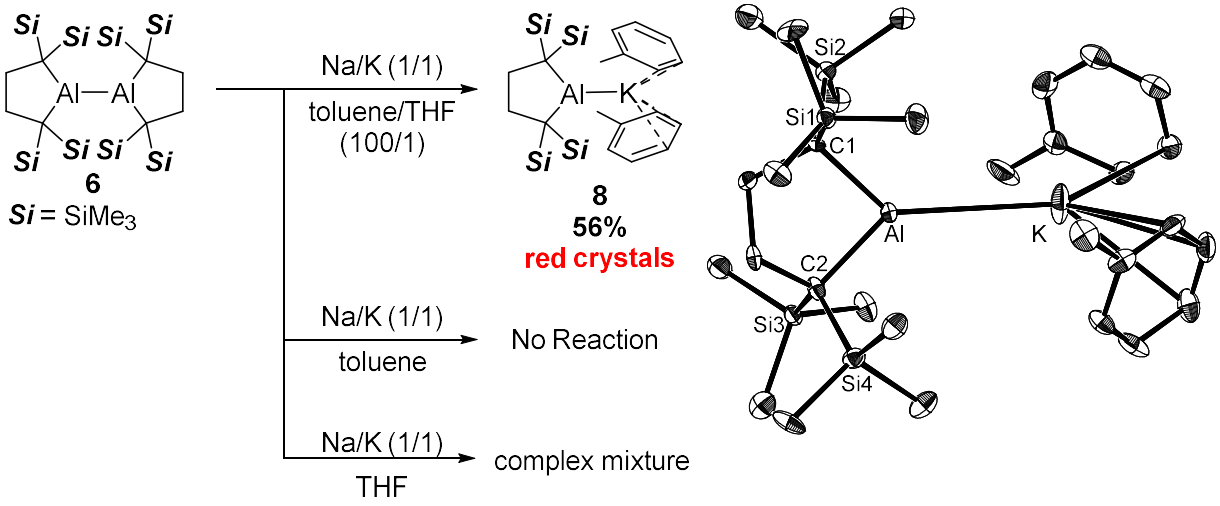

A single-crystal X-ray diffraction analysis of **8** revealed a planar and trigonal Al center (angle sum around Al, 360°) (Table 2-2-1). The Al–K bond in **8** (3.4549(5)Å) is slightly longer than the sum of the covalent radii of Al and K (3.28Å),[6] and much/slightly shorter than the Al···K distance in potassium salt of amino-substituted Al anion **A-D** (3.499-6.660 Å).[7-10] A structural comparison of **8** with its precursor **6** showed that the two Al–C bonds (2.0846(9)Å) in **8** are longer than those in **6** (2.005(3)–2.011(3)Å) and that the C–Al–C bond angle (90.40(5)°) in the former is narrower than that in the latter (97.78(12)°). These results suggest a higher p character of the C–Al bond on the Al atom and a more pronounced s character of the Al–K bond on the Al atom in **8**, which is supported by a natural bond orbital (NBO) analysis (Al–C, 80.78% p orbital of Al; Al–K, 78.98% s orbital of Al) calculated at B3LYP/6-31+G(d) level theory.

Table 2-2-1. Selected structural parameters of **8** and reference compounds.

compound	**8**	**6**	**A**	**B**	**C**	**D**
Al-K (Å)	3.4549(5)		4.070(1)/ 3.844(1)	3.5916(8)	3.499(1)	6.660
Al-C (Å)	2.0846(9)	2.005(3)/ 2011(3)				
C-Al-C(°)	90.40(5)	97.78(12)				
C-Al-K(°)	134.9(3)/ 134.7(3)					
ΣAl(°)	360.0					

The three most characteristic molecular orbitals of **8**, calculated at the B3LYP/6-31+G(d) level of theory, are illustrated in Figure 2-2-1(a). The highest occupied molecular orbital (HOMO) of **8** is a lone pair of electrons that is located mainly on the Al atom, whereas the lowest occupied molecular orbital (LUMO) of **8** consists of the π* orbitals of the toluene molecules coordinated to the K atom. An almost non-perturbed Al 3p-orbital was found in the LUMO+8. The properties of the Al–K bond were estimated by atoms in molecules (AIM) analyses (Figure 2-2-1(b)). The AIM analysis suggested a polar character of the Al–K bond with a small ρ(r) value (0.01173 $e=a_0^3$) and a positive $\nabla^2\rho(r)$ value (0.02083 $e=a_0^5$). A natural population analysis (NPA) of **8** suggested a character of slightly polarized Al-K bond in Al^- and K^+, with a charge (+0.5956) and (+0.8340), respectively (Figure 2-2-1(c)). To summarize these results, it was found that **8** has the electronic structure with a lone pair and unoccupied 3p-orbital on Al atom as describe in Figure 2-2-1(d).

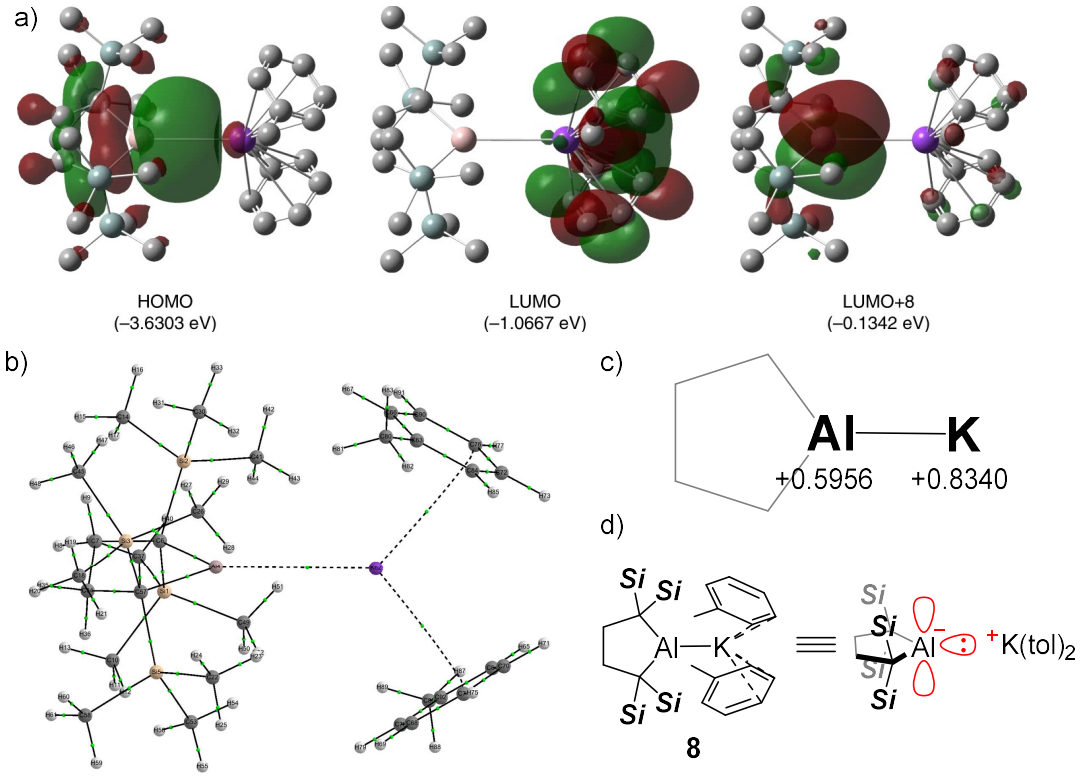

Figure 2-2-1. DFT calculations of **8** (B3LYP/6-31+G(d) level theory). The summary of (a) molecular orbitals, (b) AIM analysis, (c) NPA charges (silyl groups and toluene molecules were omitted to clarify), and (d) proposed electronic structure.

The second-order perturbation energy analysis provided weak donor–acceptor interactions from the σ_{SiC} bonding electrons to the unoccupied 3p-orbital on the Al atom (9.38–13.57 kcal mol^{-1}, Table 2-2-2), indicating it is said that Al atom in **8** has an almost non-perturbed vacant 3p-orbital.

Table 2-2-2. Interactions from the σ_{SiC} bonding electrons to the unoccupied 3p-orbital on the Al atom in **8**.

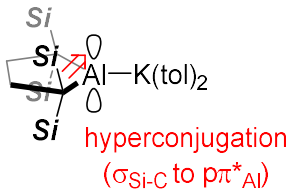

Donor NBO (i)	Acceptor NBO (j)	*E*(2) [kcal/mol]	*E*(j)-E(i) [a.u.]	*F*(i,j) [a.u.]
BD (1)Si1 - C6	LP*(2)Al4	13.57	0.57	0.084
BD (1)Si1 - C6	LP*(3)Al4	9.38	0.57	0.067
BD (1)Si2 - C6	LP*(2)Al4	12.16	0.55	0.078
BD (1)Si2 - C6	LP*(3)Al4	10.90	0.55	0.071
BD (1)Si3 - C57	LP*(2)Al4	12.70	0.56	0.081
BD (1)Si3 - C57	LP*(3)Al4	9.60	0.56	0.067
BD (1)Si5 - C57	LP*(2)Al4	12.37	0.58	0.080
BD (1)Si5 - C57	LP*(3)Al4	11.29	0.57	0.074

The color of Al(I) anions **A**-**D** were reported as yellow or bright yellow, especially, the optical absorption at 422 nm was examined for **D** (Figure 2-2-2a).[1-4] Whereas, the electronically non-perturbed Al(I) anion **8** was isolated as a red crystal. The optical absorption of **8** was examined by UV-vis spectroscopy in toluene (Figure 2-2-2b). At –50 °C, **8** exhibited two absorption maxima at 309 (ε = 981) and 468 nm (ε = 327), which is red-shifted from that in **D**. Moreover, TD-DFT calculations indicated that a combination of transitions from HOMO to LUMO and LUMO+8 reproduces the characteristic absorptions observed in the UV-vis spectrum of **8**. Thus, the electronically non-perturbed Al(I) anion **8**, possessing narrower energy gap between a lone-pair and an unoccupied 3p-orbital on Al atom than those of other anionic Al(I) species, show the characteristic optical property.

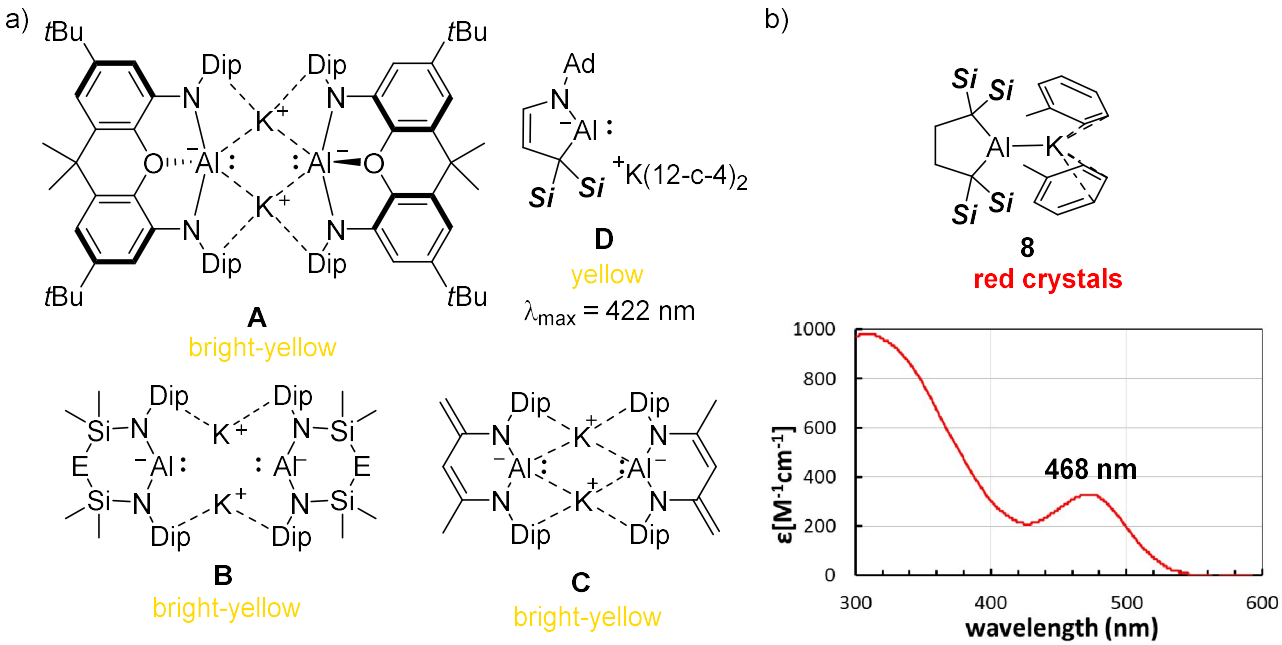

Figure 2-2-2. (a) Reported color and optical absorption of Al(I) anions **A**-**D**. (b) UV-vis spectrum of **8** in toluene in a 1 mm sealed cuvette (T = –50 °C, [**8**] = 1.07×10^{-3} M).

In summary, the four-step synthesis of the monomeric potassium salt of an alkyl-substituted aluminum anion **8** was described. The structural features of **8** in the crystal indicate that **8** is stabilized by a small C–Al–C angle, a long C–Al bond and the shortest hitherto reported Al–K contact. The characteristic absorption of **8** at 468nm suggests the presence of a lone pair of electrons and an unoccupied p orbital on the Al atom, which is supported by the results of DFT calculations. NBO and AIM analyses indicate a polar bond between Al^- and K^+.

2-3. Synthesis of dialkyl-alumanyl anion with non-solvated potassium cation

In the same manner with amino-substituted alumanyl anions **A-X** are possessing non-solvated potassium cation as dimer structure in the solid state, dialkyl-alumanyl anion dimer **8'** was synthesized by the reduction of **5・Br** with $(Me_3Si)_2O$ solvent, which is an ether having low nucleophilicity on the oxygen atom (Scheme 2-3-1). ^1H NMR spectrum of **8'** in C_6D_6 and toluene-d_8 gave same signals with **8**, suggesting **8'** takes monomeric structure in such polar solvents. The single crystal structural analysis of **8'** revealed the dimeric structure with two Al-K-Al 3 centered-2 electron bonds, supported by the shorter Al-K and Al-K' distance (3.133 Å, and 3.308 Å) than a sum of covalent radius (4.36 Å), and non-planer Al center (Σ_{Al} = 356°).

Scheme 2-3-1. Reduction of bromoalumane **5・Br** with Na/K alloy in $(Me_3Si)_2O$, which is the less-polar solvent, to afford dialkyalumanl anion **8'** with non-solvated potassium cation.

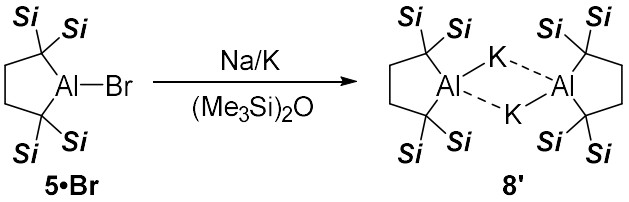

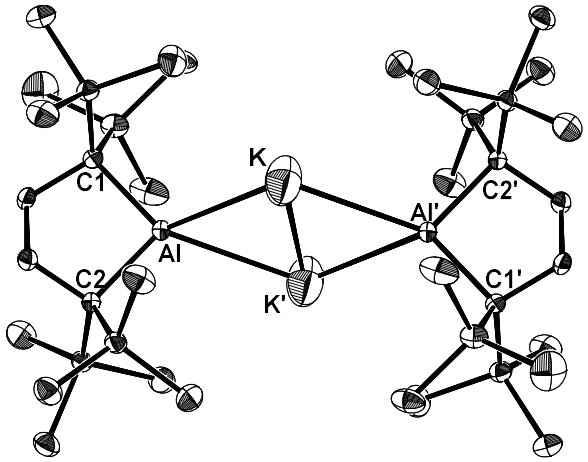

Because of the low solubility of dialumane **6**, which is the proposed intermediate of this reaction, or low reducing potential of Na/K alloy under less-polar $(Me_3Si)_2O$ solution, the reduction of **5・Br** in $(Me_3Si)_2O$ had a low reproducibility. To overcome the problems, a mechanochemistry, which is an effective and powerful method for the organic synthesis with low solubility compounds or metal(0) reductants,[11] was taken for synthesis of **8'** (Table 2-3-1). Firstly, the effect of solvent was examined under milling at 15 Hz for 5 minutes with Na/K alloy as reductant (5 equivalent). Using $(Me_3Si)_2O$, similarly with pre-examination (Scheme 2-3-2), allowed to generate **8'** but dialumane **6** remained (Entry 1). Reduction accelerating more polar solvent Et_2O gave a low yield of **8'** and **6'** with unknown products (Entry 2), and solvent free condition did not allow to generate **8'** with low conversion of **5・Br** (Entry 3). The condition of long time, or high frequency improved the selectivity of **8'** but **6** was still remained (Entry 4-6), and increasing an amount of $(Me_3Si)_2O$ solution gave better selectivity (Entry 7). On the other hand, the use of Et_2O as additive was not very effective (Entry 8).

Table 2-3-1. Trials for synthesis **8'** with ball-milling.

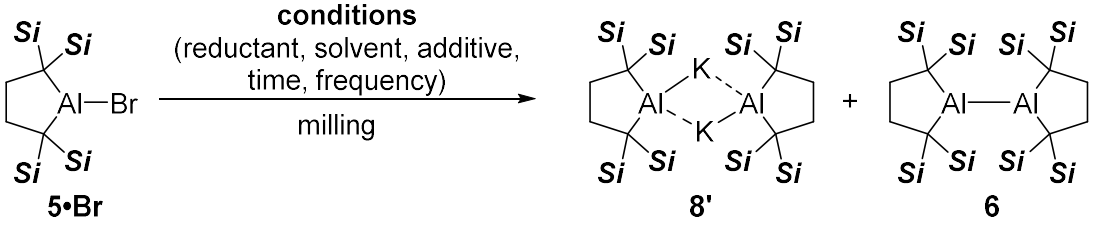

Entry	conditions					NMR yield[a] (%)	
	Reductant (eq.)	Solvent (μL)	Additive (eq.)	Time (min.)	Frequency (Hz)	**8'**	**6**
1	Na/K (5)	$(Me_3Si)_2O$ (10)	-	5	15	15	20
2[b]	Na/K (5)	Et_2O (10)	-	5	15	4	22
3[c]	Na/K (5)	-	-	5	15	0	38
4	Na/K (5)	$(Me_3Si)_2O$ (10)	-	30	15	27	37
5	Na/K (5)	$(Me_3Si)_2O$ (10)	-	30	30	27	41
6	Na/K (5)	$(Me_3Si)_2O$ (10)	-	99	30	34	41
7	Na/K (5)	$(Me_3Si)_2O$ (100)	-	5	15	33	34
8	Na/K (5)	$(Me_3Si)_2O$ (100)	-	99	30	46	36
9	Na/K (5)	$(Me_3Si)_2O$ (90)	Et_2O (10)	99	30	47	32

[a]Yield was determined by ^{1}H NMR with *t*-$Bu_3C_6H_3$ as an internal standard. [b]Unknown signals were observed in ^{1}H NMR. [c]**5•Br** was recovered (58% by ^{1}H NMR).

Subsequently, the method performing pre-milling to activate Na/K alloy was taken. After milling Na/K alloy with $(Me_3Si)_2O$ solvent at 30 Hz for 15 minutes, forming a highly dispersed Na/K alloy was visually confirmed, and then, additional milling in presence of **5•Br** gave **8'** with a higher selectivity (Entry 10). By referring the method to prepare the dispersible reducing agents,[12] KI was used as additive but there was no significant improvement (Entry 11). Further increased the solvent (Entry 12-13), the selectivity improved the most when it was used totally 500 μL of $(Me_3Si)_2O$.

Table 2-3-2. Trials for synthesis **8'** with ball-milling via pre-milling of Na/K alloy.

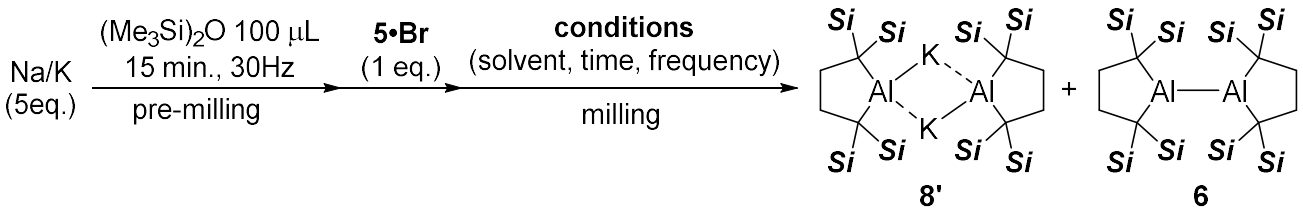

Entry	conditions				NMR yield[a] (%)	
	Solvent (μL)	Additive (eq.)	Time (min.)	Frequency (Hz)	**8'**	**6**
10	-	-	30	30	40	29
11	-	KI (5)	30	30	33	18
12	$(Me_3Si)_2O$ (400)	-	30	30	48	18

13	$(Me_3Si)_2O$ (900)	-	30	30	26	34

[a]Yield was determined by ^1H NMR with tBu$_3$C$_6$H$_3$ as an internal standard.

Since dialumane **6** was observed in all cases and the selectivity was improved by pre-milling, the following can be considered; i) possible intermediate aluminum radical **I** had been consumed by two pathway, dimerization, and further reduction to afford **6** and **8'**, and ii) the reduction of **6** to was slow (Scheme 2-3-2). In other words, suppressing a dimerization of **I** by letting it be low concentration, and accelerating a reduction of **I** by activated reductant are important to obtain **8'** effectively.

Scheme 2-3-2. Summary of the mechanochemical reduction of **6** to afford **8'**.

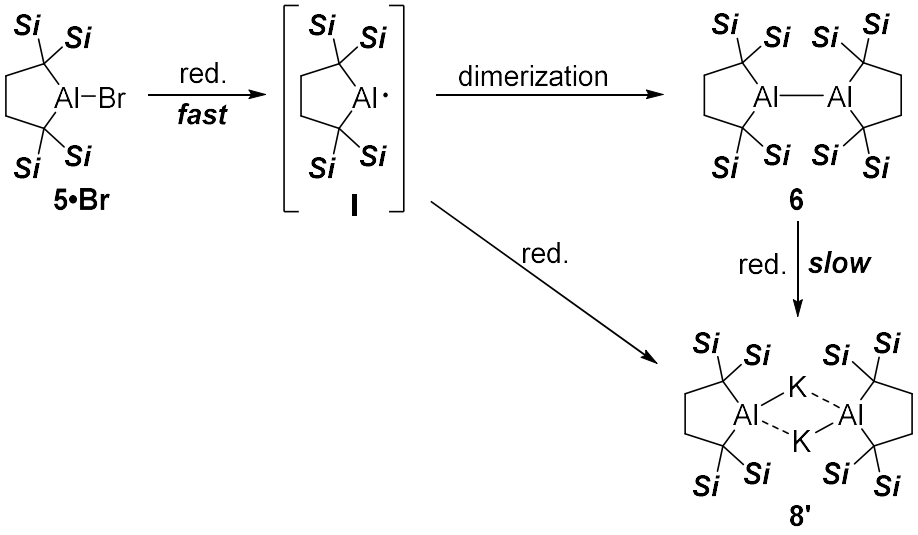

2-4. Supplementally Information

Methods

Experimental Section

General

All manipulations involving the air- and moisture-sensitive compounds were carried out under an argon atmosphere using standard Schlenk and glovebox (Korea KIYON) technique. All glassware were dried for 20 min in the 250 °C oven before use. Toluene, hexane, Et_2O, and THF were purified by passing through a solvent purification system (Grass Contour). C_6D_6 and THF-d_8 were dried by distillation over sodium-benzophenone followed by vacuum transfer. Benzene and pentane were purchased from Kanto chemical (dehydrated) and used in the glovebox without further purification. The nuclear magnetic resonance (NMR) spectra were recorded on JEOL ECS-400 (400 MHz for ^1H, 101 MHz for ^{13}C) or ECZ-600 (600 MHz for ^1H, 151 MHz for ^{13}C) Spectrometers. Chemical shifts are reported in ppm relative to the residual protiated solvent for ^1H, deuterated solvent for ^{13}C used as references. The absolute values of the coupling constants are given in Hertz (Hz). Multiplicities are abbreviated as singlet (s), doublet (d), triplet (t), quartet (q), multiplet (m), and broad (br). Melting points were determined on an Optimelt (SRS) melting point apparatus and were uncorrected. Elemental analyses were performed on a Perkin Elmer 2400 series II CHN analyzer.

Synthesis of 4

This compound was prepared in a similar manner to the previous report using THF as a solvent.1 In a glovebox, a pre-cooled (–35 °C) Et_2O solution (1.5 mL) of bis(trimethylsilyl)ethylene **3** (1.29 g, 7.50 mmol) was added to a pre-cooled (–35 °C) Et_2O suspension (1.5 mL) of Li (130 mg, 18.8 mmol) in a 30 mL vial. After stirring the reaction mixture for 12 hours at –35 °C, all the excess amount of lithium was removed by a filtration through a pad of Celite. The resulting filtrate was evaporated under reduce pressure. The residue was recrystallized from Et_2O to afford colorless crystals of dilithiobutane **4** (1.52 g, 3.00 mmol, 81%). ^1H NMR (Figure 2-4-1, 400 MHz, C_6D_6) δ 0.40 (s, 36H, CH_3 of $SiMe_3$), 1.01 (t, J = 6.9 Hz, 6H, CH_3 of Et_2O), 1.97 (s, 4H, CH_2), 3.11 (q, J = 6.9 Hz, 4H, CH_2 of Et_2O); ^{13}C NMR [Figure 2-4-2, 126 MHz, toluene-d_8, –35 °C, a signal of the Li-bonded carbon atom was not observed probably due to overlapping with the CD_3 signal of toluene-d_8 at δ 20.56 (Cf. A Li-bonded carbon atom of $PhC(SiMe_3)Li(dme)$-$C(SiMe_3)_2Li(dme)$ resonated at δ 18.6 in toluene-d_8)] δ 4.65 ($SiMe_3$), 14.94 (CH_3 of Et_2O), 45.76 (CH_2), 66.21 (CH_2 of Et_2O); mp 52.3-52.6 °C (decomp.); A highly hygroscopic nature of **4** prohibited us to obtain a reasonable elemental analysis data.

Synthesis of 5

In a glovebox, a pre-cooled (–35 °C) hexane solution (15 mL) of **4** (152 mg, 0.300 mmol) was added to a pre-cooled (–35 °C) hexane suspension (15 mL) of AlI_3 (122 mg, 0.300 mmol) in a 30 mL vial. After stirring the reaction mixture for 5 hours at –35 °C and 1 hour at room temperature, generated LiI was removed by a filtration through a pad of Celite®.The resulting filtrate was evaporated under reduce pressure. The residue was recrystallized from hexane to afford colorless crystals of iodoalumane **5** (84.5 mg, 0.169 mmol, 56%). ^1H NMR (Figure 2-4-3, 400 MHz, C_6D_6) δ

0.24 (s, 36H, CH_3 of $SiMe_3$), 1.92 (s, 4H, CH=); ^{13}C NMR (Figure 2-4-4, 126 MHz, C_6D_6) δ 2.54 ($SiMe_3$), 15.08 (br, 4°), 31.89 (CH_2); mp 80.4-87.2 °C (decomp.); A highly hygroscopic nature of **5** prohibited us to obtain a reasonable elemental analysis data.

Synthesis of 6

In a glovebox, a pre-cooled (–35 °C) hexane solution (8.0 mL) of **5** (84.5 mg, 0.169 mmol) was added to a pre-cooled (–35 °C) hexane suspension (8.0 mL) of Li (11.7 mg, 1.69 mmol) in a 30 mL vial. After stirring the reaction mixture for 20 hours at –35 °C and 1 hour at room temperature, generated LiI was removed by a filtration through a pad of Celite®. The resulting filtrate was evaporated under reduce pressure. The residue was recrystallized from hexane to afford colorless crystals of dialumane **6** (18.9 mg, 25.4 μmol, 30%). ^1H NMR (Figure 2-4-5, 400 MHz, C_6D_6) δ 0.31 (s, 36H, CH_3 of $SiMe_3$), 2.18 (s, 4H, CH_2); ^{13}C NMR (Figure 2-4-6, 126 MHz, C_6D_6) δ 4.38 ($SiMe_3$), 19.47 (4°), 34.98 (CH_2), mp 226.3-231.1 °C; Anal. Calcd for $C_{30}H_{80}Al_2Si_8$: C, 51.69; H, 10.84; Found: C, 51.65; H, 11.14.

Synthesis of 8

In a glovebox, a pre-cooled (–35 °C) toluene/THF (100/1) solution (500 μL) of **6** (16.0 mg, 21.4 μmol) was added to a pre-cooled (–35 °C) toluene/THF (100/1) suspension (500 μL) of Na/K alloy (1/1, 5.5 mg, 87.9 μmol as K) in a 3 mL vial. After stirring the reaction mixture for 15 hours at –35 °C, all the excess amount of Na/K alloy was removed by a filtration through a pad of Celite®. The resulting filtrate was evaporated under reduce pressure. The residue was recrystallized from toluene to afford red crystals of **8** (14.0 mg, 23.4 μmol, 55%). ^1H NMR (Figure 2-4-7, 400 MHz, toluene-d_8, –50 °C, toluene molecules coordinating to K^+ appeared as free toluene due to exchange with toluene-d_8) δ 0.54 (s, 36H, CH_3 of $SiMe_3$), 2.40 (s, 4H, CH_2); ^{13}C NMR (Figure 2-4-8, 101 MHz, tol-d8, –50 °C) δ 4.38 ($SiMe_3$), 19.47 (4°), 34.98 (CH_2); mp 75.7-86.6 °C (decomp., red color gradually disappeared); Anal. Calcd for $C_{30}H_{56}AlKSi_4$: C, 60.54; H, 9.48; Found: C, 60.32; H, 9.67.

Details for X-Ray Crystallography

Crystallographic data for **4**, **5**, **6**·hexane, and **8**, crystalized from hexane (**4**-**7**) or toluene (**8**) are summarized in Table 2-4-1. The crystals were coated with immersion oil and put on a MicroMountTM (MiTeGen, LLC), and then mounted on diffractometer. Diffraction data were collected on a Rigaku Saturn CCD or a Bruker Photon detectors using MoKα radiation. The Bragg spots were integrated using CrysAlisPro program package.[13] Absorption corrections were applied. All the following procedure for analysis, Yadokari-XG 2009[14] was used as a graphical interface. The structure was solved by a direct method with programs of SIR2014[15] and refined by a full-matrix least squares method with the program of SHELXL-2018.[16] Anisotropic temperature factors were applied to all non-hydrogen atoms. The hydrogen atoms were put at calculated positions, and refined applying riding models. The detailed crystallographic data have been deposited with the Cambridge Crystallographic Data Centre: Deposition code CCDC 1869762-1869770. A copy of the data can be otained free of charge via http://www.ccdc.cam.ac.uk/products/csd/request.

Computational Methods

Gaussian 16 (rev. A.03) software package[17] was employed to perform all of the calculations. The full model of **8**

and[18-22] were optimized from the crystallographically obtained structure of **8** was calculated by geometry optimization at the B3LYP[23-25]/6-31+G(d)[26] level of theory in the presence of solvent toluene using the CPCM solvation method.[27,18] The TD-DFT calculations[19, 20] were performed to estimate UV-vis spectrum of **8** with LC-ωHPBE[21-22, 28-29] /6-31G(d) [26] level of theory in the presence of toluene as a solvent using the CPCM solvation method. [27,18] AIM analysis[30,31] was performed by using AIMAll program package[32] with wavefunction file generated by Gaussian program.

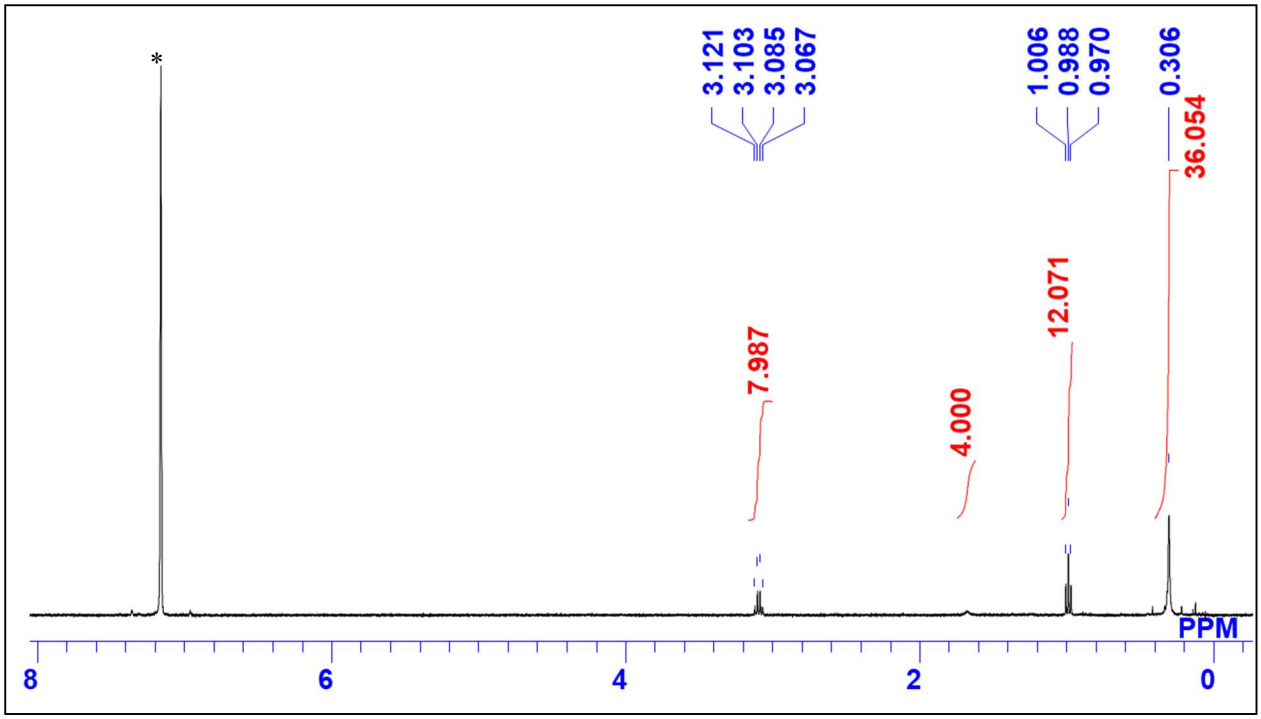

Figure 2-4-1. The ^{1}H NMR spectrum of **4** (*: C_6D_5H).

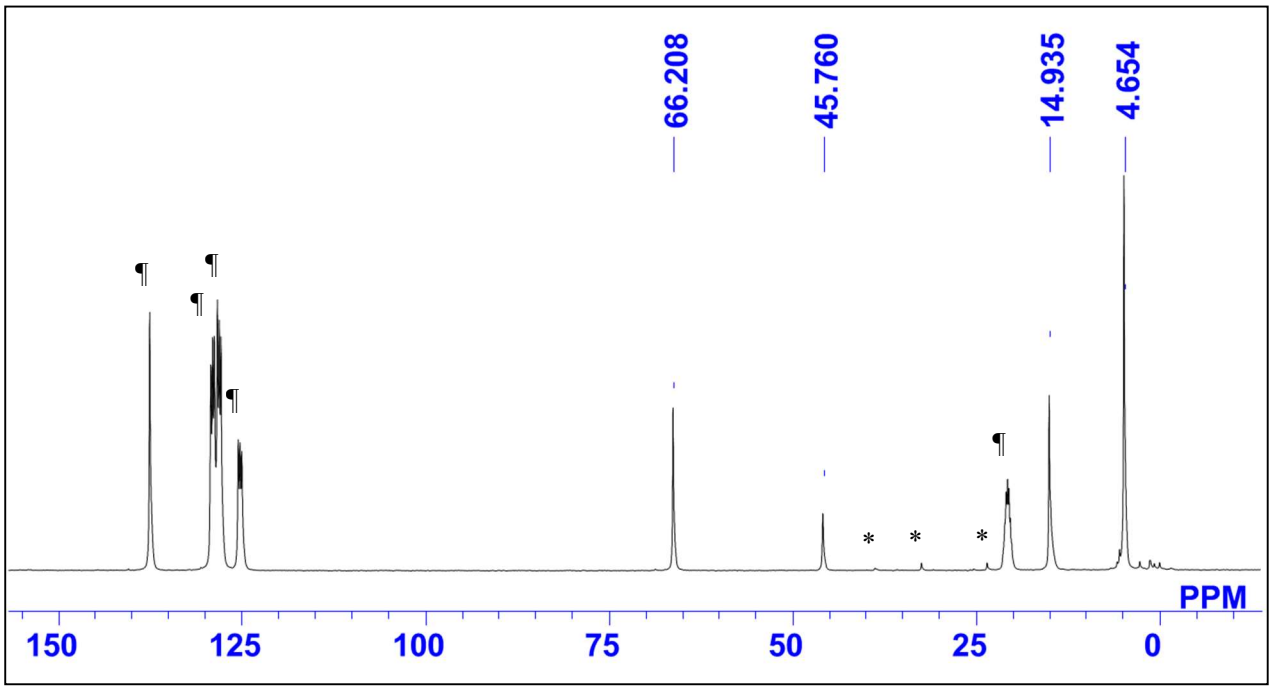

Figure 2-4-2. The ^{13}C NMR spectrum of **4** (*: hexane, ¶: toluene-d_8).

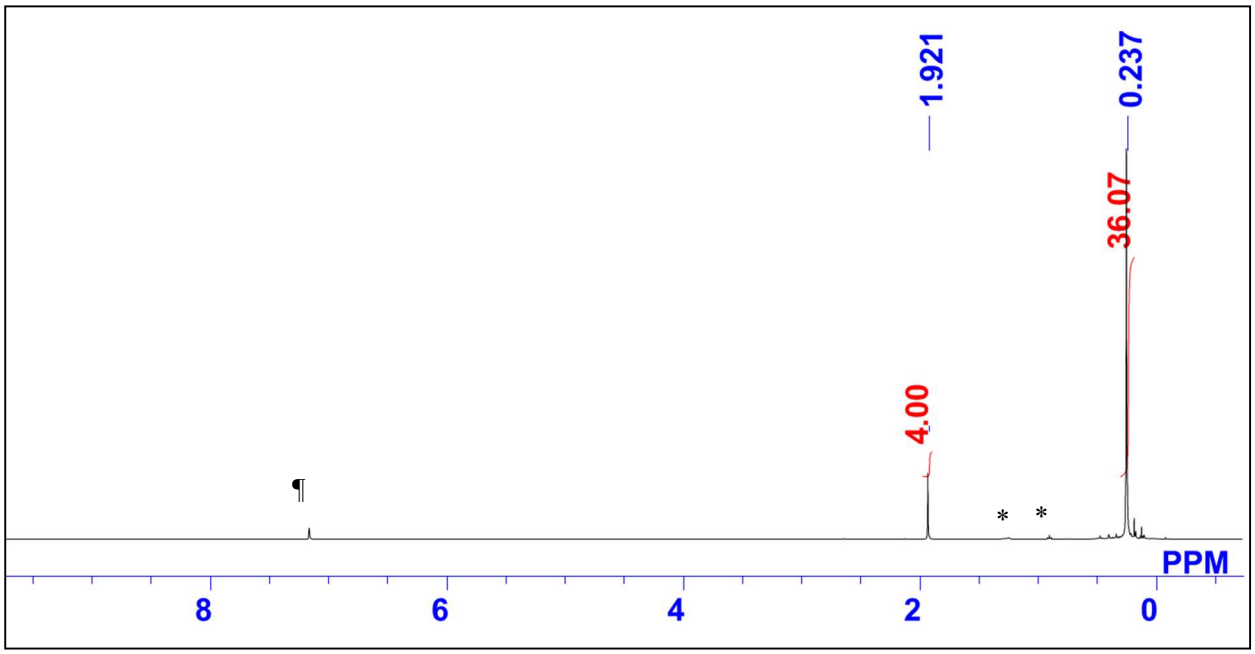

Figure 2-4-3. The ^{1}H NMR spectrum of **5** (*: hexane, ¶: C_6D_5H).

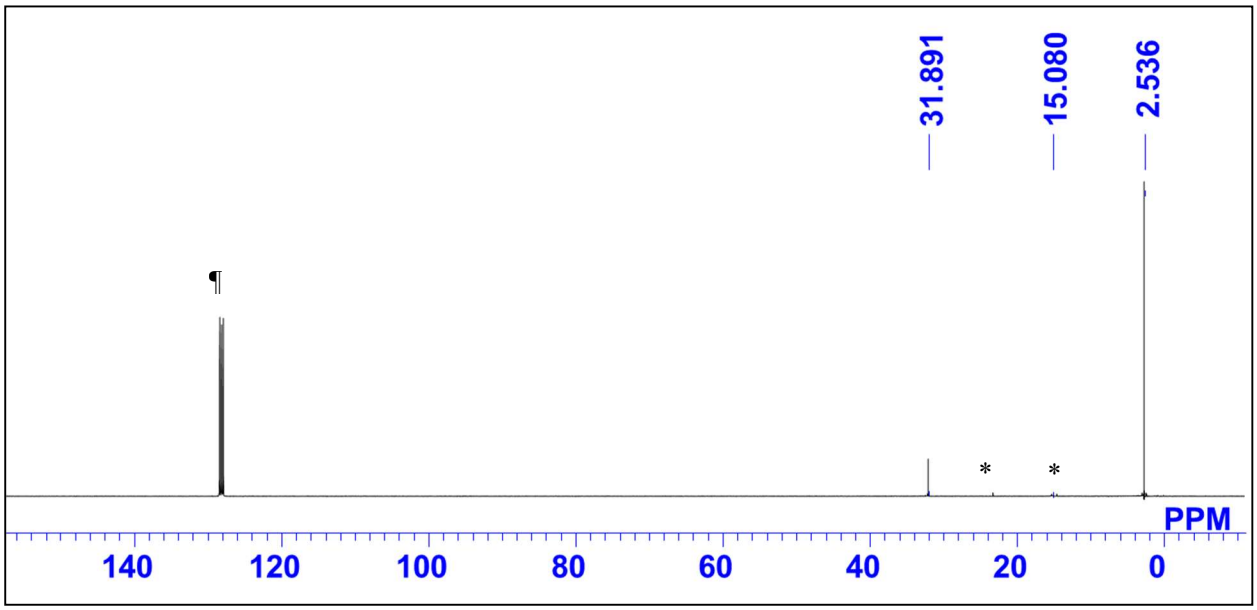

Figure 2-4-4. The ^{13}C NMR spectrum of **5** (*: hexane, ¶: C_6D_6).

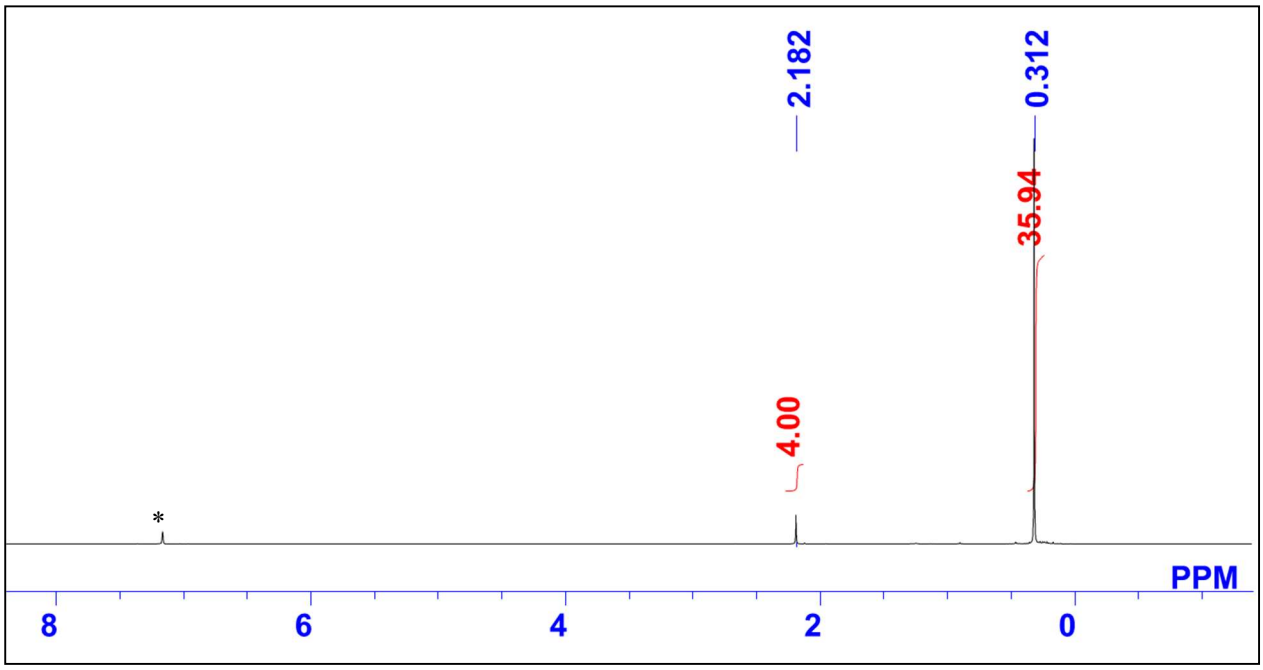

Figure 2-4-5. The ^{1}H NMR spectrum of **6** (*: C_6D_5H).

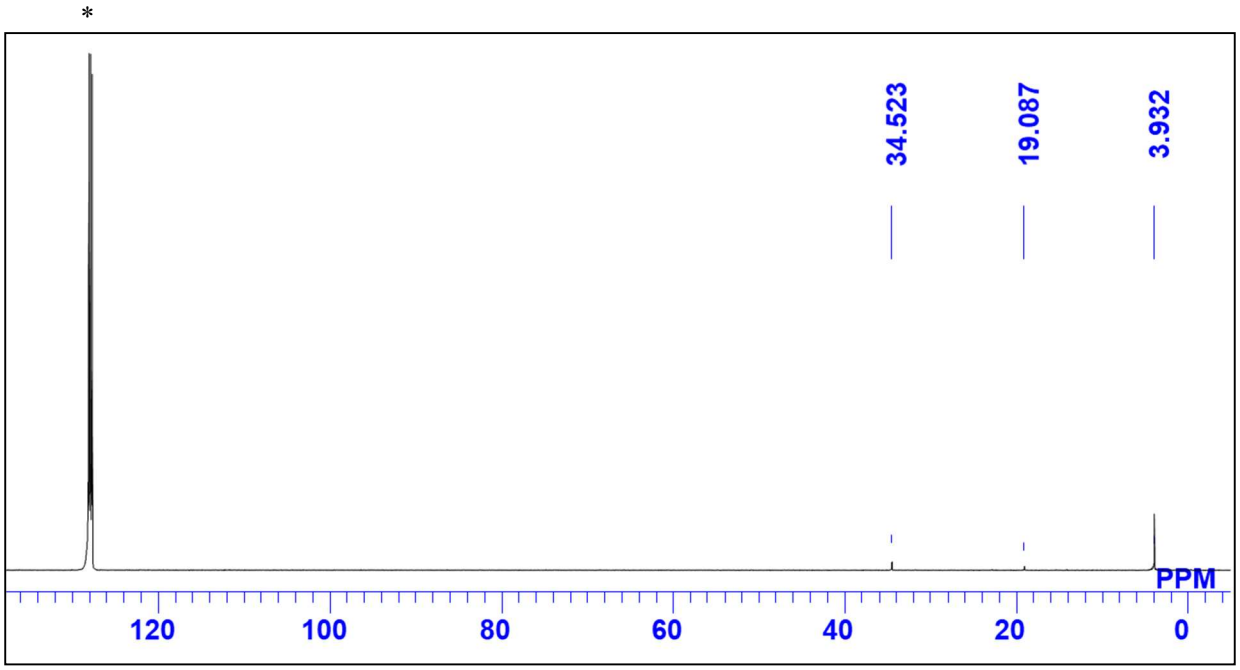

Figure 2-4-6. The ^{13}C NMR spectrum of **6** (*: C_6D_6).

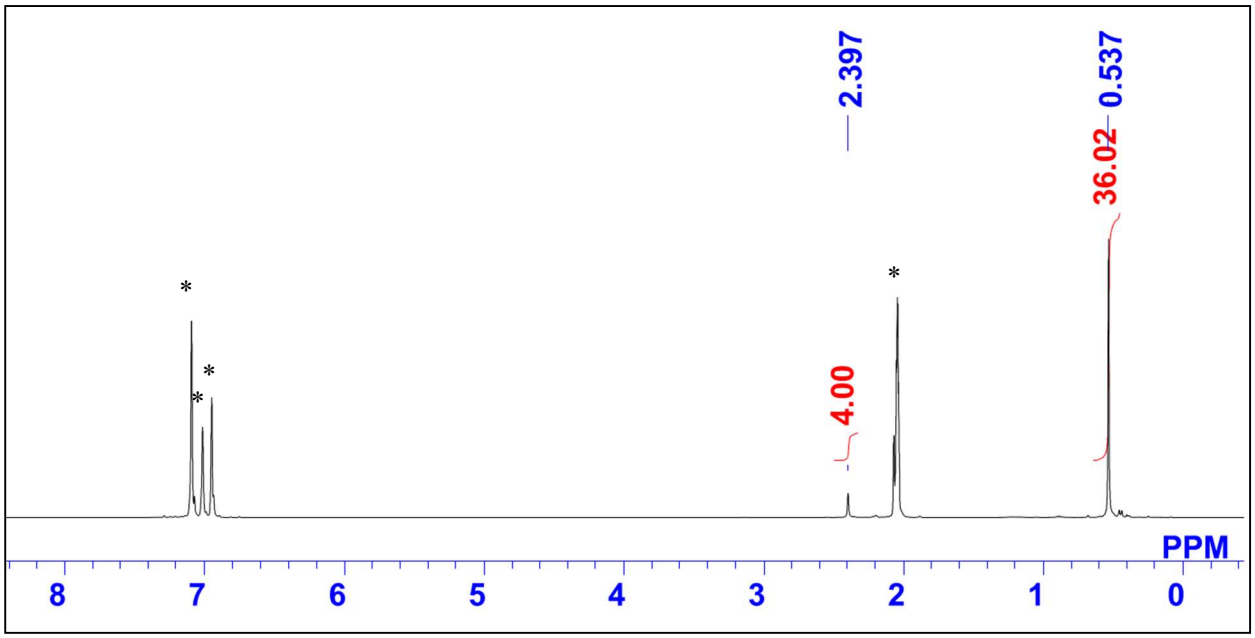

Figure 2-4-7. The ^{1}H NMR spectrum of **8** (*: toluene-d_7).

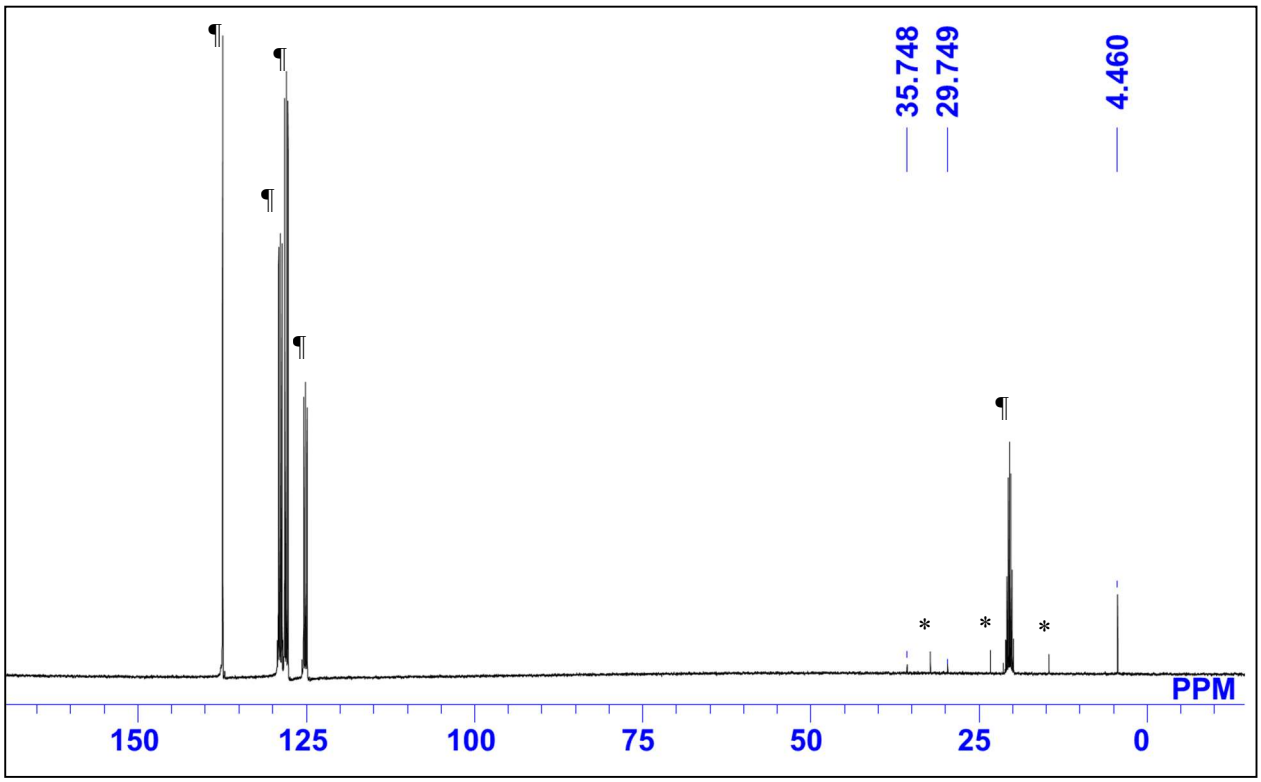

Figure 2-4-8. The ^{13}C NMR spectrum of **8** (*: toluene, ¶: toluene-d_8).

Table 2-4-1. Crystallographic data and structure refinement details for **4**, **5**, **6**·hexane, and **8**.

compound #	**4**	**5**	**6·hexane**	**8**
CCDC deposit #	1869762	1869763	1869764	1869765
Empirical formula	$C_{24}H_{60}Li_2O_2Si_4$	$C_{16}H_{40}AlISi_4$	$C_{32}H_{80}Al_2Si_8 \cdot C_6H_{14}$	$C_{30}H_{56}AlKSi_4$
Formula weight	506.96	498.72	829.81	595.18
T (K)	93(2)	93(2)	93(2)	93(2)
λ (Å)	0.71073	0.71073	0.71073	0.71073
Crystal system	*Orthorhombic*	*Monoclinic*	*Monoclinic*	*Monoclinic*
Space group	$P2_12_12_1$	$P2_1/c$	$P2_1/n$	C_2/c
a (Å)	12.7825(4)	14.314(5)	11.6041(5)	16.8617(4)
b (Å)	15.8213(4)	11.518(5)	13.4158(7)	12.1818(2)
c (Å)	16.4525(5)	15.980(5)	33.898(2)	18.1343(4)
a (°)	90	90	90	90
b (°)	90	105.465(5)	91.821(5)	103.600(2)
g (°)	90	90	90	90
V (Å^3)	3327.28(17)	2539.2(16)	5274.5(5)	3620.45(13)
Z	4	4	4	4
$D_{calc,}$ (g/m^3)	1.012	1.305	1.045	1.092
μ (mm^{-1})	0.195	1.482	0.260	0.320
F(000)	1128	1032	1840	1296
Crystal size (mm)	0.36×0.21×0.11	0.43×0.38×0.37	0.45×0.08×0.04	0.55×0.30×0.29
2q range (°)	2.018-31.338	1.476-28.552	2.321-28.767	2.083-32.616
reflns collected	31815	18717	39212	19639
Indep reflns/R_{int}	9854/0.0629	5335/0.0330	11167/0.0649	6056/0.0359
param	305	211	433	171
GOF on F^2	1.031	1.150	1.035	1.039
R_1, wR_2 [I>2σ(I)]	0.0534, 0.1069	0.0294, 0.0793	0.0562, 0.1231	0.0333, 0.0884
R_1, wR_2 (all data)	0.0741, 0.1173	0.0381, 0.1065	0.0946, 0.1420	0.0400, 0.0920

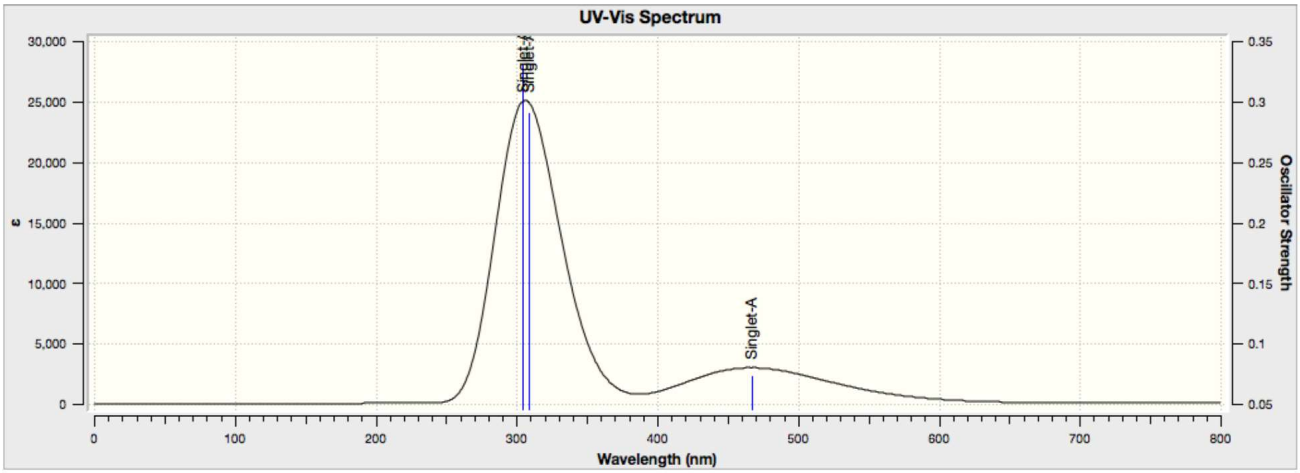

Figure 2-3-9. A simulated UV-vis spectrum for **8** at TD[16,17]-LC-ωHPBE[18-21]/6-31G(d)[13]//B3LYP[10-12]/6-31+G(d)[13] level of theory with solvent effect of toluene (cpcm).[14,15]

Table 2-4-2. Calculated excitation energies and oscillator strengths for **8** at TD[16,17]-LC-ωHPBE[18-21]/6-31G(d)[13]//B3LYP[10-12]/6-31+G(d)[13] level of theory with solvent effect of toluene (cpcm). [14,15]

Excited State 1: Singlet-A 2.6565 eV 466.73 nm f=0.0726 <S**2>=0.000

162 ->164	0.10052
162 ->166	-0.43714
162 ->168	-0.22424
162 ->171	0.47834

This state for optimization and/or second-order correction.

Total Energy, E(TD-HF/TD-DFT) = -3175.84357497

Copying the excited state density for this state as the 1-particle RhoCI density.

Excited State 2: Singlet-A 4.0208 eV 308.36 nm f=0.2907 <S**2>=0.000

162 ->164	0.39504
162 ->167	0.17810
162 ->172	0.53209

Excited State 3: Singlet-A 4.0733 eV 304.38 nm f=0.3311 <S**2>=0.000

162 ->163	0.43796
162 ->169	-0.17122
162 ->170	-0.42959
162 ->173	0.24666
162 ->175	-0.10777

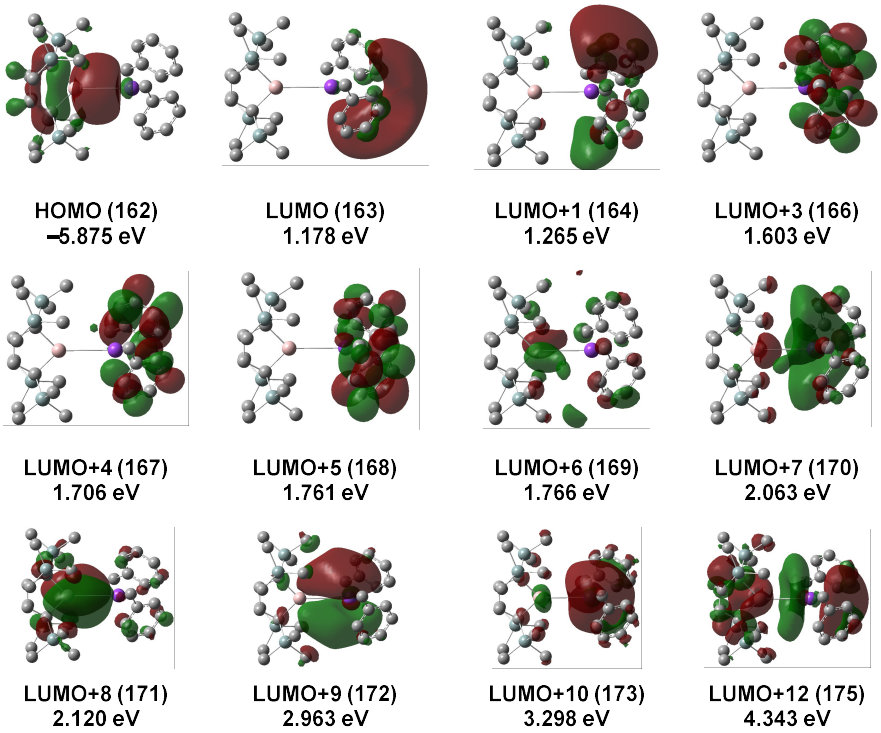

2-5. References

1. Kira, M., Ishida, S., Iwamoto, T., Kabuto, C. *J. Am. Chem. Soc.* **1999**, *121*, 9722–9723.
2. Ishida, S., Hirakawa, F., Iwamoto, T. *J. Am. Chem. Soc.* **2011**, *133*, 12968–12971.
3. Kira, M., Hino, T., Kubota, Y., Matsuyama, N., Sakurai, H. *Tetrahedron Lett.* **1988**, *29*, 6939–6942.
4. Wong, A.; Chakraborty, A.; Bawari, D.; Wu, G.; Dobrovetsky, R.; Menard G. *Chem. Commun.,* **2021**, *57*, 6903–6906
5. (a) Uhl, W.; Vester, A.; Fenske, D.; Baum, G. *J. Organometal. Chem.* **1994**, *464*, 23-34. (b) Uhl, W.; Gerding, R.; Vester, A. *J. Organometal. Chem.* **1996**, *513*, 163-172.
6. IUPAC *Compendium of Chemical Terminology* 2nd edn (compiled by McNaught, A. D. & Wilkinson, A.) (Blackwell Scientifc Publications, 1997); https://doi.org/10.1351/goldbook
7. (a) Hicks, J.; Vasko, P.; Goicoechea, J. M.; Aldridge, S. *Nature* **2018**, *557*, 92-95; (b) Hicks, J.; Vasko, P.; Goicoechea, J. M.; Aldridge, S.,*J. Am. Chem. Soc.* **2019**, *141*, 11000-1100.
8. (a) Schwamm, R. J.; Anker, M. D.; Lein, M.; Coles, M. P. *Angew. Chem. Int. Ed.* **2019**, *58*, 1489-1493. (b) Evans J. M., Anker, M. D., McMullin, L. C., Neale, E. S., Coles, M. P. *Angew. Chem. Int. Ed.* **2021**, *60*, 22289-22292.
9. Harder, S.; Grams, S.; Eyselein, J.; Langer, J.; Färber, C. *Angew. Chem. Int. Ed.* **2020**, *59*, 15982-15986.
10. Koshino, K.; Kinjo, R. *J. Am. Chem. Soc.* **2020**, *142*, 9057-9062.
11. Takahashi, R.; Hu, A.; Gao, P.; Gao, Y.; Pang, Y.; Seo, T.; Maeda, S.; Jiang, J.; Takaya, H.; Kubota, K.; Ito, H. *Nature Commun*. **2021**, *12*, 6691.
12. Hicks, J.; Juckel, M.; Paparo, A.; Dange, D.; Jones, C. *Organometallics* **2018**, *37*, 4810−4813.
13. CrysAlisPRO (Oxford Diffraction/Agilent Technologies UK Ltd, Yarnton, England,2015).
14. Kabuto, C., Akine, S. Kwon, E. *J. Cryst. Soc. Jpn.* **2009**, *51*, 218-224.

15. Burla, M. C. *et al*. *J. Appl. Crystallogr.* **2015***, 48*, 306-309.
16. Sheldrick, G. *Act. Cryst. Sec.* **2015**, *C 71*, 3-8.
17. Gaussian 16 (Wallingford, CT, 2016).
18. Cossi, M., Rega, N., Scalmani, G., Barone, V. *J. Comput. Chem.* **2003**, *24*, 669-681.
19. Adamo, C., Jacquemin, D. *Chem. Soc. Rev.* **2013**, *42*, 845-856.
20. Laurent, A. D., Adamo, C., Jacquemin, D. *Phys. Chem. Chem. Phys.* **2014**, *16*, 14334-14356.
21. Henderson, T. M., Izmaylov, A. F., Scalmani, G., Scuseria, G. E. *J. Chem. Phys.* **2009**, *131*, 044108.
22. Vydrov, O. A., Scuseria, G. E. *J. Chem. Phys.* **2006**, *125*, 234109.
23. Lee, C., Yang, W., Parr, R. G. *Phys. Rev.* **1988**, *B 37*, 785-789.
24. Becke, A. D. *Phys. Rev.* **1988**, *A 38*, 3098-3100.
25. Miehlich, B., Savin, A., Stoll, H., Preuss, H. *Chem. Phys. Lett.* **1989**, *157*, 200-206.
26. Huzinaga, S. et al. Gaussian basis sets for molecular calculations. (Elsevier, 1984).
27. Barone, V., Cossi, M. *J. Phys. Chem.* **1998**, *A 102*, 1995-2001.
28. Vydrov, O. A., Heyd, J., Krukau, A. V., Scuseria, G. E. *J. Chem. Phys.* **2006**, *125*, 074106.
29. Vydrov, O. A., Scuseria, G. E. Perdew, J. P., *J. Chem. Phys.* **2007**, *126*, 154109.
30. Bader, R. F. W. Atoms In Molecules - A Quantum Theory. (Oxford University Press, 1990).
31. Bader, R. F. W. A. *Chem. Rev.* **1991**, *91*, 893-928.
32. AIMALL (version 14.04.17) (TK Gristmill Software, Overland Park KS, USA, 2014).

Chapter 3:
Reactivity of Dialkyl-Substituted Aluminum Anion

3-1. Introduction

Since the first aluminum anion emerged in 2018,[1] reactivity of aluminum anions has been widely investigated. The reactivity of these reported aluminum anions can be classified into five patterns: a) nucleophilic substitution, b) transmetallation, c) oxidative addition, d) cycloaddition, and e) reduction.

Similar to the boryl anion, the alumanyl anions can nucleophilically introduce the aluminum unit through the reaction with electrophiles. Nucleophilic substitution, which is the most typical reactivity of anionic species, was only reported toward methyl electrophiles, such as MeI and MeOTf, to furnish the corresponding methylalumane **I** (Scheme 3-1-1a).[1] Transmetallation of **A**,[1,2] **F**,[3,4] or **8**[5] have been reported for magnesium, calcium, aluminum, copper, and gold (Scheme 3-1-1b). Reductive insertion of carbodiimide and CO_2 into Al-Au and Al-Cu bonds in copper complex **III** and gold complex **VII** has been reported. Moreover, the reaction mechanism, both aluminum and gold in **III** behave as nucleophile (radical like mechanism) toward CO_2 was supported by DFT calculations. Furthermore, a sole effort of transmetalation for early metal was reported by using dialkyl-alumanyl anion.[5] The alumanyl yttrium complex **IV** has a low energy level of $d\pi^*$ orbitals on the Y atom due to the introduction of electron accepting aluminum, and characteristic optical absorption and emission have been reported.

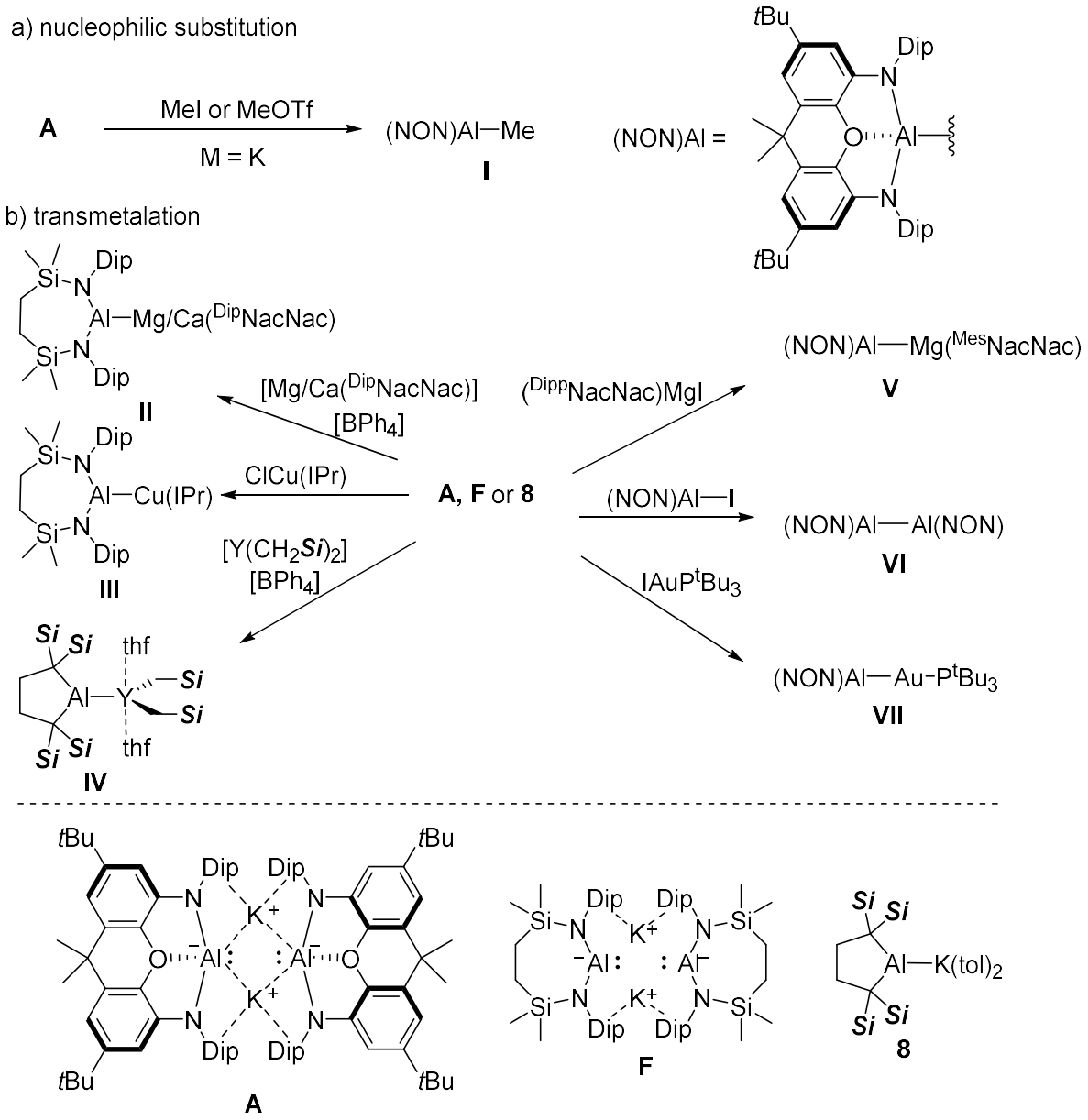

Figure 3-1-1. Reactivity of alumanyl anion; a) nucleophilic substitution and b) transmetalation.

The aluminum anions, which have a negative charge on electropositive aluminum atom, undergoes oxidative addition toward generally inert σ-bonds to afford the corresponding aluminum(III) compounds. The H-H, N-H, and Si-H bonds are cleaved by **A** and **H**. In addition, (alkyl)(amino)alumanyl anion **H** adds to robust C-C bond. [6] The reaction of **A** with benzene afforded monoaluminated **XI**, [1] whereases **G** afforded 1,4-dialuminated **XII**.[7] Cycloaddition, which is a classical reactivity of six-electron species such as carbenes and silylenes,[8,9] has also been reported for negatively charged aluminum anions to alkenes via (1+2) cycloaddition.[10,11] Moreover, (1+4) cycloaddition of **8** have been reported for naphthalene or anthracene.[12]

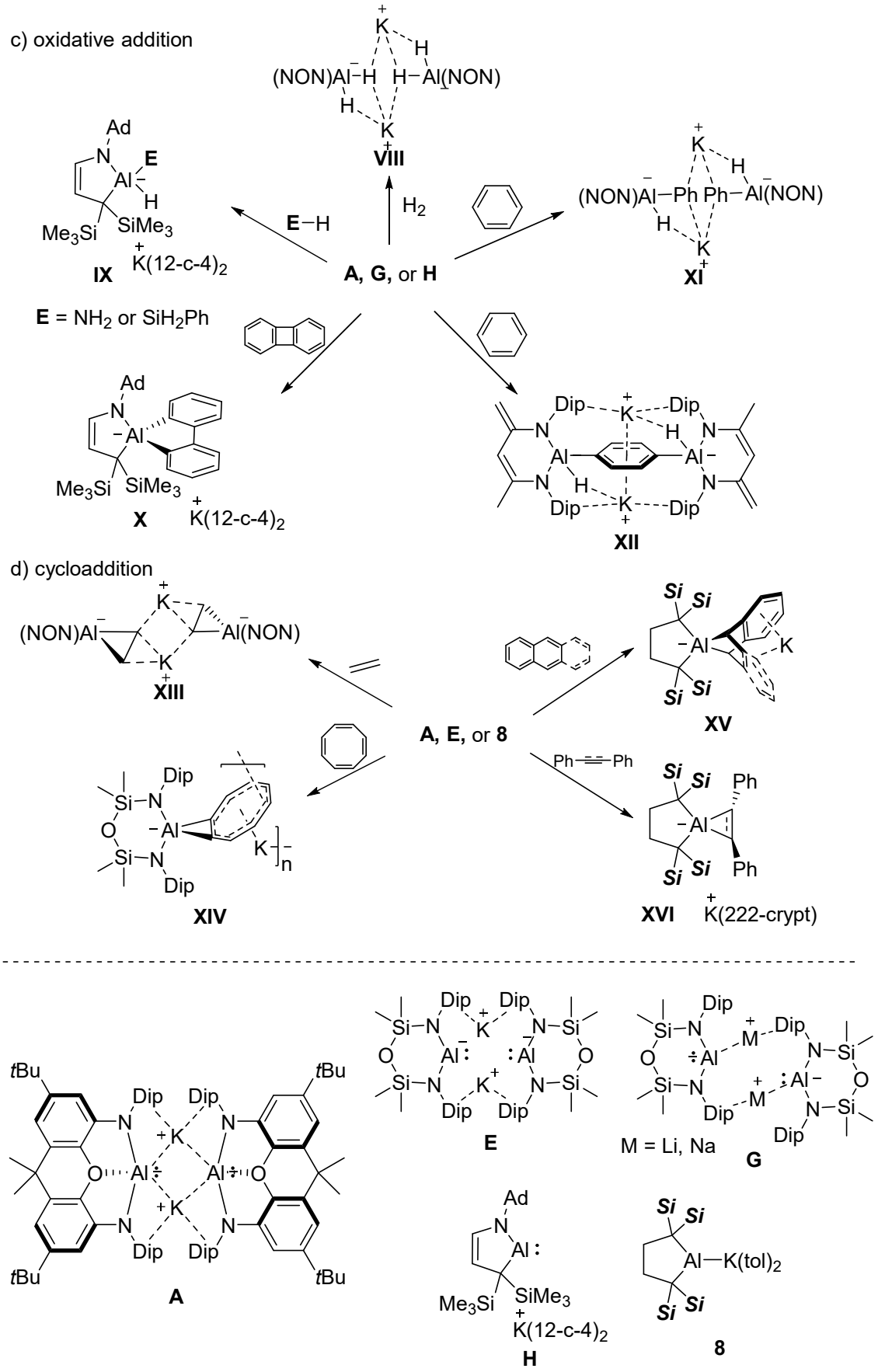

Figure 3-1-2. Reactivity of alumanyl anion; c) oxidative addition and b) cycloaddition.

Highly reducing nature due to the negative charge on electropositive Al atom in aluminum anions were used for affording anionic group 15 and 16 elements species. The aluminoxanes, having negatively charged Al-O bond, were obtained by two electron reduction of N_2O, CO_2, or PhNCO with the desorption of N_2, CO, or PhNC.[12] These species were highly reactive to undergo H-H cleavage of H_2 and reductive coupling with another equivalent of N_2O, CO_2, or PhNCO. Moreover, the heavy analogue possessing Al-E (E = Se, Te) also be isolated by treatment of element E.[13] On the other hand, dialkyl-alumanyl anion **8** gave Ti(III) complex **XXI** via one-electron reduction of Ti(IV) complex.[14]

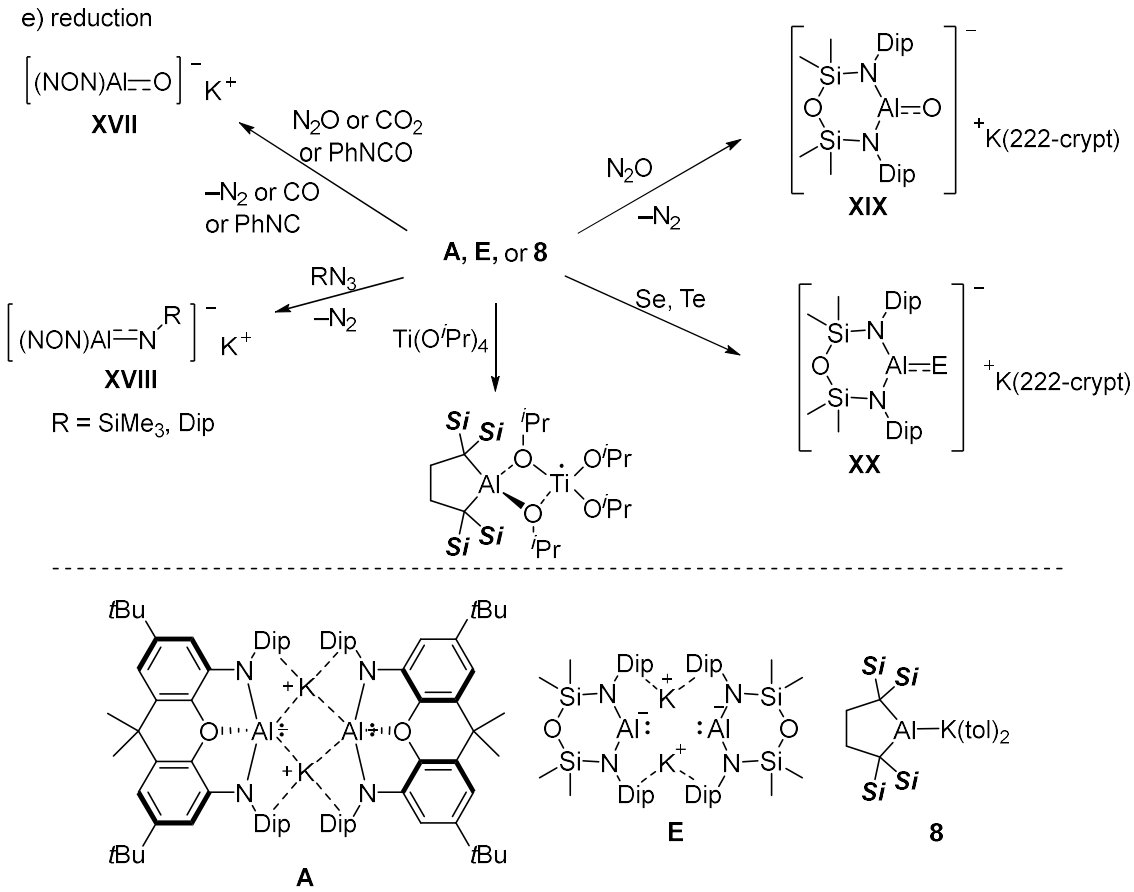

Figure 3-1-3. Reactivity of alumanyl anion; e) reduction.

In this chapter, nucleophilic substitution reactions and oxidative additions of dialkyl aluminum anion **8** are described, along with their characteristics as carbon-substituted species.

3-2. Reactivity of dialkylalumanyl anion

Nucleophilic substitution reactions using alumanylpotassium **8** were examined (Scheme 3-2-1). The reaction of **8** with methyl trifluoromethanesulfonate (MeOTf) afforded the corresponding methylalumane **9**, characterized by ^{1}H NMR spectrum with C_{2V} pattern signals (one silyl group and methylene) and Me group at high magnetic field similar to the reported signal of $AlMe_3$.[15] Further, it should be noted that the same signals also were observed by the treatment of MeLi with iodoalumane **5**. Owing to the low crystallinity of **9**, the corresponding (*N,N*-dimethylamino)pyridine (DMAP) adduct, **9**-DMAP, was generated to confirm the presence of the methyl group. ^{1}H NMR spectrum of **9**-DMAP gave signal of Me group at high magnetic field similar to **9** and $AlMe_3$, and unsymmetric two silyl groups and methylenes, which are characteristic for four-coordinate structure as observed in the solid state. This result clearly demonstrates the nucleophilicity of the aluminum center in **8**. Whereases, dibenzylaluminate **10** and chloroalumane **11** were obtained from the reaction with benzyl chloride, as evident from a NMR analysis. It should be noted that the generation of **11** was confirmed by comparing with the mixture of the reaction of alkylenedianion **3** with $AlCl_3$, which was carried out similar to the reaction of **3** with AlI_3 to afford iodoalumane **5**.

Scheme3-2-1. Reaction of **8** with MeOTf and benzylchloride.

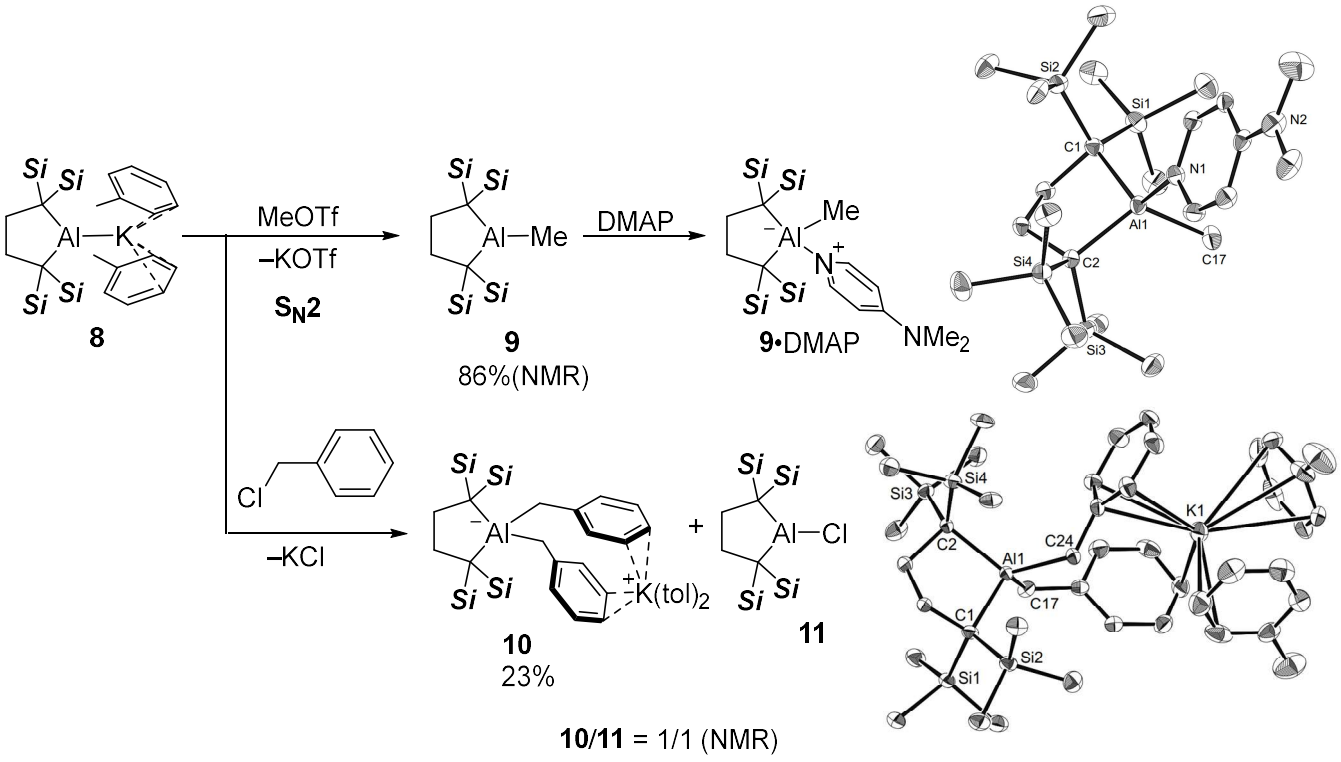

A possible reaction mechanism for the formation of **10** and **11** was illustrated in Scheme 3-2-2. That is, **8** would be susceptible to a nucleophilic substitution at the chlorine atom, rather than the sterically crowded benzylic carbon atom, to generate **11** and benzylpotassium. The resulting benzylpotassium further reacts with an equimolar amount of **11** to afford benzylalumane **12** as a potential intermediate. As an alternative pathway for **12** from **8** and benzylchloride, Al-C coupling of Al radical and benzyl radical which are generated via single-electron-transfer (SET) reaction also can be considered. Subsequently, **12** further reacts with one more equivalent of benzylpotassium to give

10. Considering that the consumption of benzylpotassium for form **10** would leave **11** unreacted.

Scheme 3-2-2. Possible reaction mechanism for dibenzylaluminate **10** and chloroalumane **11** from **8** and benzylchloride.

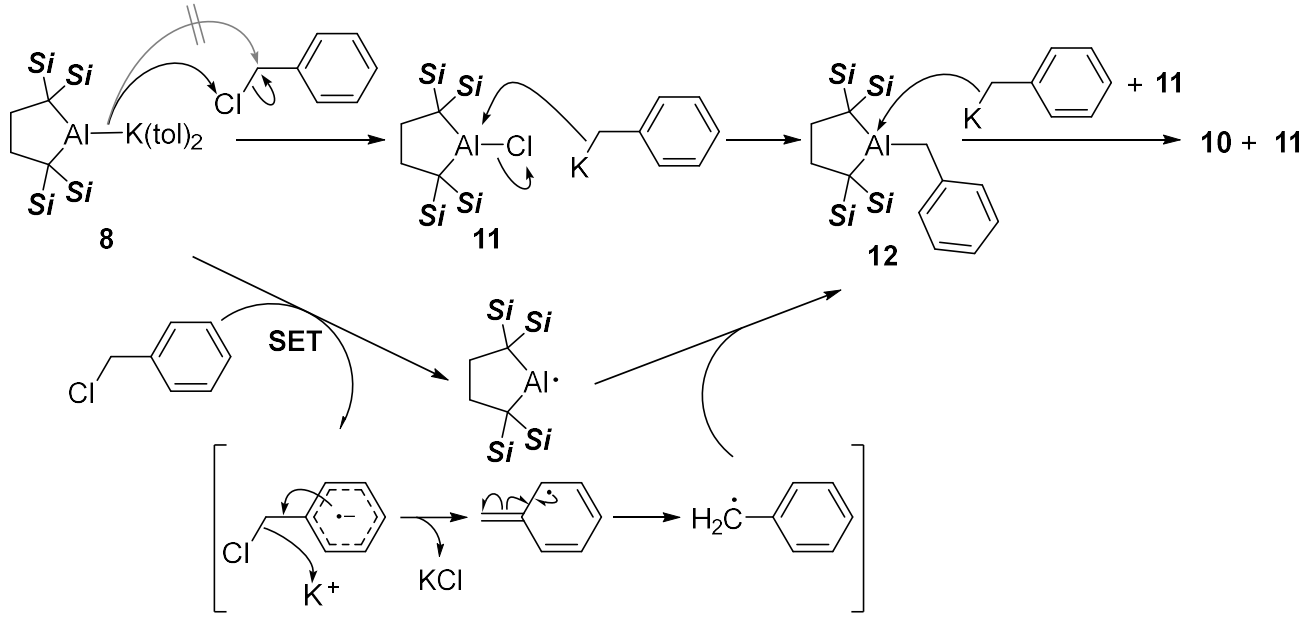

On the other hand, the oxidative addition of **8** was demonstrated in the reactions with Ar-F species (Scheme 3-2-3). Treatment of **8** with C_6F_6 afforded a mixture of **12** and **13** via one and two S_NAr type oxidative addition(s) in which the ratio of **12**/**13** varied with the stoichiometry of C_6F_6. In the reaction with 0.5 equiv. C_6F_6, dialuminated **13** was isolated as the major product, which led to the full structural characterization of **12** by a single-crystal X-ray diffraction analysis. ^{1}H NMR spectrum of **12** gave the two silyl groups and methylenes, which are characteristic for four corrdinate structure. Moreover, ^{19}F NMR spectrum showed two signal in the ratio of 1/2, reflecting the 1,4-dialuminated structure of **12** as observed in the solid state. Increasing the stoichiometry of C_6F_6 (1 equiv.) afforded a mixture of **12** and **13** at a ratio of **12**/**13**=4/3, confirmed by ^{1}H and ^{19}F NMR spectra. Here, **13** was characterized by ^{1}H NMR spectrum with unsymmetric silyl groups and methylenes like **13**, and ^{19}F NMR spectrum with three signals in the ratio of 1/1/2. Even in the reaction with 10 equiv. of C_6F_6, a significant amount of **13** was formed (**12**/**13**=3/1). These results indicate that monosubstituted **13** is more reactive toward **8** than C_6F_6.

Scheme 3-2-3. C-F oxidative addition of C_6F_6 by **8** afforded dialuminated **12** and mono-aluminated **13**.

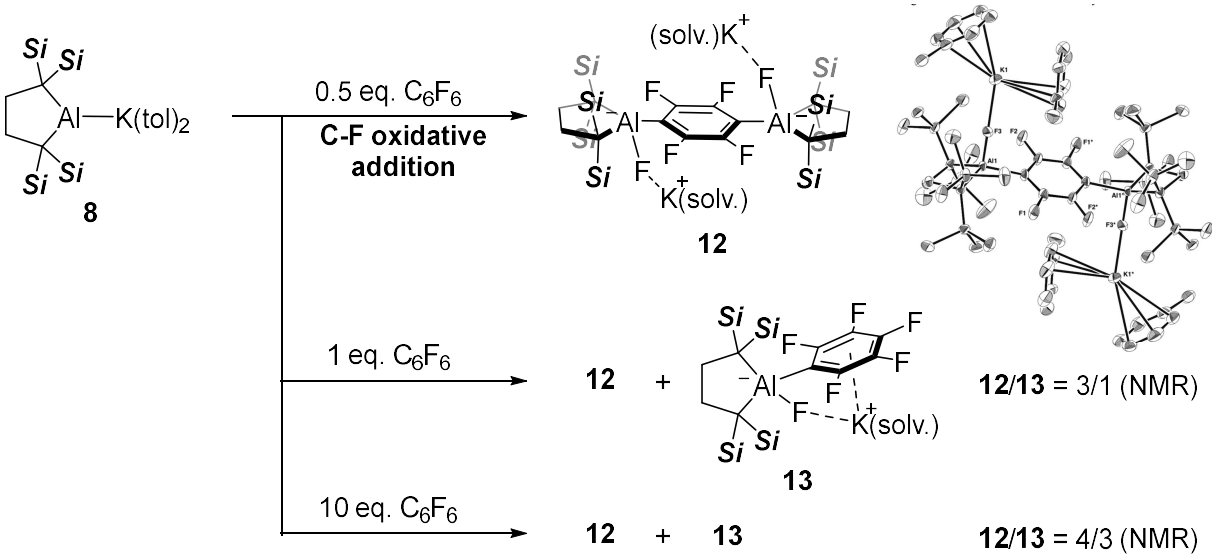

The results of the reaction of **8** with C_6F_6 indicate that monosubstituted **13** is more reactive **8** than C_6F_6, and the reaction mechanism via a S_NAr type C-F oxidative addition of **8** were proposed (Scheme 3-2-4). The monoaluminated **12** would be generated through the 1,2-fluoride shift from Meisenheimer type intermediate, or Al-C coupling of Al radical and C_6F_5 radical generated via SET reaction. A following the second nucleophilic *para*-C-F oxidative addition of another **8** afforded the bisaluminated **12**. Here, (dialkyl)(fluoro)alumanuidyl substituent probably decreases the electron density of the C_6F_5 moiety compared to that of C_6F_6, and thus enhances the reactivity towards oxidative addition reactions.

Scheme 3-2-4. Proposed mechanism for the reaction of **8** with C_6F_6.

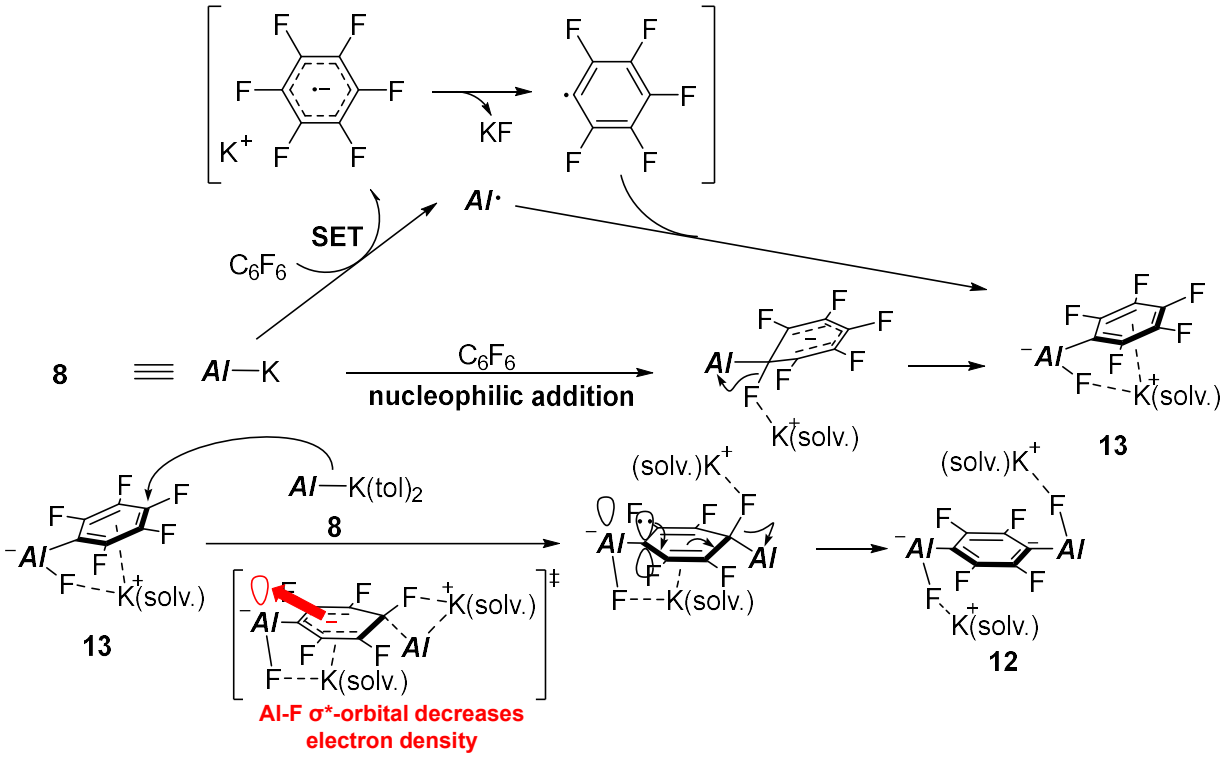

On the other hand, keeping a benzene solution of **8** at room temperature led to the formation of (hydrido)(phenyl)aluminate **14**, via the C-H oxidative addition of benzene by anionic aluminum atom (Scheme 3-2-5). I could not find the signal attributed to the aluminum bound hydrogen in ^{1}H NMR spectrum, but the signals characteristic of four coordinate structure (unsymmetrical two silyl groups and methylenes) indicated the existence of another substituents except phenyl group on the aluminum atom. Whereases, the aluminum bound hydrogen was found as a peak from the Fourier difference map in X-ray structural analysis. Note that this reaction was completed within 2.5 hours at room temperature. In contrast, the reported aluminum nucleophiles **A** and **C** required harsher conditions to give a similar compound.[1,6] I assumed that the electronically non-stabilized lone-pair on Al atom in **8** would be responsible to the very high ability for oxidative addition.

Scheme 3-2-5. C-H oxidative addition of benzene with **8** and the related reactions of aluminum anon **A** and **C**.

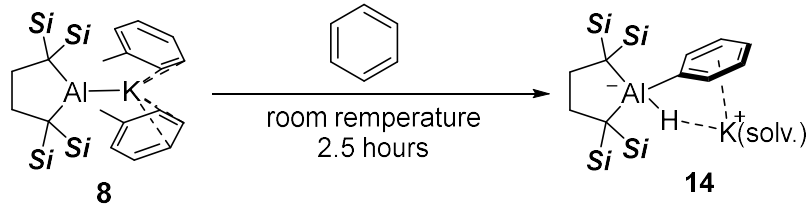

cf. reported C-H cleavage with Al(I) anions **A** and **C**

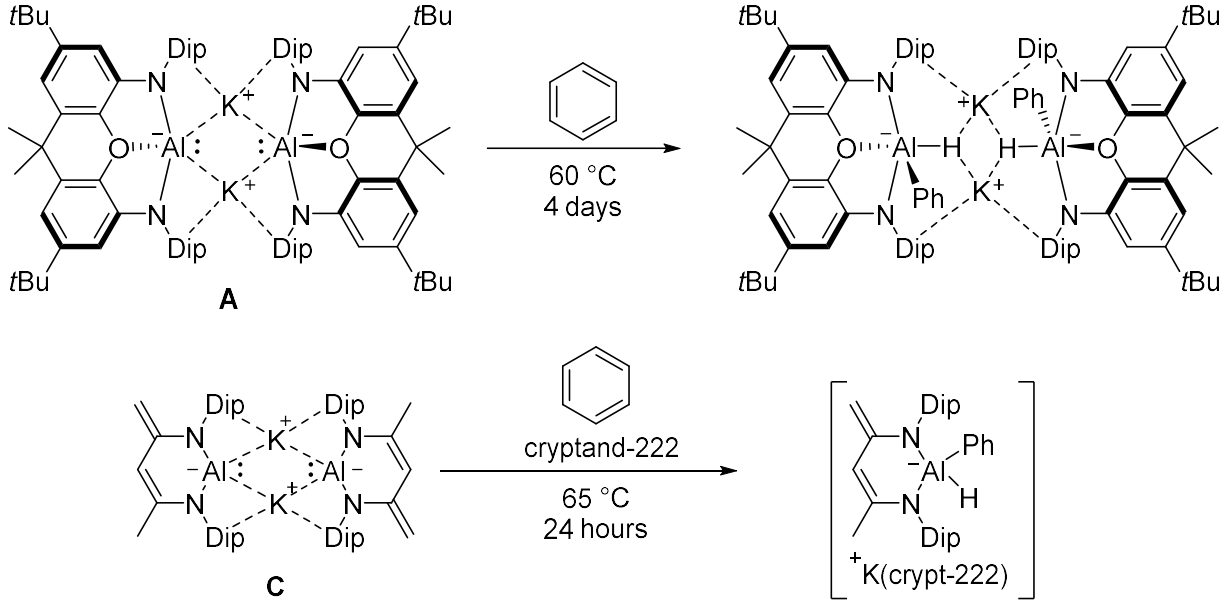

Next, the reactivity of **8** toward mono-substituted benzenes were examined. Leaving a toluene solution of **8** at room temperature led to the formation of (hydrido)(*m*-tolyl)aluminate **15** as a crystalline solid in 63% yield (Scheme 3-2-6). The ^{1}H NMR spectrum of the crude product exhibited no signal that corresponds to other isomers (NMR yield: 99%). I could not find the signal attributed to a proton bound to the aluminum atom in ^{1}H NMR spectrum, whereases a hydrogen to the alumination was found as a peak from the Fourier difference map in X-ray structural analysis. The perfect *meta*-selectivity is apparently in contrast to those in the recently reported reactions

of toluene with **A** (*meta*:*para* = 3:1) or neutral Al(I) **F** in the presence of [(nacnac)-CaH]$_2$ catalyst (meta:para = 9:1).[16,17]

Scheme 3-2-6. Perfectly *meta*-selective C-H oxidative addition of toluene with **8** and the related reactions of Al(I) species **A** and **F**.

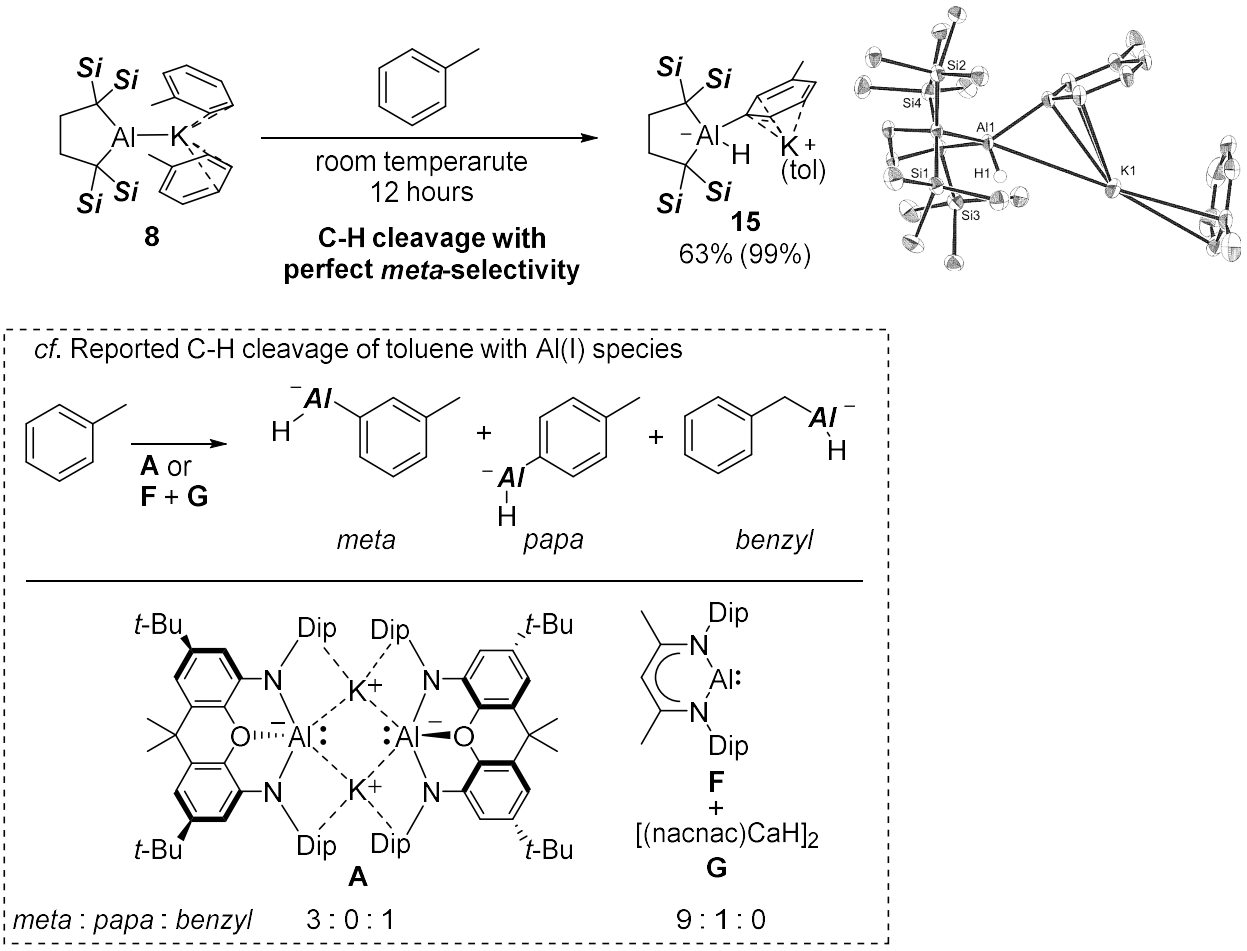

I originally assumed alumanyl anion **8** has high Brønsted basicity, considering the low electronegativity of Al (1.61) and the similar reactivity of diaminobory anion toward benzene (Scheme 1-2-1a) [18] and had proposed the deprotonating mechanism as shown in Scheme 3-2-7. Since the diaminoboryl anion **A** deprotonated benzylic C–H bond of toluene, *meta*-selective C–H cleavage by **8** is completely different.[19]

Scheme 3-2-7. Proposed deprotonating mechanism of **8** toward benzene.

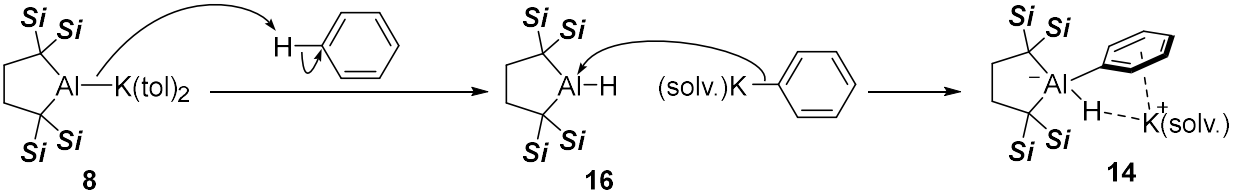

Therefore, the kinetic isotope effect (KIE) was investigated to reveal further details of the reaction mechanism (Scheme 3-2-8). Consumption of **8** or **8**-d_{16} (prepared by recrystallization of **8** from cooled toluene-d_8) in either toluene or toluene-d_8 were monitored at 35 °C by UV-vis spectroscopy. The decay of the absorption at 468 nm obeyed pseudo-first order kinetics with rate constants of $k_H = 5.42 \times 10^{-4}$ s^{-1} and $k_D = 3.58 \times 10^{-4}$ s^{-1}. The obtained KIE (k_H/k_D = 1.51) is smaller than the reported values for the deprotonation of benzene with either ethylpotassium (k_H/k_D = 2.0),[16] *n*BuLi/*t*BuOK (k_H/k_D = 2.7),[17] or boryl anion (k_H/k_D = 2.3).[14] This relatively small value of k_H/k_D in the present study would reflect the "triangular" or "non-linear" transition state, where the change in C–H bending is more important than the change in C–H stretching.

Scheme 3-2-8. Kinetic isotope effect (KIE) of the C-H cleavage of toluene with **8**.

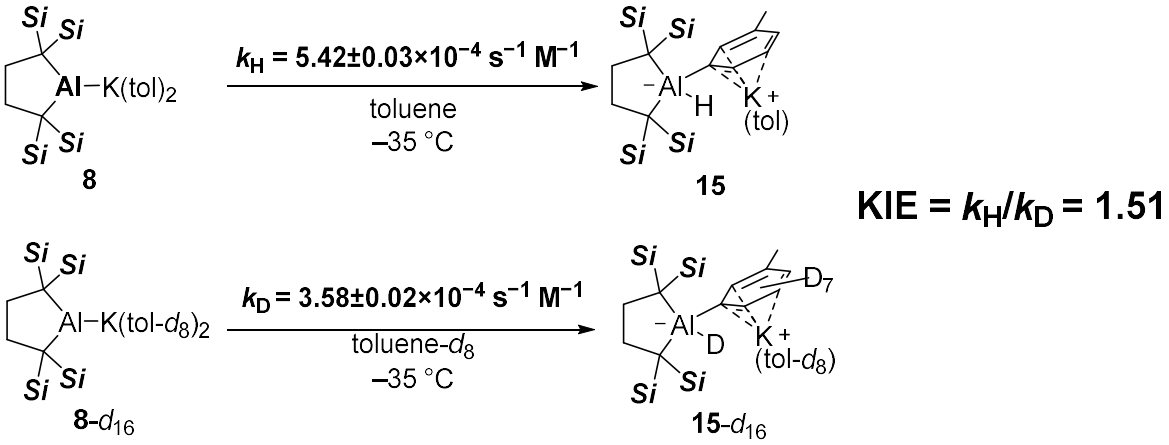

To shed light on the origin of *meta*-selective C–H cleavage of toluene with **8** to furnish **15**, the reaction mechanism and the property of the transition state were examined by using DFT calculations. Energy profiles for C–H cleavage at *meta*-, *para*-, and *benzylic* positions were summarized in Figure 3-2-1. The obtained pathway for *meta*-C–H cleavage is two-step reaction involving the formation of Meisenheimer intermediate ***meta*-INT.** The first transition state, ***meta*-TS1**, for the nucleophilic attack of Al anion has an almost coplanar configuration of the eliminating hydrogen atom and benzene ring (Figure 3-2-1b) with an activation energy of 26.1 kcal/mol. The second transition state, ***meta*-TS2**, for the hydride-migration to the Al center has a lower activation energy (4.2 kcal/mol) where the aluminum atom is almost coplanar with the benzene ring. The sum of two TSs having non-linear arrangement of Al, C, and H atoms would contribute to the experimentally obtained small KIE value. Similar two-step pathway for para-C–H cleavage was found to have a slightly higher activation energy (27.8 kcal/mol). In the case of *benzylic* C–H cleavage, reaction proceeds through a concerted pathway without an intermediate. The difference between two transition states, ***para*-TS1** and ***meta*-TS1**, would arise from the electron-donating character of the methyl group. In fact, HOMO of both transition states has large coefficients at *ortho*- and *para*-positions of the carbon atom being attacked by Al anion (Figure 3-2-1c), therefore, the methyl group on the *para*-position in ***para*-TS1** contributes to destabilize the transition state. Thus, the absence of destabilizing effect by methyl group in ***meta*-TS1** would be the reason why the *meta*-selective C–H cleavage. It should be noted that the second transition states ***para*-TS2** and ***meta*-TS2** having a coplanarity of the aluminum atom with the benzene ring seem to be similar to that

found in the reaction of **F** with toluene with an assistance of a calcium catalyst. The electronical properties of ***meta*-TS2** were examined by using natural bond orbital (NBO) analysis. The second perturbation analysis of ***meta*-TS2** shows significant donor-acceptor interaction between *ipso*-C-H bond and Al atom. This result indicates Lewis acidic Al center enables a generally disadvantageous hydride-eliminating S_NAr reaction.

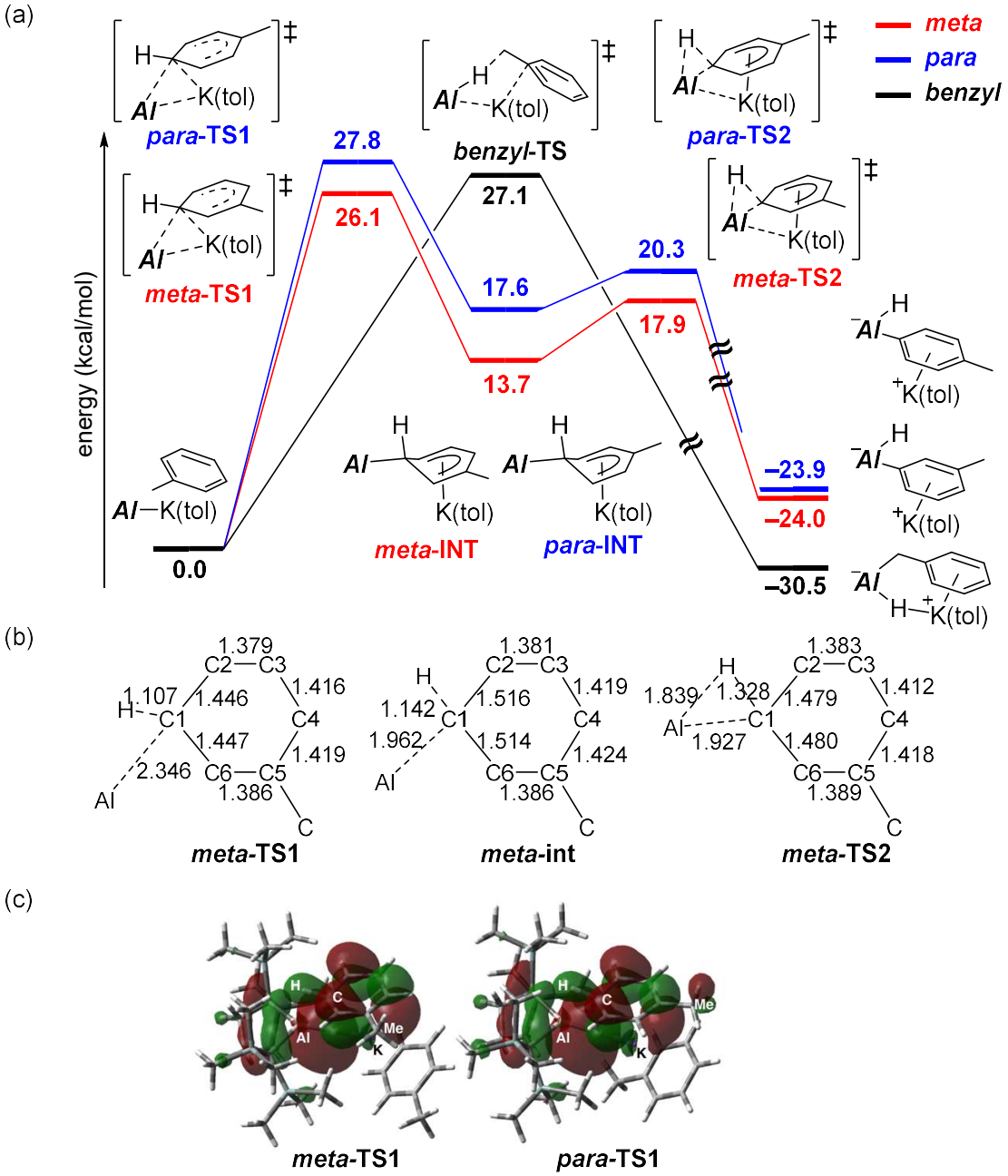

Donor NBO (i)	Acceptor NBO (j)	E(2) [kcal/mol]	E(j)-E(i) [a.u.]	F(i,j) [a.u.]
BD (1)C 69 – H 70	LP*(1)Al 1	16.20	0.55	0.090
BD (1)C 69 – H 70	LP*(2)Al 1	30.63	0.60	0.125
BD (1)C 69 – H 70	LP*(4)Al 1	25.20	0.75	0.123

Figure 3-2-1. a) Energy profiles of the DFT-based mechanism for C-H cleavage of toluene by **8**, including schematic structures of transition states, calculated at the PBE0/def2-SVP/ PCM(SMD, Toluene)//M06-HF/def2-TZVP level of theory. Relative Gibbs free energies are given in kcal/mol. b) Selected bond lengths (Å) of ***meta*-TS1**. c) HOMO of ***meta*-TS1** and ***para*-TS1** (isovalue=0.02). Al, C, and H atoms around the reaction center are labeled.

Subsequently, we examined the reactivity of alumanyl anion **8** toward mono-substituted benzenes (Scheme 3-2-8). The reaction of **8** with fluorobenzene followed by an addition of I_2 gave a crude reaction mixture, which involves 3-fluoroiodo benzene **16** (25%) and iodobenzene **17** (28%) as judged by the ^{1}H NMR spectrum. The former would be generated from a *m*-fluorophenyl-substituted aluminate, which has a similar structure of **14**. The latter would form via S_NAr reaction at the *ipso*-carbon of the fluorine substituent, as found for the reaction of **8** with C_6F_6. Treatment of **8** with anisole gave (methyl)(phenoxy)aluminate **18** in 90% yield through S_N2 reaction at methyl group with phenoxide anion as a leaving group. The structure of **18** was determined by NMR spectroscopy and X-ray crystallographic analysis. The signal of aluminum bounded Me group was observed at high magnetic field, which is similar to **9**. On the other hand, the reaction of **8** with diphenyl ether gave (hydrido)(*m*-phenoxyphenyl)aluminate **19** through C-H bond cleavage at *meta*-position. A similar unsymmetrical type signals in the ^{1}a peak from the Fourier difference map in X-ray structural analysis supported the occurrence of the C-H oxidative addition.

Scheme 3-2-8. Reactivity of **8** toward mono-substituted benzenes.

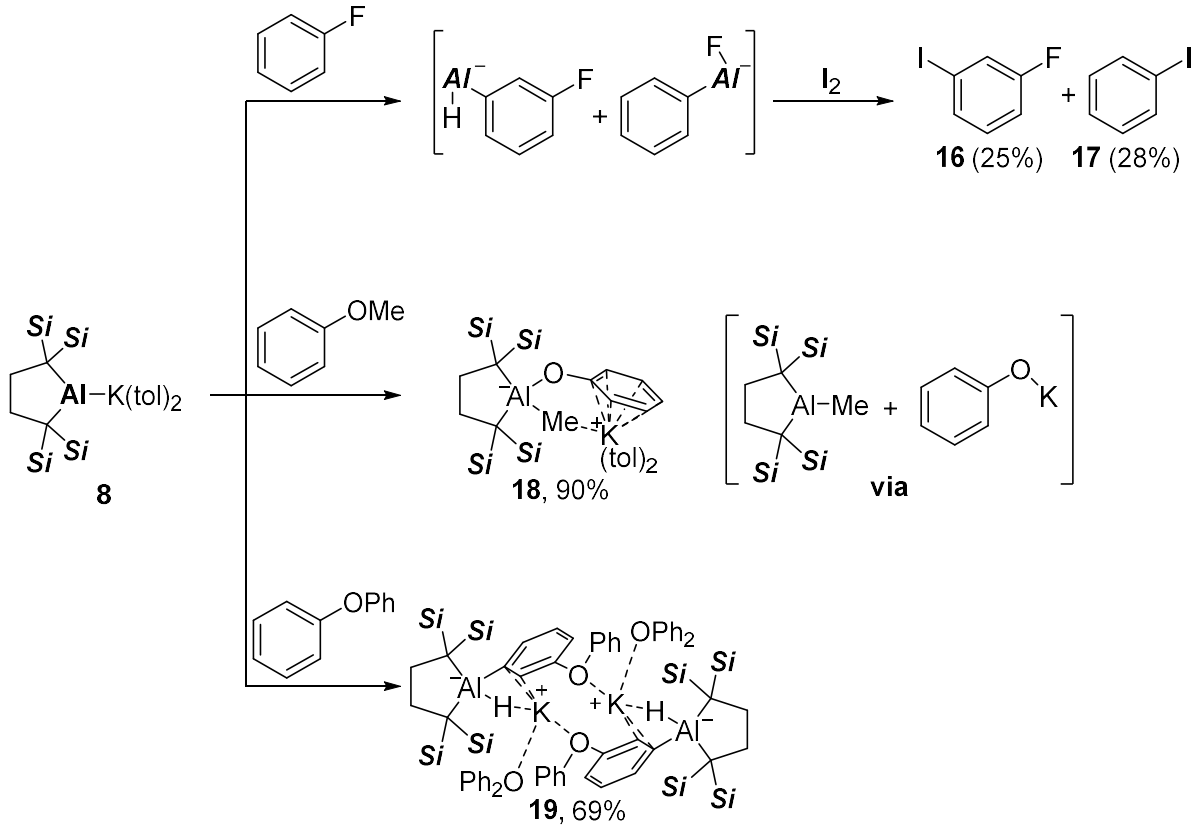

Scheme 3-2-9. A formation dialumane **6** from **8** via 1-electron transfer toward electron-deficient (trifluoromethyl)benzene.

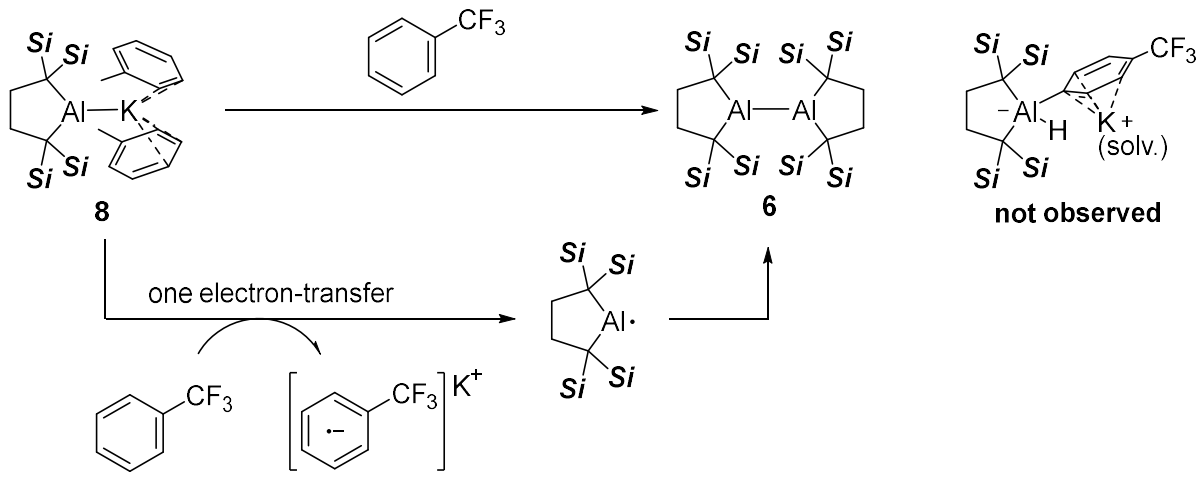

In summary, the nucleophilic substitution and oxidative additions of dialkyl-aluminum anion **8** were described in this chapter. The Al anion **8** underwent S_N2 reaction toward MeOTf to furnish corresponding methylalumane **9**. Whereases, oxidative additions were performed in the reaction of **8** with aryl fluoride and aromatic hydrocarbons afforded C-F or C-H cleaved compounds. Especially, **8** exhibited highly reactivity toward benzene to react at milder condition than that of amino-substituted aluminum anions. Furthermore, a detailed mechanism of the perfectly *meta*-selective C-H oxidative addition toward toluene, reflecting the electronic structure with a lone-pair and vacant 3p-orbital, was revealed by small KIE (=1.51) and DFT calculations.

3-3. Supplementally Information

Methods

Experimental Section

General

All manipulations involving the air- and moisture-sensitive compounds were carried out under an argon atmosphere using standard Schlenk and glovebox (Korea KIYON) technique. All glassware were dried for 20 min in the 250 °C oven before use. Toluene, hexane, Et_2O, and THF were purified by passing through a solvent purification system (Grass Contour). C_6D_6 and THF-d_8 were dried by distillation over sodium-benzophenone followed by vacuum transfer. Benzene and pentane were purchased from Kanto chemical (dehydrated) and used in the glovebox without further purification. The nuclear magnetic resonance (NMR) spectra were recorded on JEOL ECS-400 (400 MHz for ^{1}H, 101 MHz for ^{13}C) or ECZ-600 (600 MHz for ^{1}H, 151 MHz for ^{13}C). Chemical shifts are reported in ppm relative to the residual protiated solvent for ^{1}H, deuterated solvent for ^{13}C used as references. The absolute values of the coupling constants are given in Hertz (Hz). Multiplicities are abbreviated as singlet (s), doublet (d), triplet (t), quartet (q), multiplet (m), and broad (br). Melting points were determined on an Optimelt (SRS) meltingpoint apparus and were uncorrected. Elemental analyses were performed on a Perkin Elmer 2400 series II CHN analyzer.

Reaction of 8 with MeOTf and estimation of NMR yield for the formation of 9

In a glovebox, a pre-cooled (–35 °C) toluene solution (1.0 mL) of MeOTf (2.8 mg, 0.17 mmol) was added to a pre-cooled (–35 °C) toluene solution (1.0 mL) of **8** (10.0 mg 0.167 mmol) in a 3 mL vial. Just after stirring the reaction mixture in minutes at –35 °C, generated LiOTf was removed by a filtration through a pad of Celite. The resulting filtrate was evaporated under reduce pressure. The residue was dissolved in C_6D_6 and pipetted to a screw-capped NMR tube. After bringing the NMR tube out from the glovebox, a ^{1}H NMR spectrum was recorded to estimate the NMR yield of methylalumane **9** (84%, Figure 3-3-1): ^{1}H NMR (400 MHz, C_6D_6.) δ –0.09 (s, CH_3, Al-Me), 0.17 (s, 36H, CH_3 of $SiMe_3$), 1.93 (s, 4H, CH_2).

Independent synthesis of 9 from 8 and isolation as a DMAP adduct 9·DMAP

In a glovebox, a hexane suspension (4.0 mL) of MeLi(thf) (4.0 mg, 42.1 μmol) was added to a pre-cooled (–35 °C) hexane suspension (4.0 mL) of **8** (20.0 mg, 40.1 μmol) in a 15 mL vial. After stirring the reaction mixture for 5 hours at room temperature, generated LiI was removed by a filtration through a pad of Celite and the resulting filtrate was evaporated under reduce pressure. After addition of C_6D_6 to the residue, the solution was taken into an NMR tube to measure the ^{1}HNMR spectrum of the crude product. The resulting ^{1}H NMR spectrum suggested the existence of methylalumane **9** (Figure 3-3-2, compared with Supplementary Figure 3-3-1; ^{1}H NMR of **9** (400 MHz, C_6D_6) δ –0.09 (s, CH_3, Al-Me), 0.17 (s, 36H, CH_3 of $SiMe_3$), 1.93 (s, 4H, CH_2)]. The residue recovered from the NMR sample was vacuumed for removal of C_6D_6, and a toluene solution (4.0 mL) of DMAP (4.9 mg, 40.1 μmol) was added. After stirring the reaction mixture for 1 hour at room temperature, it was evaporated under reduce pressure. The residue was recrystallized from THF to afford colorless crystals of **9**·DMAP (18.9 mg, 16.9 μmol, 42%). ^{1}H NMR (Figure 3-3-3, 400 MHz, C_6D_6) δ –0.13 (s, 3H, CH_3 of Al-Me), 0.34 (s, 18H, CH= of $SiMe_3$), 0.52 (s, 18H, CH_3 of $SiMe_3$),

1.85 (s, 6H, CH_3 of DMAP), 2.26-2.41 (m, 4H, CH_2), 5.73 (d, J = 7 Hz, 2H, 2,6-ArH of DMAP), 8.26 (d, J = 7 Hz, 2H, 3,5-ArH of DMAP); ^{13}C NMR (Figure 3-3-4, 126 MHz, C_6D_6) d 2.18 (Al-Me), 4.39 ($SiMe_3$), 5.17 ($SiMe_3$), 5.34 (4°), 34.0 (CH_2), 38.1 (CH_3 of DMAP), 106.3 (2,6-ArH of DMAP), 147.0 (3,5-ArH of DMAP), 155.1 (4°); mp 184.0-190.3 °C (decomp.); Anal. Calcd for $C_{24}H_{53}AlN_2Si_4$: C, 56.63; H, 10.50; N, 5.50; Found: C, 56.56; H, 10.67; N, 5.42.

Reaction of 8 with $PhCH_2Cl$ to form 10 and 11

In a glovebox, pre-cooled (–35 °C) toluene solution (1.7 mL) of **8** (20.0 mg, 33.5 μmol) was added to pre-cooled (–35 °C) toluene solution (1.7 mL) of benzylchloride (4.2 mg 33.5 μmol) in 15 mL vial. After stirring the reaction mixture for several minutes at -35 °C, the reaction mixture was evaporated under reduce pressure. After addition of C_6D_6 to the residue, an aliquot was taken into an NMR tube to measure the ^1H NMR spectrum of the crude product. The resulting ^1H NMR spectrum suggested the existence of dibenzylaluminate **10** and chloroalumane **11** (Figure 3-3-5.). The remaining residue after extraction with hexane was recrystallized from toluene to afford colorless crystals of dibenzylaluminate **10** (5.7 mg, 5.8 μmol, 23%). Isolated **10**: ^1H NMR (Figure 3-3-6, 400 MHz, C_6D_6) δ 0.51 (s, 36H, CH_3 of $SiMe_3$), 2.05 (s, 4H, CH_2Ph), 2.45 (s, 4H, CH_2), 6.20 (t, J = 7 Hz, 2H, 4-CH of Bn), 6.59 (t, J = 7 Hz, 4H, 3,5-CH of Bn), 7.08 (d, J = 7 Hz, 4H, 2,6-CH of Bn); ^1H NMR (Figure 3-3-7, 400 MHz, THF-d_8) δ –0.02 (s, 36H, CH_3 of $SiMe_3$), 1.93 (s, 4H, CH_2), 1.97 (s, 4H, CH_2), 6.56 (t, J = 7 Hz, 2H, 4-CH of Bn), 6.82 (t, J = 7 Hz, 4H, 3,5-CH of Bn), 6.95 (d, J = 7 Hz, 4H, 2,6-CH of Bn); ^{13}C NMR (Figure 3-3-8, 126 MHz, THF-d_8) δ 5.39 ($SiMe_3$), 7.74 (br, 4°), 28.52 (br, CH), 35.23 (CH_2), 119.57 (ArH), 127.14 (ArH), 129.13 (ArH), 152.68 (4°); mp 151.2-158.1 °C (decomp.); Anal. Calcd for $C_{30}H_{54}AlKSi_4 \cdot 1.70$(toluene) [calculated from ^1H NMR spectrum of vacuumed solid for a long time]: C, 67.10; H, 9.09; Found: C, 66.94; H, 9.24.

Reaction of 8 with 0.5 equivalent of C_6F_6 to isolate 12

In a glovebox, a pre-cooled (–35 °C) toluene solution (1.7 mL) of **8** (10.0 mg, 16.7 μmol) was added to pre-cooled (–35 °C) toluene solution (850 μL) of C_6F_6 (1.6 mg 8.3 μmol) in 3 mL vial. After stirring the reaction mixture for several minutes at –35 °C, the reaction mixture was evaporated under reduce pressure. The residue was recrystallized from toluene to afford colorless crystals of **12** (8.0 mg, 5.8 μmol, 70%). ^1H NMR (Figure 3-3-9, 400 MHz, C_6D_6) 0.37(s, 18H, CH_3 of $SiMe_3$), 0.50 (s, 18H, CH_3 of $SiMe_3$), 2.11 (s, 5.42H, CH_3 of 1.81·toluene), 2.29-2.46 (m, 4H, CH_2), 6.99 (m, 5.42H, ArH of 1.81·toluene), 7.11-7.14 (m, 3.84H, ArH of 1.92·toluene); ^{19}F NMR (Figure 3-3-10, 376 MHz, C_6D_6) δ –142.79 (brs, fwhm = 64 Hz, Al-F), –119.60 (s, fwhm = 19 Hz, Ar-F); ^{13}C NMR (Figure 3-3-11, 126 MHz, THF-d_8) δ 4.19 ($SiMe_3$), 4.45 ($SiMe_3$), 5.44 (br, 4°), 34.15 (CH_2), 126.42 (d, $^1J_{FC}$ = 208 Hz, ArF), 145.65 (d, $^2J_{FC}$ = 41 Hz, ArAl); mp 200.1-206.7 °C (decomp.); Anal. Calcd for $C_{38}H_{80}Al_2F_6K_2Si_8 \cdot 1.81$(toluene) [calculated from ^1H NMR spectrum of vacuumed solid for a long time]: C, 51.78; H 8.11; Found C, 51.43; H, 7.87.

Reaction of 8 with 1 equivalent of C_6F_6

In a glovebox, a pre-cooled (–35 °C) toluene solution (1.7 mL) of **8** (10.0 mg, 16.7 μmol) was added to pre-cooled (–35 °C) toluene solution (850 μL) of C6F6 (3.1 mg 16.7 μmol) in 3 mL vial. After stirring the reaction mixture for several minutes at –35 °C, the reaction mixture was evaporated under reduce pressure. The resulting ^1H NMR spectrum and ^{19}F NMR suggested the existence of **12** and **13** in the ratio of 4 to 3 (Figure 3-3-12, 13).

Reaction of 8 with 10 equivalents of C_6F_6

In a glovebox, a pre-cooled (–35 °C) toluene solution (1.3 mL) of 5 (7.7 mg, 12.9 μmol) was added to pre-cooled (–35 °C) toluene solution (650 μL) of C_6F_6 (24.5 mg 13.2 μmol) in 3 mL vial. After stirring the reaction mixture for several minutes at –35 °C, the reaction mixture was evaporated under reduce pressure. The resulting ^{1}H NMR spectrum and ^{19}F NMR suggested the existence of **12** and **13** ratio of 3 to 1 (Figure 3-3-14,15).

Synthesis of 15

In a glovebox, red crystals of **8** (10.0 mg, 16.8 μmol) was dissolved in 1.7 mL of toluene. After leaving the resulting solution at room temperature for 12 h, the reaction mixture was evaporated under reduced pressure. Then a C_6D_6 solution of adamantane (0.0281 M, 600 μL, 2.30 mg, 16.9 μmol) was added to the residue. An aliquot of the resulting solution was pipetted to a screw-capped NMR tube. After bringing the NMR tube out from the glovebox, a ^{1}H NMR spectrum was recorded to estimate the NMR yield of (hydride)(*m*-tolyl)aluminate **15** (>99%, Figure 3-3-16). Afterwards, the solution was recovery from the NMR tube and was evaporated under reduce pressure. The reinsure was recrystallized from toluene to afford colorless crystals of **15** (6.3 mg, 10.6 μmol, 63%). ^{1}H NMR (Figure 3-3-17, crude reaction mixture, 400 MHz, C_6D_6) δ 0.46 (s, 18H, CH_3 of $SiMe_3$), 0.49 (s, 18H, CH_3 of $SiMe_3$), 2.21 (s, 3H, CH_3 of *m*-tolyl), 2.40 (s, 4H, CH_2, fwhm = 7 Hz, probably two magnetically inequivalent 2H signals were coalesced due to rapid exchange), 6.79 (d, *J* = 7 Hz, 1H, *m*-tolyl), 6.95 (t, *J* = 7 Hz, 1H, *m*-tolyl), 7.56 (d, *J* = 7 Hz, 1H, *m*-tolyl), 7.86 (s, 1H, *m*-tolyl); ^{1}H NMR (Figure 3-3-18, 400 MHz, THF-d_8) δ −0.04 (s, 18H, CH_3 of $SiMe_3$), 0.07 (s, 18H, CH_3 of $SiMe_3$), 1.83-2.01 (m, 4H, CH_2), 2.18 (s, 4H, CH_3 of *m*-tolyl), 6.71 (d, *J* = 7 Hz, 1H, *m*-tolyl), 6.87 (t, *J* = 7 Hz, 1H, *m*-tolyl), 7.17 (d, *J* = 7 Hz, 1H, *m*-tolyl), 7.67 (s, 1H, *m*-tolyl); ^{13}C NMR (Figure 3-3-19, 151 MHz, THF-d_8) δ 4.17 ($SiMe_3$), 4.66 (br, 4°), 4.78 ($SiMe_3$), 34.76 (CH_2), 125.27 (CH, *m*-tolyl), 125.73 (CH, *m*-tolyl), 133.30 (4°, *m*-tolyl), 133.72 (4°, *m*-tolyl), 136.39 (CH, *m*-tolyl), 140.48 (CH, *m*-tolyl); mp 207.5-210.7 °C (decomp.); Anal. Calcd for $C_{30}H_{56}AlKSi_4$: C, 60.54; H, 9.48; Found: C, 60.39; H, 9.71.

Reaction of 8 with fluorobenzene and estimation of NMR yield for the formation of 16 and 17

In a glovebox, red crystal of **1** (10.0 mg, 16.8 μmol) was dissolved in 200 μL of fluorobenzene. After leaving the solution at room temperature for 5 h, the reaction mixture was evaporated under reduced pressure. Then a C_6D_6 solution of adamantane (0.0281 M, 600 μL, 2.30 mg, 16.9 μmol) was added to the residue. An aliquot of the resulting solution was pipetted to a screw-capped NMR tube. After bringing the NMR tube out from the glovebox, a small piece of I_2 was added to the mixture. Then a ^{1}H NMR spectrum was recorded to estimate the NMR yield of 3-fluoroiodobenezene **3** (25%) and iodobenzene **4** (28%, Figure 3-3-20).

Synthesis of 18

In a glovebox, red crystals of **1** (10.0 mg, 16.8 μmol) was dissolved in 200 μL of anisole. After leaving the solution at room temperature for 5 h, the reaction mixture was evaporated under reduced pressure. The residue was recrystallized from toluene to afford colorless crystals of **5** (10.6 mg, 15.1 μmol, 90%). ^{1}H NMR (Figure 3-3-21, 400 MHz, C_6D_6) δ −0.68 (s, 3H, CH_3), 0.026 (s, 18H, CH_3 of $SiMe_3$), 0.033 (s, 18H, CH_3 of $SiMe_3$), 1.87-1.98 (m, 2H, CH_2), 1.98-2.07 (m, 2H, CH_2), 6.31 (t, *J* = 7 Hz, 1H, Ph), 6.65 (d, *J* = 7 Hz, 2H, Ph), 6.86 (t, *J* = 7 Hz, 2H, Ph); ^{13}C

NMR (Figure 3-3-22, 151 MHz, THF-d_8) δ 4.89 ($SiMe_3$), 4.95 ($SiMe_3$), 5.50 (CH_3), 6.53 (br, 4°), 34.33 (CH_2), 114.38 (CH, Ph), 120.87 (CH, Ph), 128.47 (CH, Ph), 163.60 (4°); mp 166.7-171.2 °C (decomp.); Anal. Calcd for $C_{37}H_{64}AlKOSi_4$: C, 63.19; H, 9.17; Found: C, 63.02; H, 9.51.

Synthesis of 19

In a glovebox, red crystals of **1** (10.0 mg, 16.8 μmol) was dissolved in 200 μL of diphenyl ether. After leaving the solution at room temperature for 5 h, 200 μL of hexane was added to the reaction mixture and colorless crystals of **6** (8.7 mg, 5.8 μmol, 69%) appeared in 2 h. ^{1}H NMR (Figure 3-3-23, 400 MHz, C_6D_6) δ 0.40 (s, 18H, CH_3 of $SiMe_3$), 0.41 (s, 18H, CH_3 of $SiMe_3$), 2.36 (s, 4H, CH_2, fwhm = 5 Hz, probably two magnetically inequivalent 2H signals were coalesced due to rapid exchange), 6.82-6.90 (m, 4H, ArH), 6.94-7.14 (m, 13H, ArH), 7.55 (d, J = 7 Hz, 1H, ArH), 7.68 (d, J = 3 Hz, 1H, ArH); ^{13}C NMR (Figure 3-3-24, 51 MHz, C_6D_6) δ 4.00 (br, 4°), 4.53 ($SiMe_3$), 4.82 ($SiMe_3$), 34.53 (CH_2), 117.49 (CH), 118.81 (CH), 119.26 (CH), 123.34 (CH), 128.48 (CH), 129.03 (CH), 130.28 (CH), 156.98 (4°), 157.88 (4°), 158.46 (4°), 185.22 (4°); mp 174.6-178.3 °C (decomp.); Anal. Calcd for $C_{80}H_{120}Al_2K_2O_4Si_8$: C, 63.94; H, 8.05; Found: C, 63.72; H, 7.81.

Reaction of 8 with trifluoromethylbenzene and estimation of NMR yield for the formation of tetraalkyldialumane

In a glovebox, red crystals of **1** (10.0 mg, 16.8 μmol) was dissolved in trifluoromethylbenzene (200 μL). After leaving the solution at room temperature for several minutes, the reaction mixture was evaporated under reduced pressure. Then a C_6D_6 solution of adamantane (0.0281 M, 600 μL, 2.30 mg, 16.9 μmol) was added to the residue. An aliquot of the resulting solution was pipetted to a screw-capped NMR tube. After bringing the NMR tube out from the glovebox, a ^{1}H NMR spectrum was recorded to estimate the NMR yield of tetraalkyldialumane (65%, Figure 3-3-25), although the product derived from trifluoromethylbenzene was not identified.

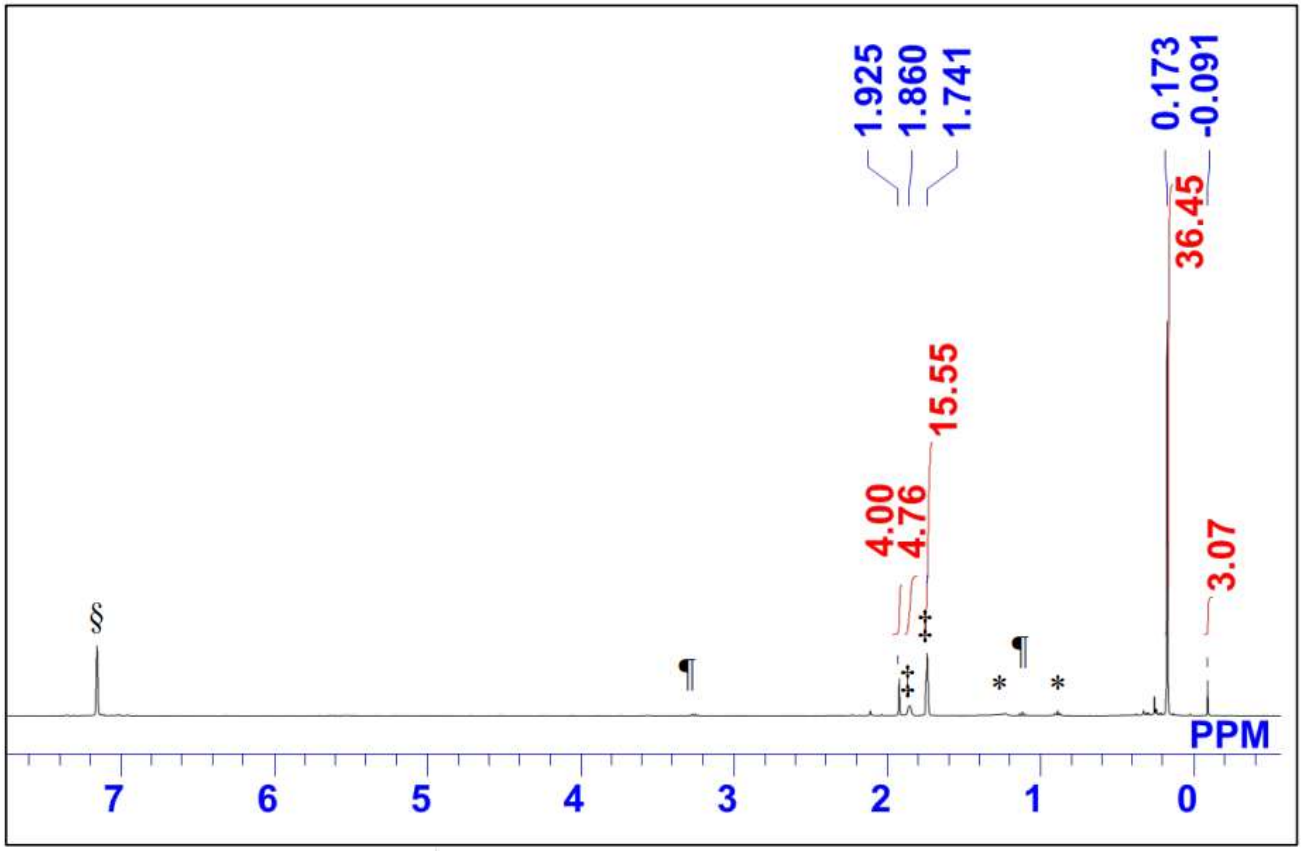

Figure 3-3-1. The ^{1}H NMR spectrum of the crude mixture in the reaction of **8** with MeOTf (*: n-hexane, ¶: Et_2O, §: C_6H_5 ‡: adamantane). The major component of the solution would be **9**.

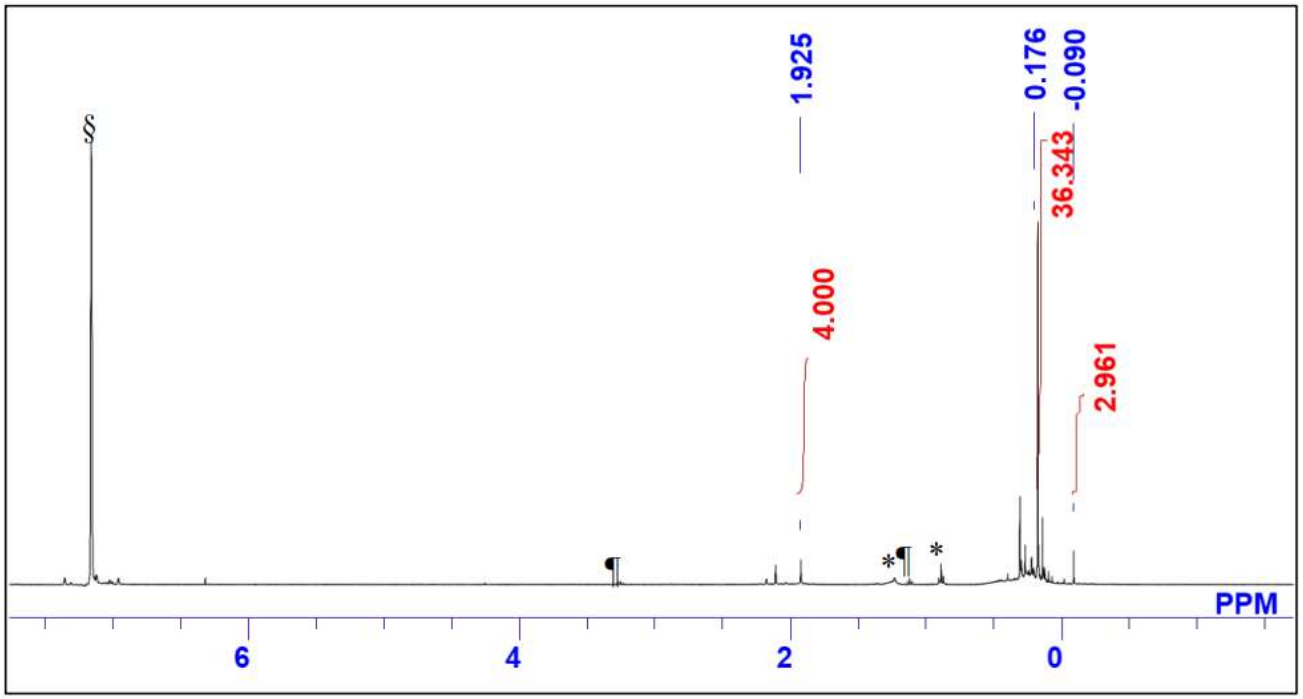

Figure 3-3-2. The ^{1}H NMR spectrum of the crude mixture in the reaction of **11** with MeLi(thf) (*: n-hexane, ¶: Et_2O, §: C_6D_5H). The major component of the solution would be **9**.

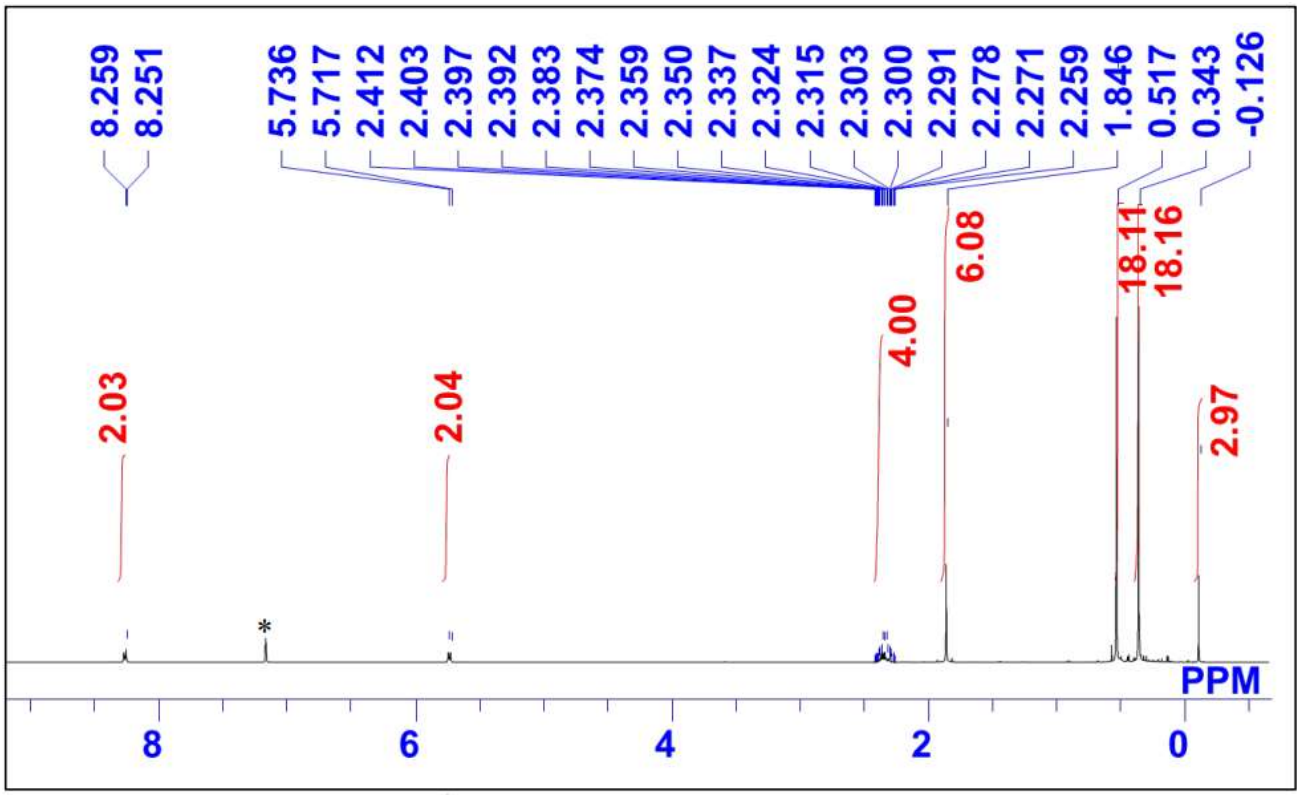

Figure 3-3-3. The ^{1}H NMR spectrum of **9**-DMAP (*: C_6D_5H).

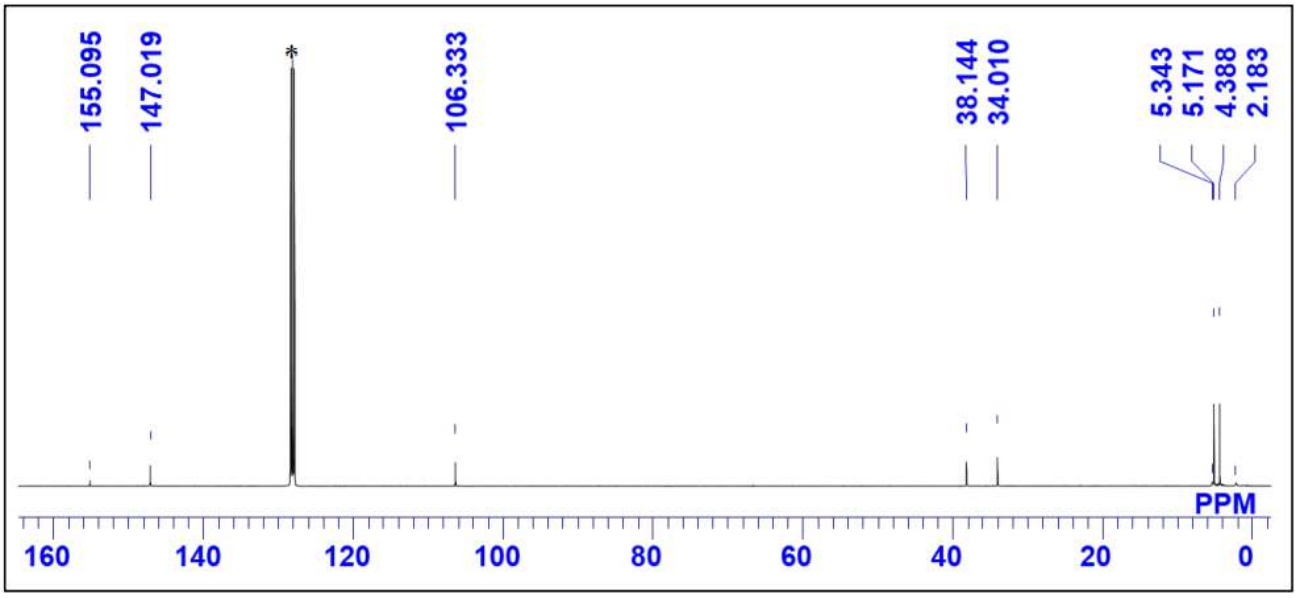

Figure 3-3-4. The ^{13}C NMR spectrum of **9**-DMAP (*: C_6D_6).

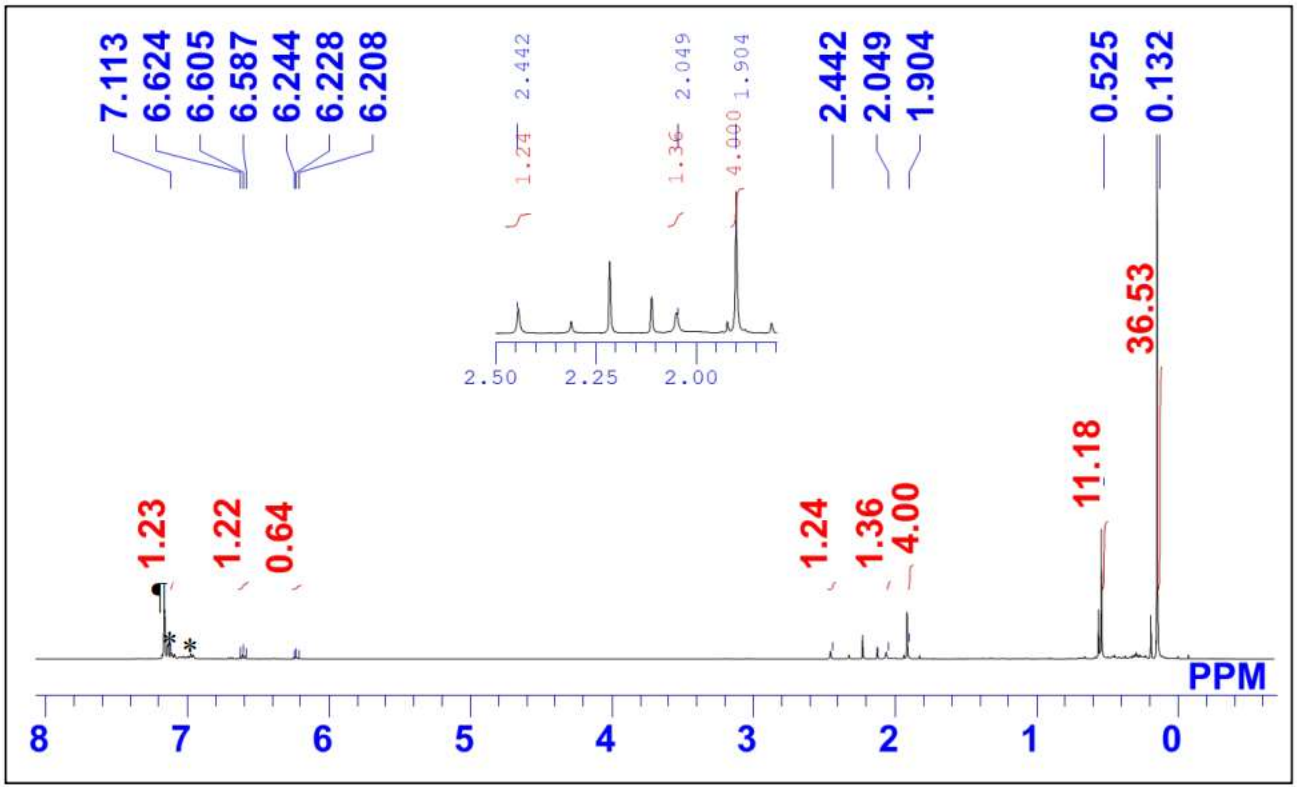

Figure 3-3-5. The ^{1}H NMR spectrum of the crude mixture in the reaction of **8** with BnCl (*: toluene, ¶: C_6H_5).

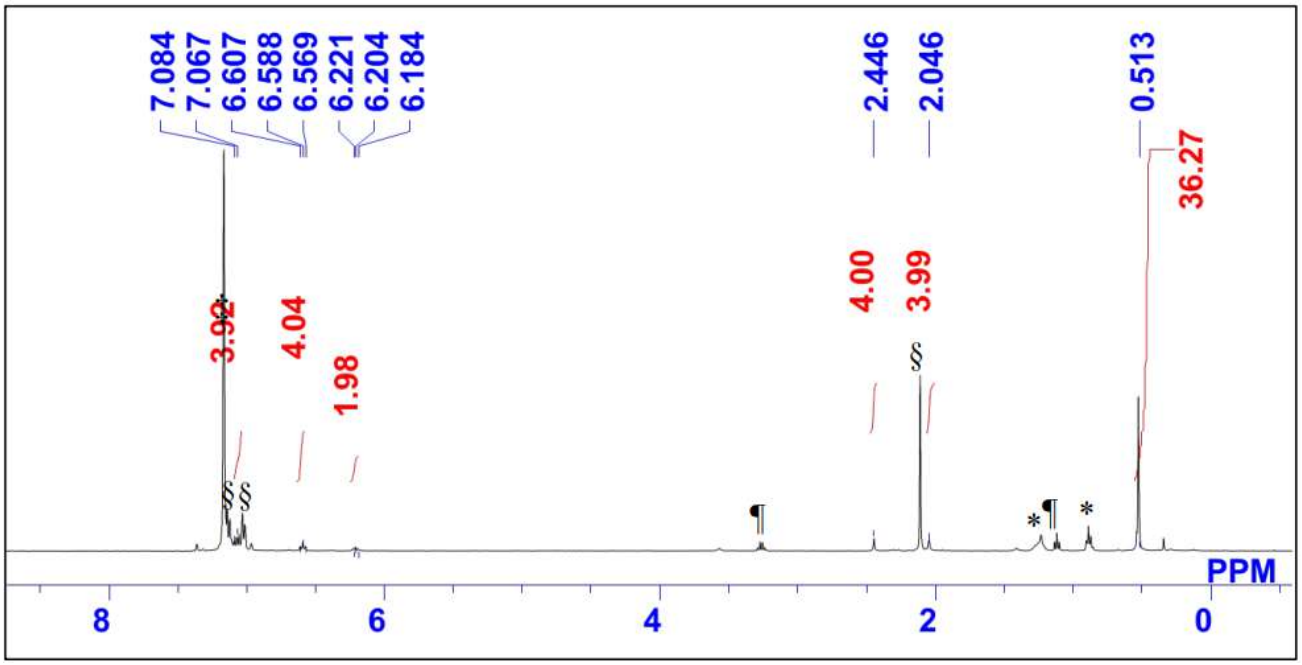

Figure 3-3-6. The ^{1}H NMR spectrum of **10** (*: n-hexane, ¶: Et_2O, §: toluene ‡:C_6D_5H).

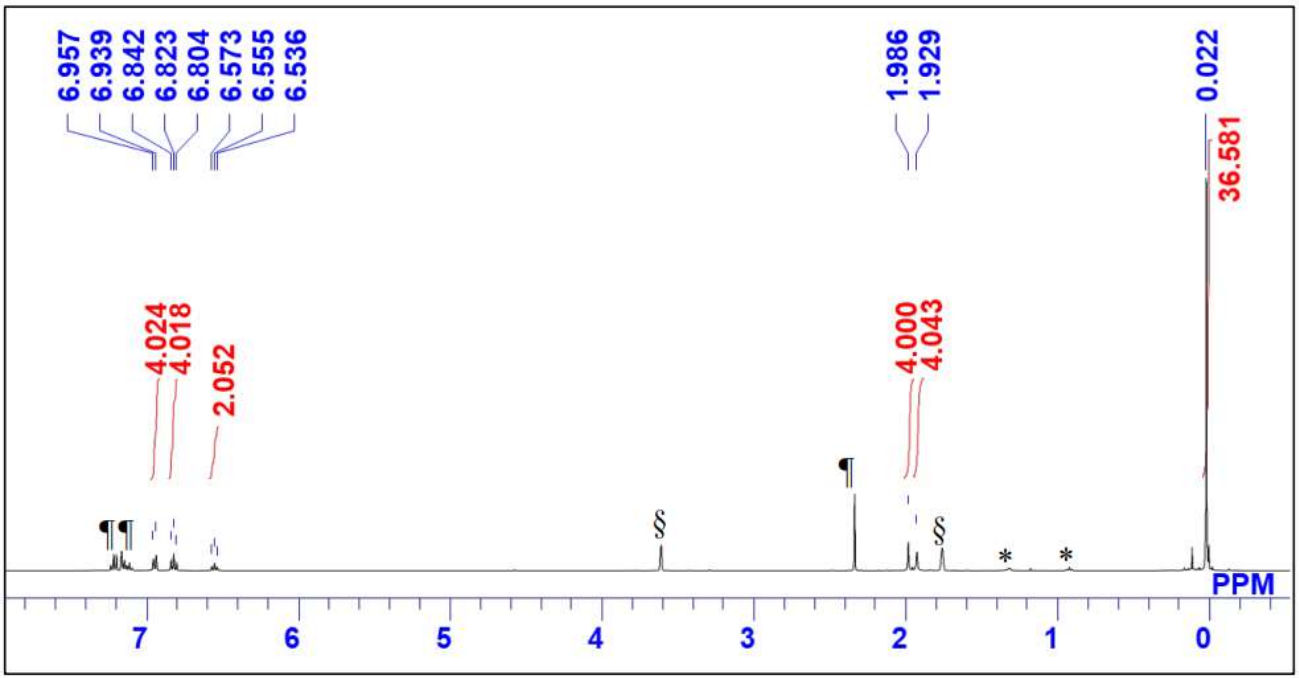

Figure 3-3-7. The ^{1}H NMR spectrum of **10** (*: n-hexane, ¶: toluene, §: THF-d_7).

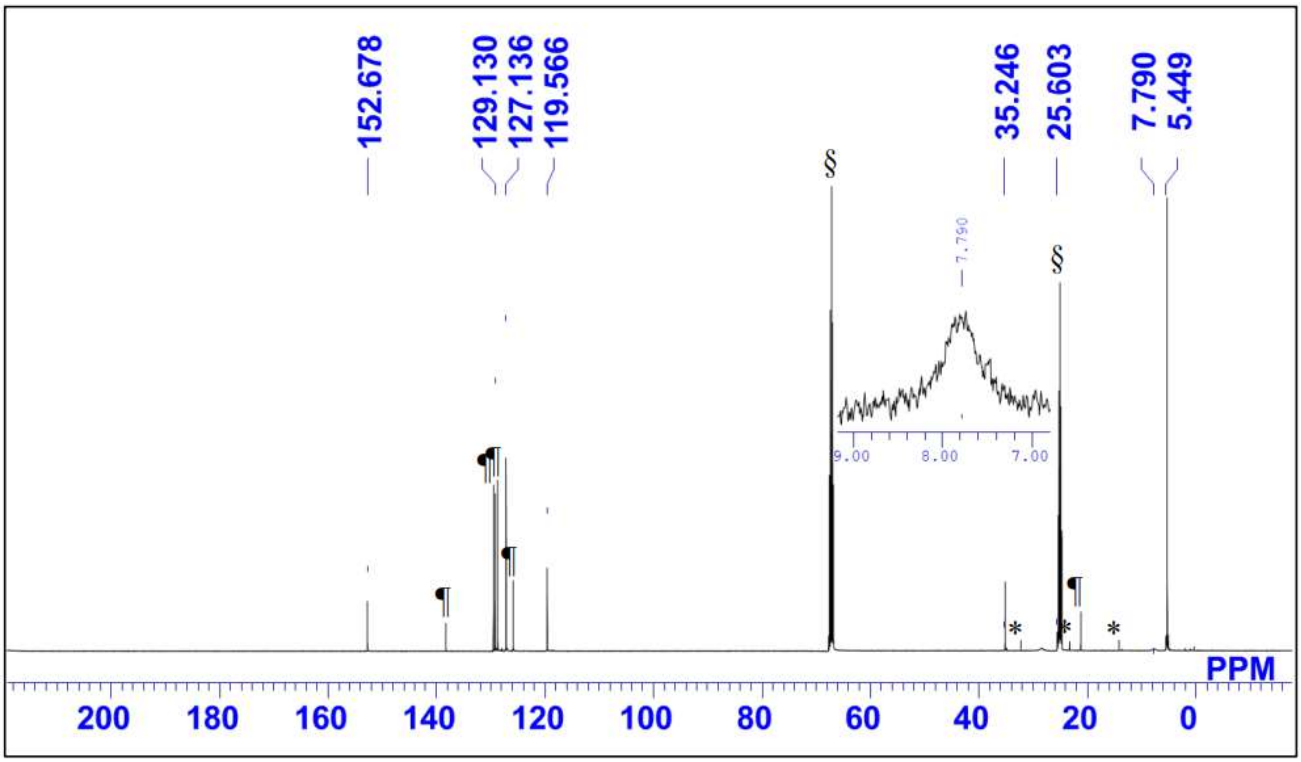

Figure 3-3-8. The ^{13}C NMR spectrum of **10** (*: n-hexane, ¶: toluene, §: THF-d_8).

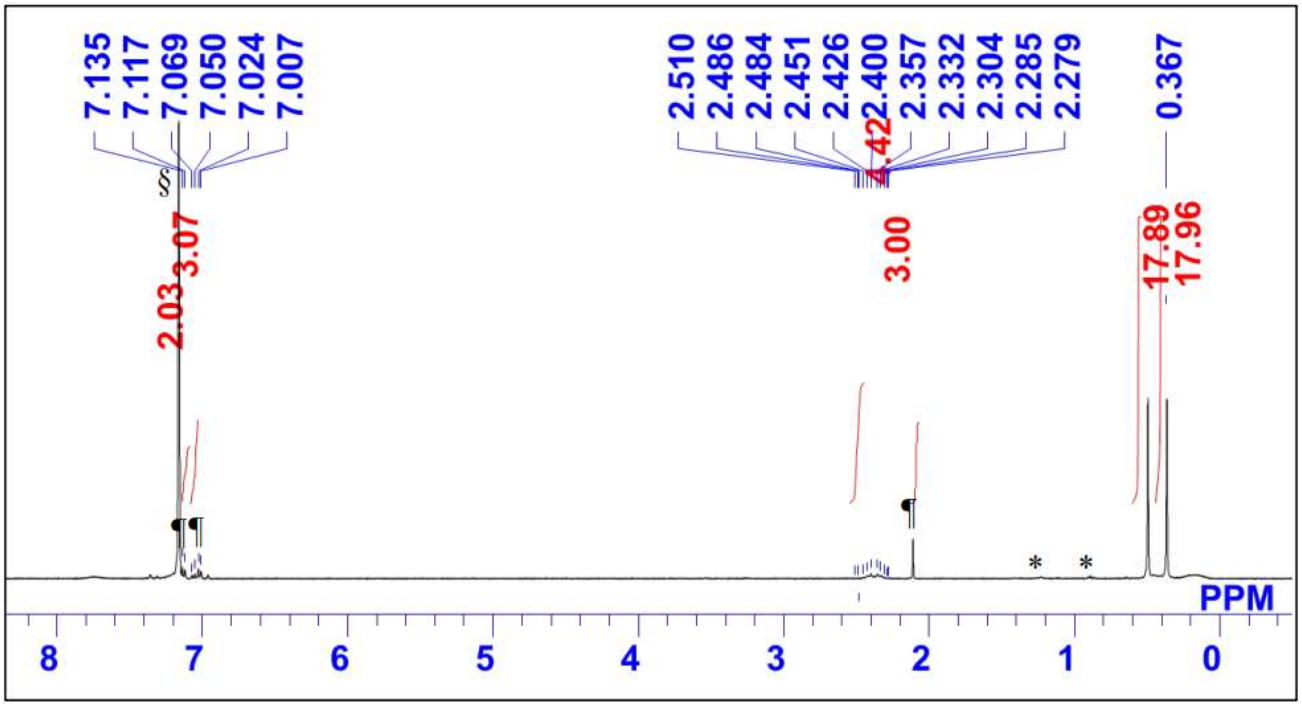

Figure 3-3-9. The ^{1}H NMR spectrum of **12** (*: n-hexane, ¶: toluene, §: C_6H_5).

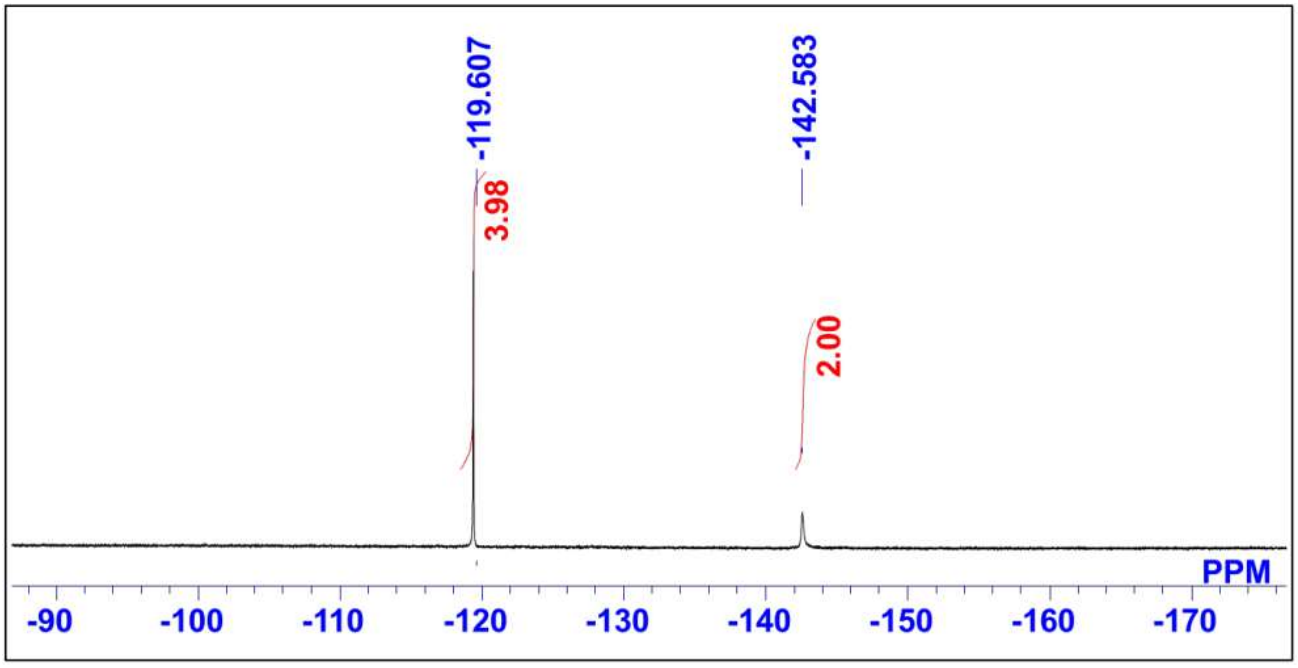

Figure 3-3-10. The ^{19}F NMR spectrum of **12**

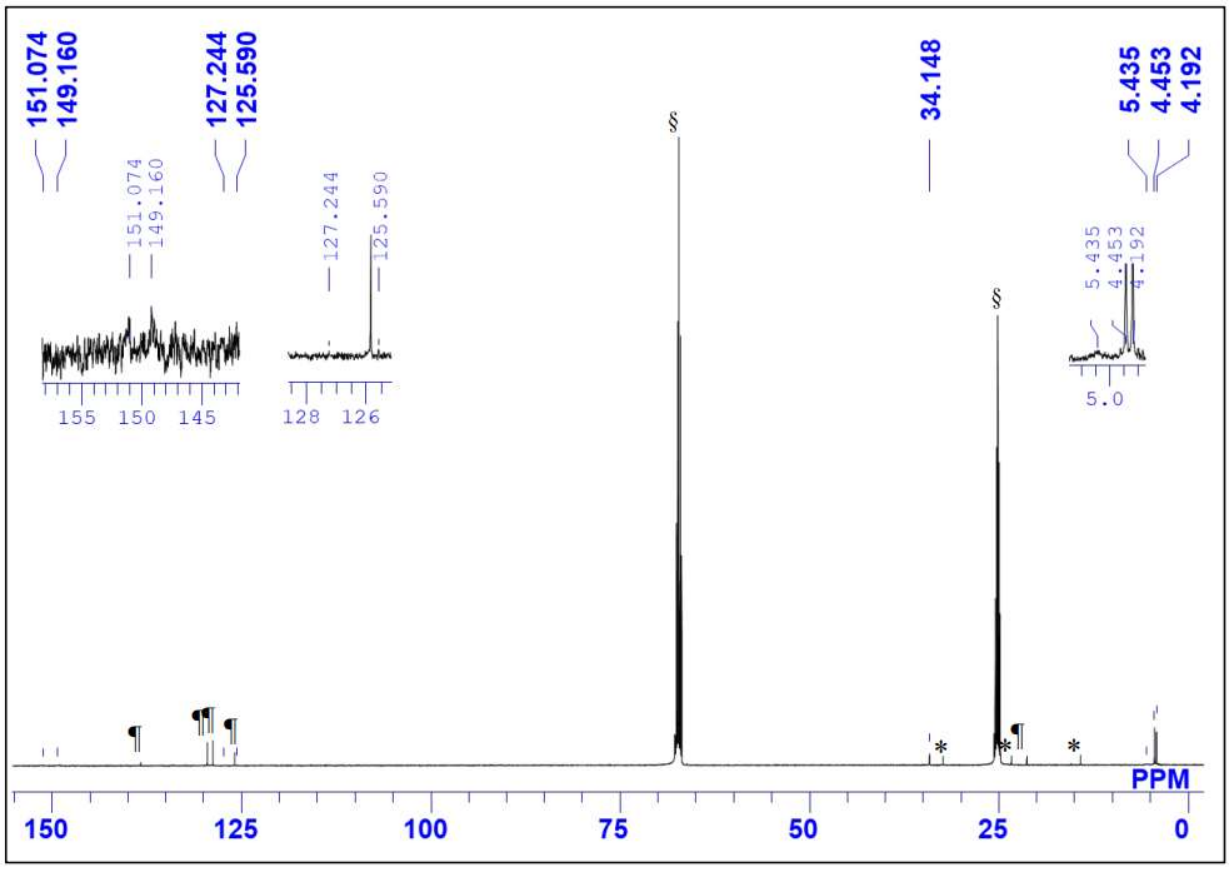

Figure 3-3-11. The ^{13}C NMR spectrum of **12** (*: n-hexane, ¶: toluene, §: THF-d_8).

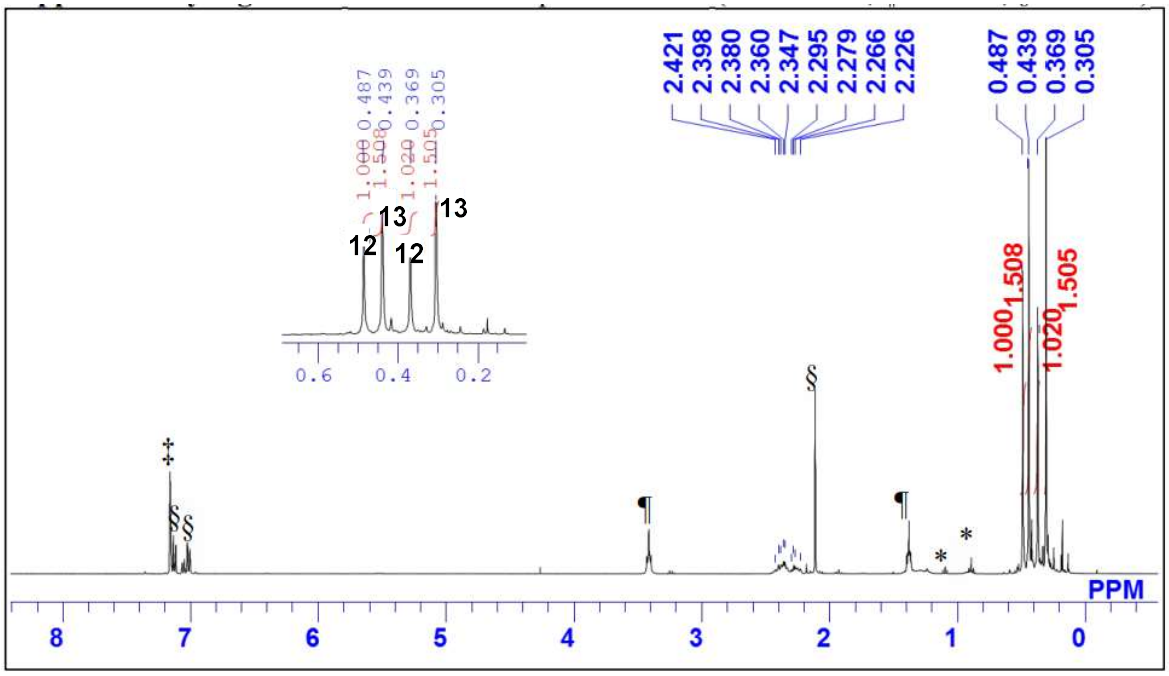

Figure 3-3-12. The ^{1}H NMR spectrum of the crude mixture in the reaction of **8** with 01 equivalent of C_6F_6 (*: hexane, ¶: THF, §: toluene, ‡: C_6D_5H).

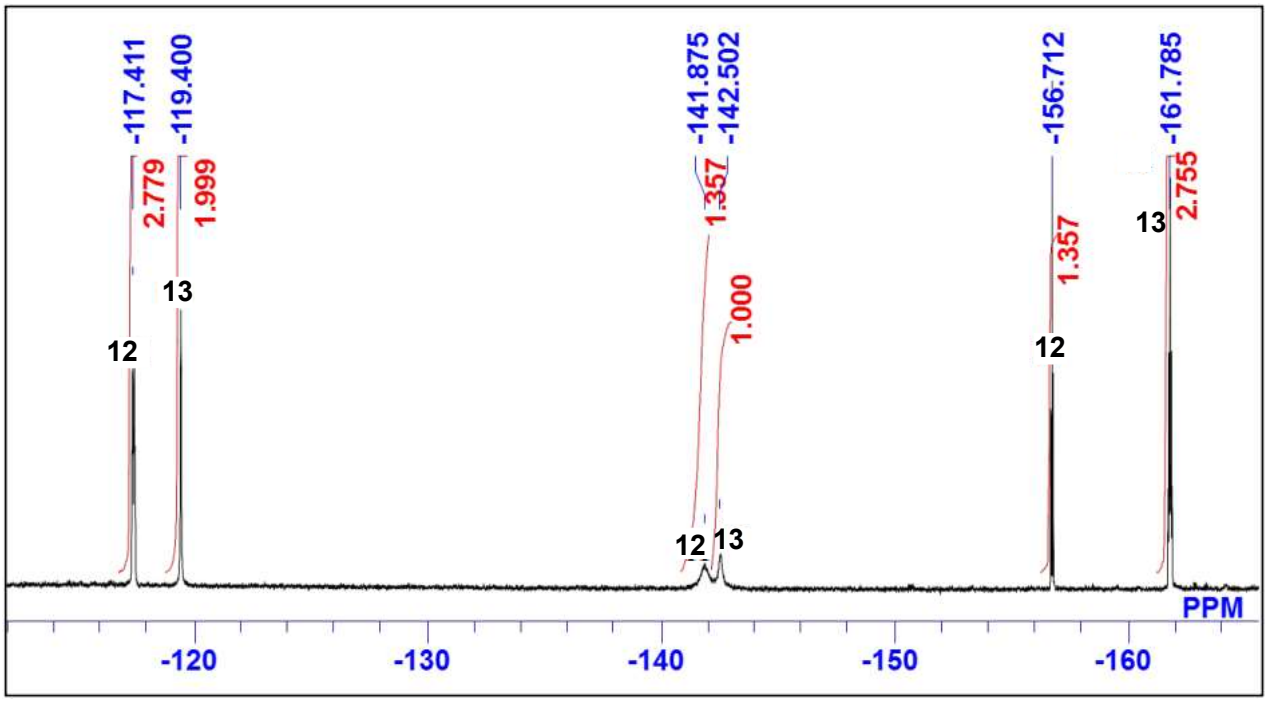

Figure 3-3-13. The ^{19}F NMR spectrum of the crude mixture in the reaction of **8** with 1 equivalent of C_6F_5

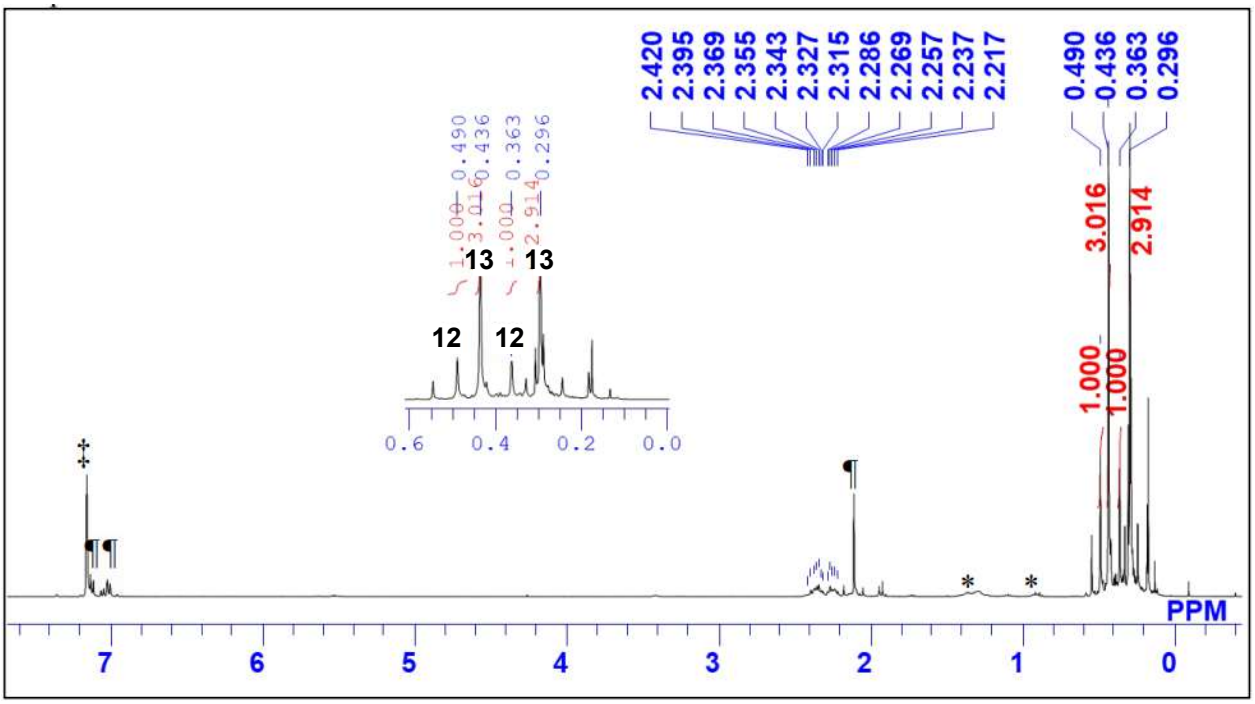

Figure 3-3-14. The ^{1}H NMR spectrum of the crude mixture in the reaction of **8** with 10 equivalents of C_6F_6 (*: hexane, ¶: toluene, §: C_6D_5H).

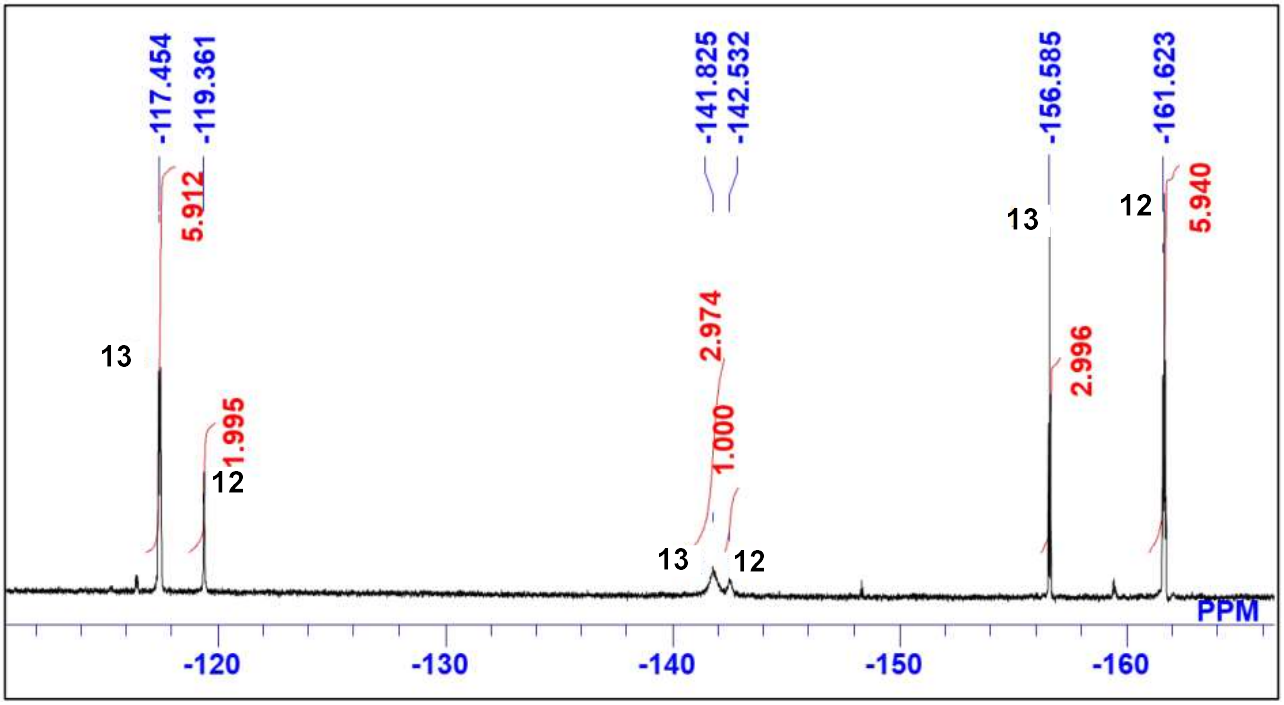

Figure 3-3-15. The ^{19}F NMR spectrum of the crude mixture in the reaction of **8** with 10 equivalents of C_6F_6.

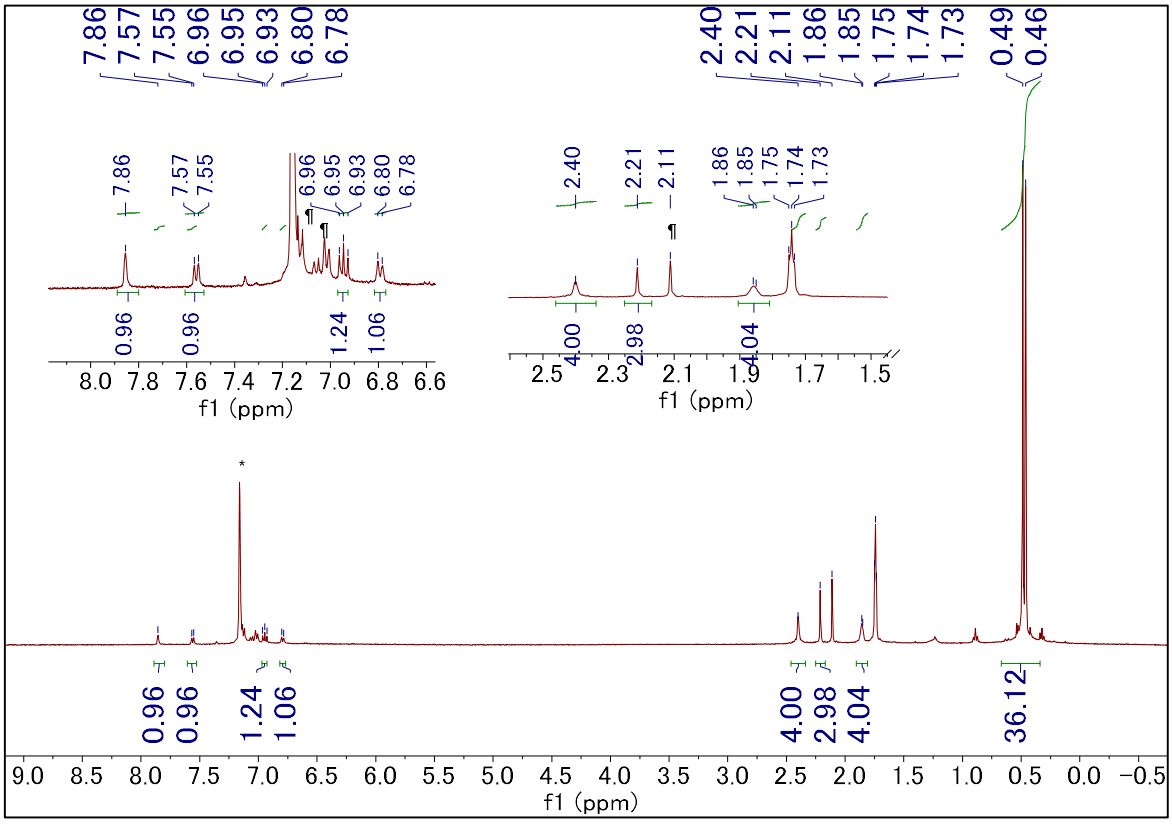

Figure 3-3-16. The ^{1}H NMR spectrum of the crude mixture in the reaction of **8** with toluene (*: C_6D_5H, ¶: toluene).

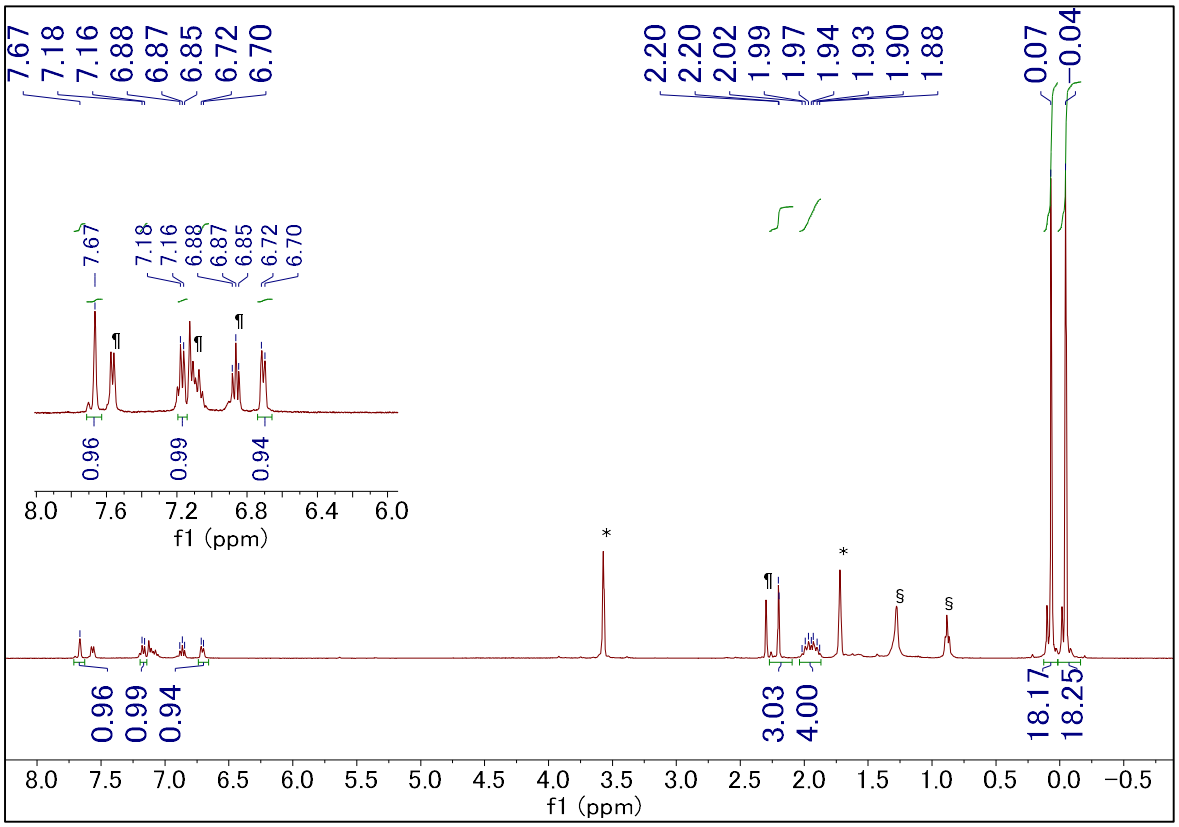

Figure 3-3-17. The ^{1}H NMR spectrum of **15** (*: THF-d_7, ¶: toluene, § ; hexane).

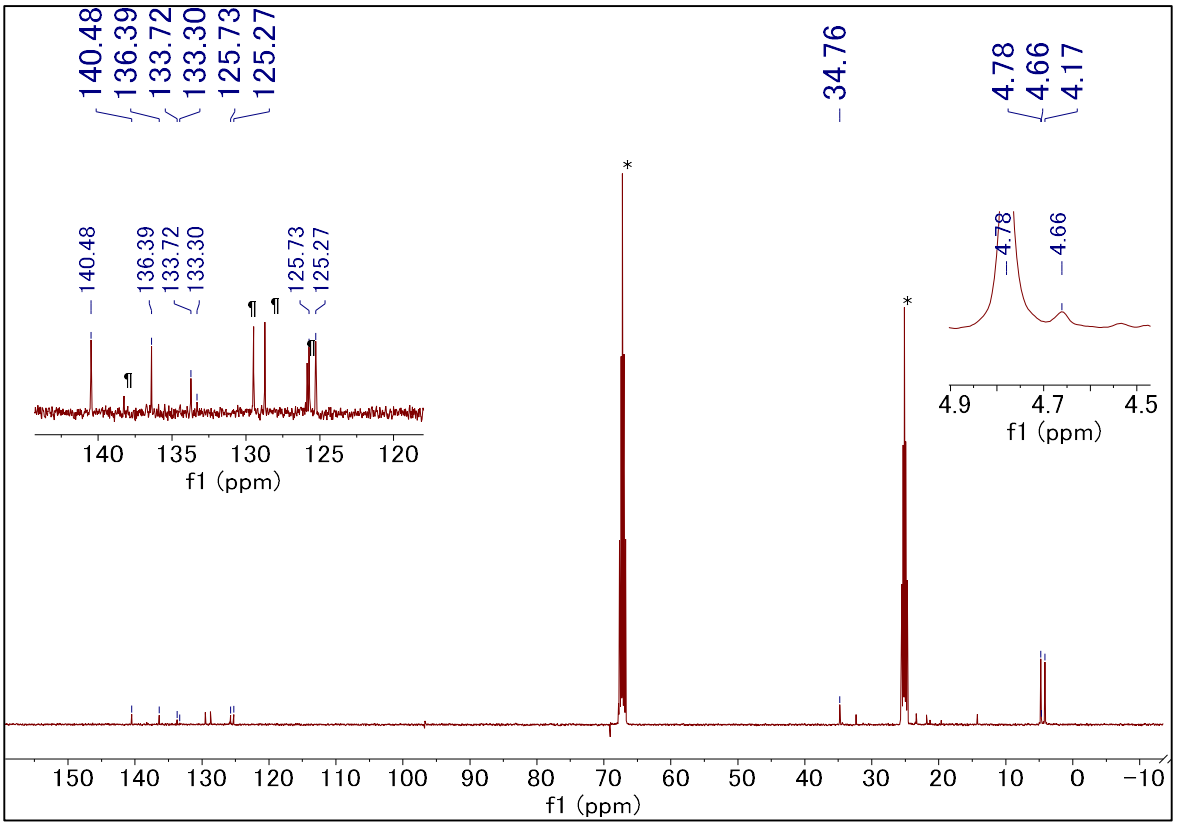

Figure 3-318. The ^{13}C NMR spectrum of **15** (*: THF-d_8, ¶: toluene)

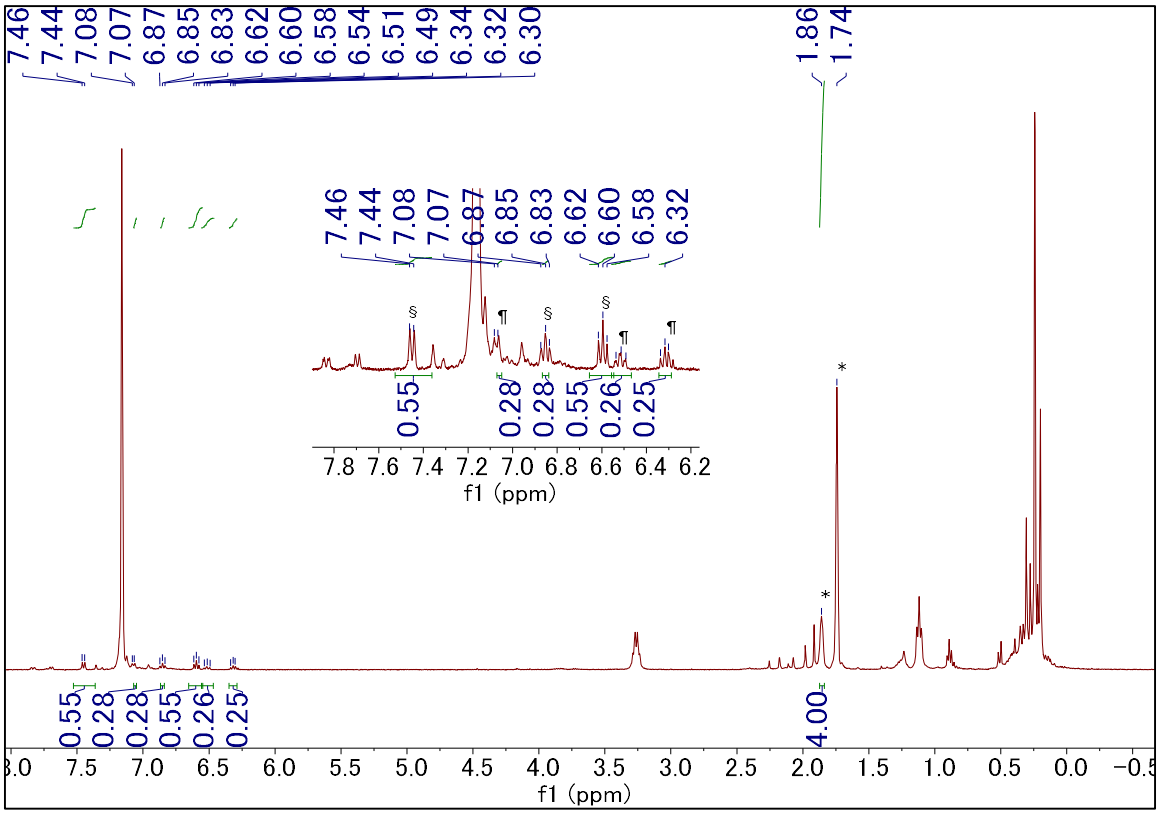

Figure 3-3-19. The ^{1}H NMR spectrum of the crude mixture in the reaction of **8** with fluorobenzene and I_2 (*: adamantane, ¶: *m*-fluoroiodobenzene, § : iodobenzene).

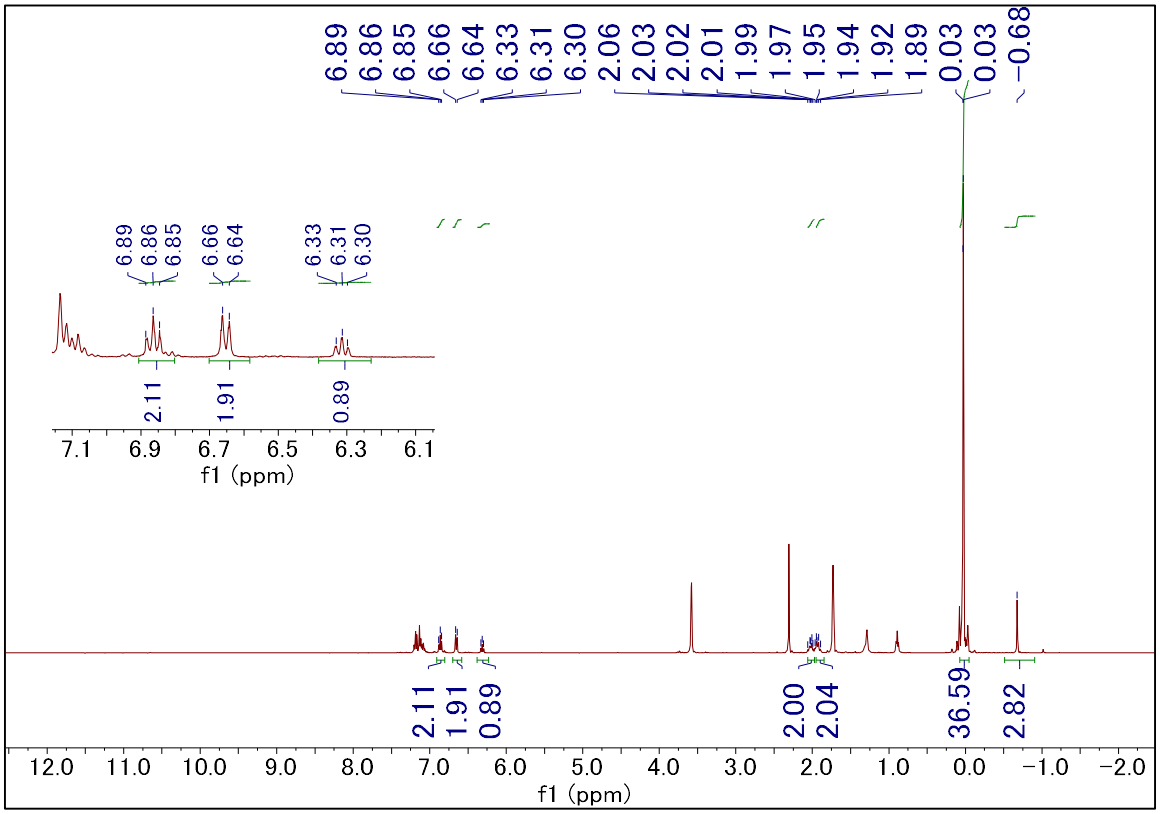

Figure 3-3-20. The ^{1}H NMR spectrum of **18** (*: THF-d_7, ¶: toluene, § ; hexane).

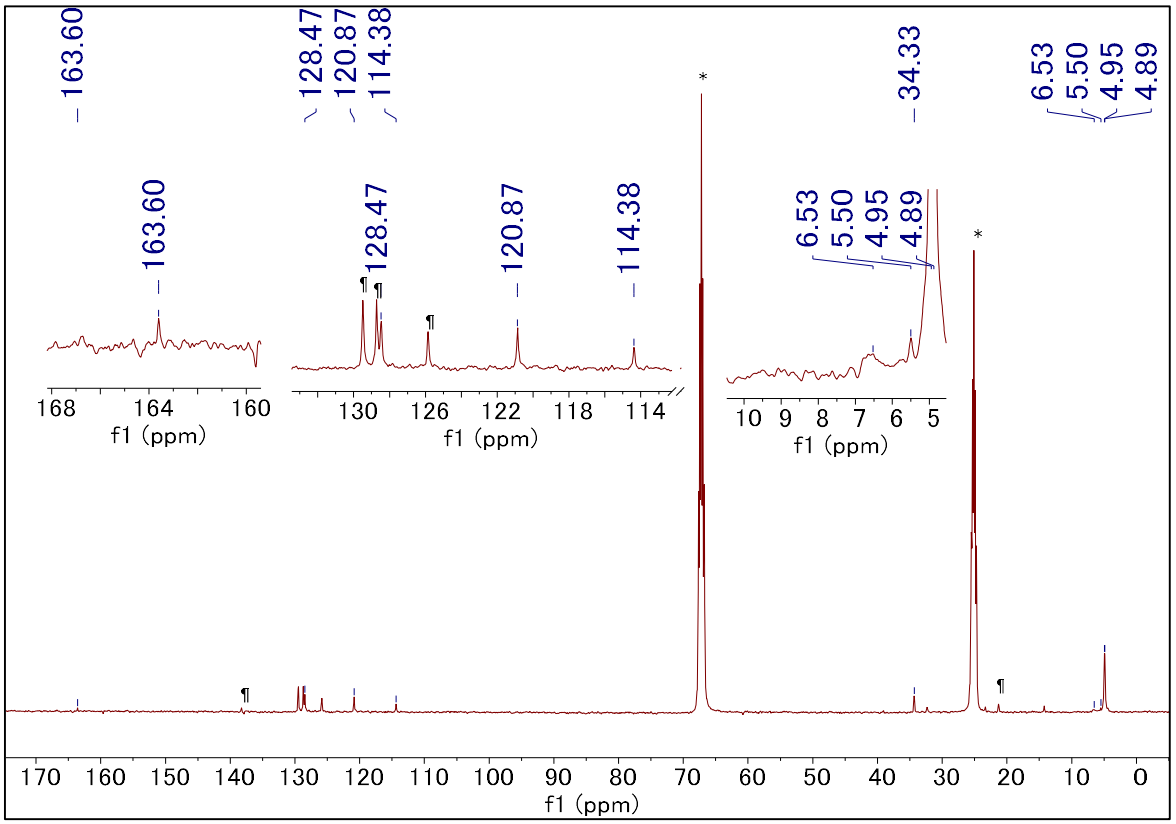

Figure 3-3-21. The ^{13}C NMR spectrum of **18** (*: THF-d_8, ¶: toluene).

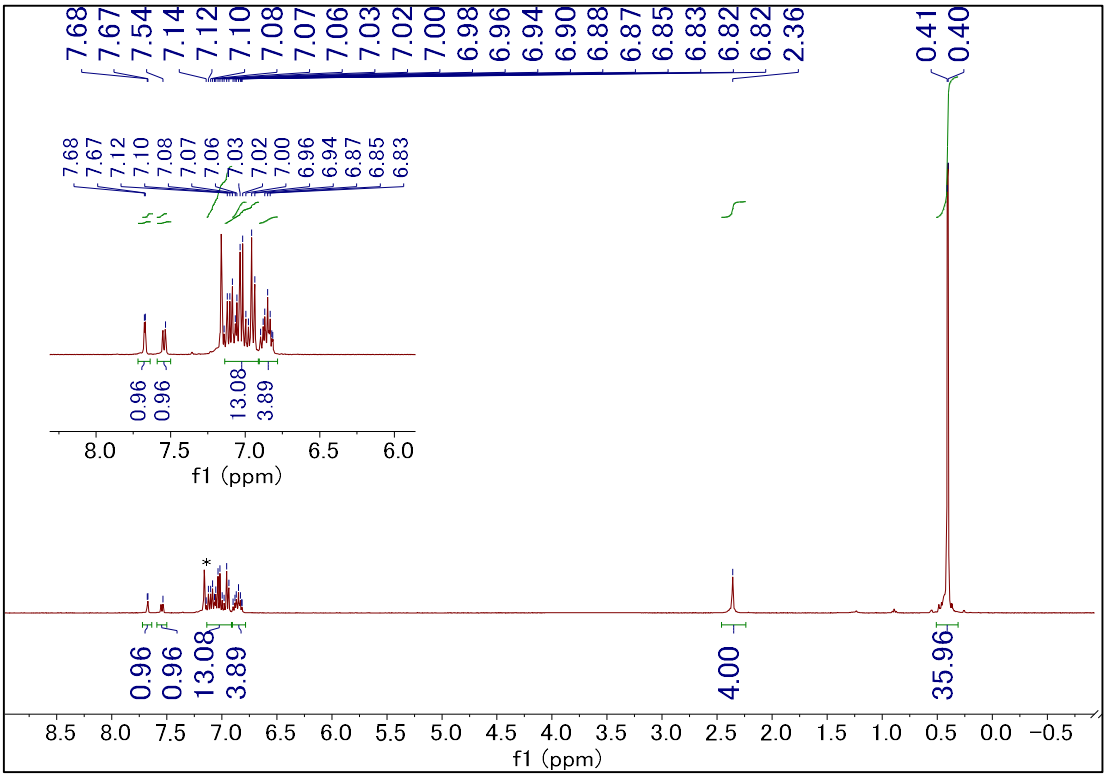

Figure 3-3-22. The ^{1}H NMR spectrum of **19** (*: C_6D_5H)

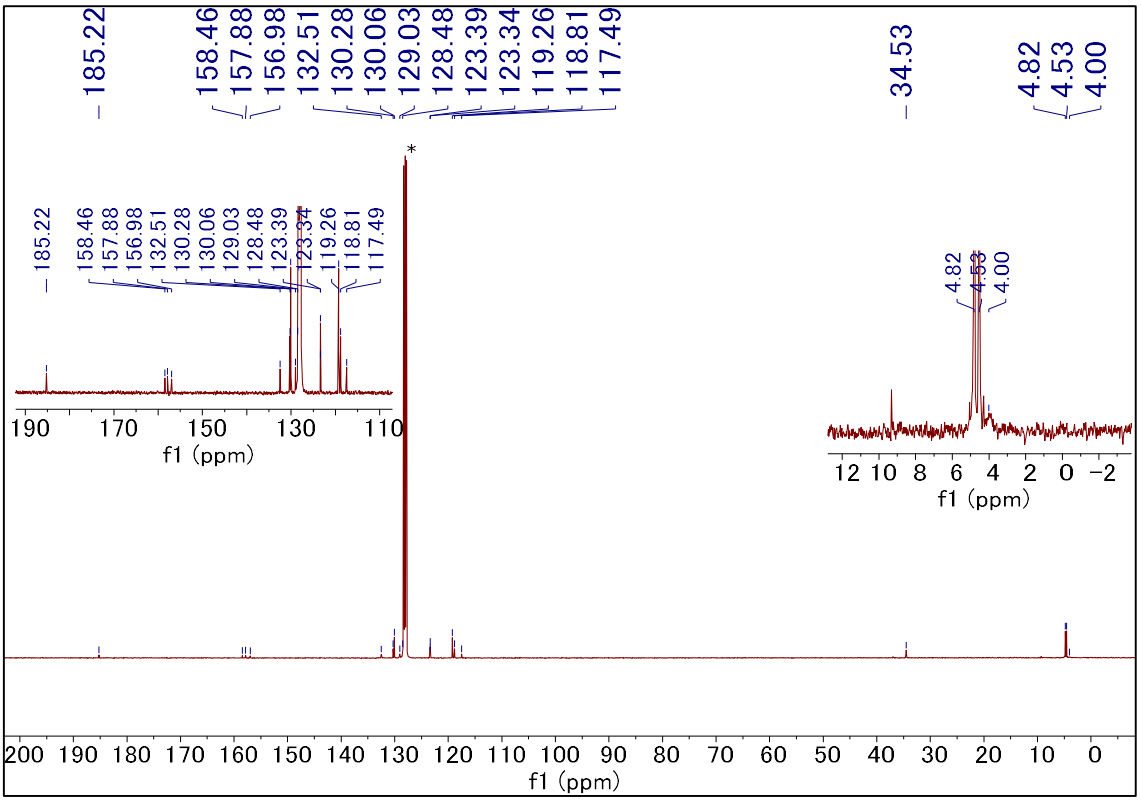

Figure 3-3-23. The ^{13}C NMR spectrum of **19** (*: C_6D_6)

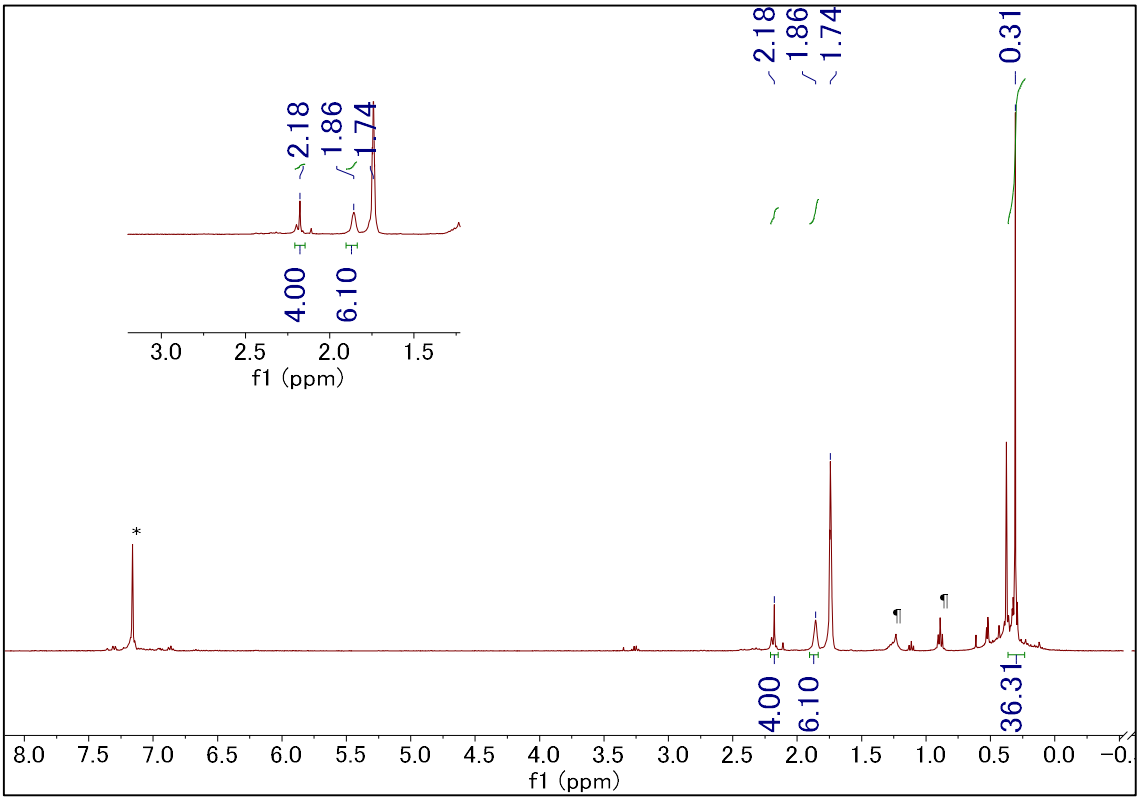

Figure 3-3-24 The ^{1}H NMR spectrum of the reaction of **8** with trifluoromethylbenzene (*: C_6D_5H, ¶: hexane).

Kinetic analysis for the reaction of 1 with toluene and 1-d_{16} with toluene-d_8

In a glovebox, isolated crystals of **8** (10.6 mg, 17.8 μmol) or **8-d_{16}** (11.0 mg, 18.2 μmol, prepared by the recrystallization of **8** from toluene-d_8) were dissolved in toluene or toluene-d_8 and the resulting solution was diluted with a volumetric flask to 4.00 mL at room temperature. Decay of **8** or **8-d_{16}** were monitored with the absorbance at 468 nm by UV-vis spectrum at 35 °C. The observed rate constants k_{obs} were determined by pseudo-first order plot resulting from concentration of **8** or **8-d_{16}** depending on time as summarized in Figure 3-3-25 [k_{obs} (toluene) = 5.42±0.03×10^{-4} s^{-1} M^{-1}, R^2 = 0.9994; k_{obs} (toluene-d_8) = 3.58±0.02×10^{-4} s^{-1} M^{-1}, R^2 = 0.9992; k_H/k_D = 1.51].

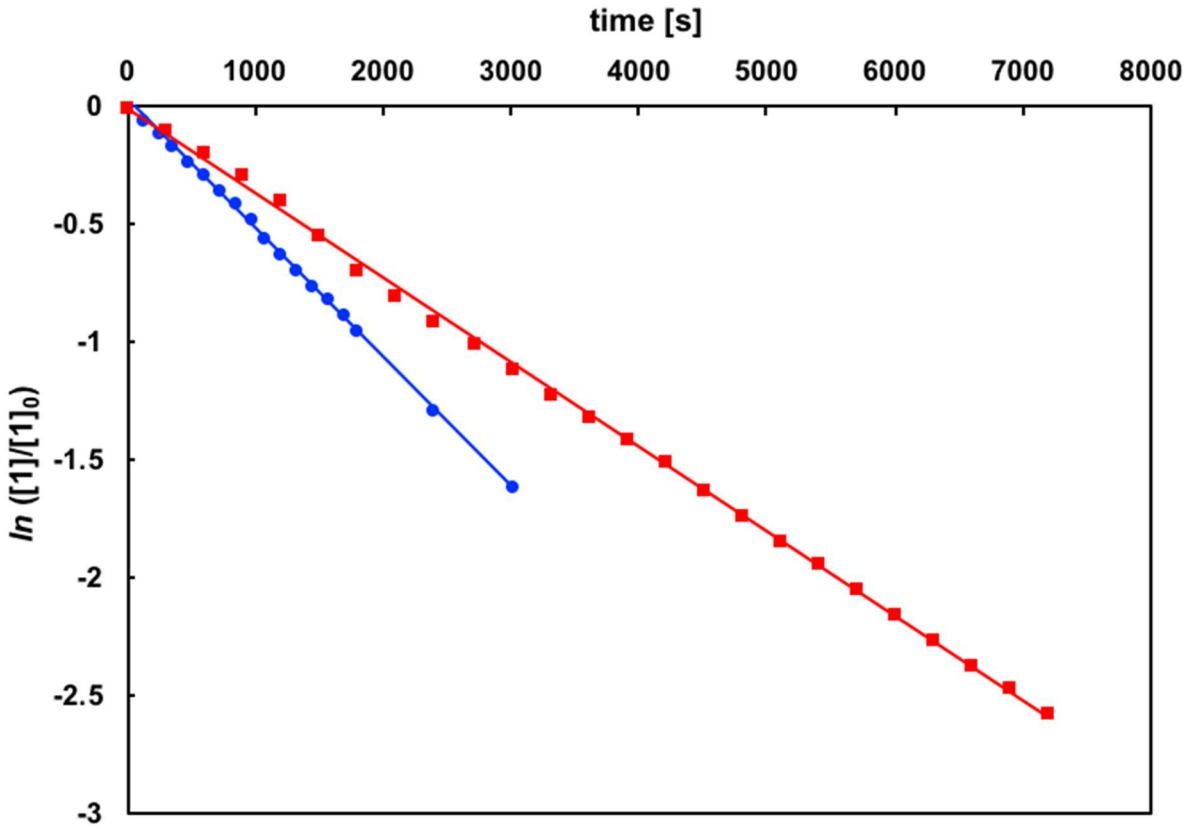

Figure 3-3-25. First-order plot for consumption of **8** or **8-d_{16}** reacting with toluene and toluene-d_8 at 35 °C (blue: reaction in toluene, red: reaction in toluene-d_8).

Details for X-ray crystallography

Crystallographic data for **9**-DMAP, **10**, **14, 15**, **18** and **19**·are summarized in Table 3-3-1. The crystals were coated with immersion oil and put on a MicroMountTM (MiTeGen, LLC), and then mounted on diffractometer. Diffraction data were collected on a Rigaku Rigaku HyPix-6000 detectors using MoKα radiation. The Bragg spots were integrated using CrysAlisPro program package.[22] Absorption corrections were applied. All the following procedure for analysis, Yadokari-XG 2009[23] was used as a graphical interface. The structure was solved by a direct method with programs of SIR2014[24] and refined by a full matrix least squares method with the program of SHELXL-2018.[22] Anisotropic temperature factors were applied to all non-hydrogen atoms. The hydrogen atoms were put at calculated positions, and refined applying riding models. The detailed crystallographic data have been deposited with

the Cambridge Crystallographic Data Centre: Deposition code CCDC 2012416 (**15**), 2012417 (**18**), and 2012418 (**19**). A copy of the data can be obtained free of charge via http://www.ccdc.cam.ac.uk/products/csd/request.

Table 3-3-1. Crystallographic data and structure refinement details for **9**, **12, 14, 15, 18** and **19**.

compound #	**9**-DMAP	**12**	**14**
CCDC deposit #	186767	1869770	1869766
Empirical formula	$C_{24}H_{53}AlN_2Si_4$	$C_{66}H_{112}Al_2F_6K_2Si_8$	$C_{36}H_{62}AlKSi_4$
Formula weight	509.02	1376.43	673.29
T (K)	93(2)	93(2)	93(2)
□ (Å)	0.71073	0.71073	0.71073
Crystal system	*Monoclinic*	*Monoclinic*	*Triclinic*
Space group	$P2_1/c$	$P2_1/n$	P-1
a (Å)	11.5195(11)	16.3949(8)	9.3326(5)
b (Å)	10.5843(8)	13.6006(7)	11.0021(5)
c (Å)	25.805(2)	18.1753(11)	20.8482(11)
α (°)	90	90	102.699(4)
β (°)	96.958(9)	108.047(6)	99.530(4)
γ (°)	90	90	101.952(4)
V (Å^3)	3123.1(5)	3853.4(4)	1992.42(18)
Z	4	2	2
D_{calc}, (g/m^3)	1.083	1.186	1.122
μ (mm^{-1})	0.233	0.3218	0.298
F(000)	1120	1476	732
Crystal size (mm)	0.27×0.21×0.18	0.46×0.32×0.19	0.26×0.22×0.19
2Θ range (°)	1.590-28.771	1.905-28.848	1.960-28.676
reflns collected	23491	29424	12041
Indep reflns/R_{int}	6467/0.0850	8233/0.0456	6819/0.0268
param	295	471	396
GOF on F^2	1.049	1.028	1.063
R_1,[a] wR_2[b] [I>2σ(I)]	0.0591, 0.1266	0.0494, 0.1141	0.0400, 0.1018
R_1,[a] wR_2[b] (all data)	0.1010, 0.1525	0.0778, 0.1324	0.0463, 0.1096

[a] $R_1 = \Sigma \, ||Fo| - |Fc|| \, / \, \Sigma \, |Fo|$, [b] $wR_2 = [\Sigma \, [w(Fo^2 - Fc^2)^2 / \Sigma \, w(Fo^2)^2]]^{1/2}$

compound #	**15**	**18**	**19**
CCDC deposit #	2012416	2012417	2012418
Empirical formula	$C_{23}H_{56}AlKSi_4 \cdot C_7H_8$	$C_{23}H_{48}AlKSi_4 \cdot 2(C_7H_8)$	$C_{40}H_{60}AlKO_2Si_4$
Formula weight	595.18	703.32	751.32
T (K)	93(2)	93(2)	93(2)
λ (Å)	0.71073	0.71073	0.71073
Crystal system	*Triclinic*	*Monoclinic*	*Triclinic*
Space group	*P*-1	$P2_1/a$	*P*-1
a (Å)	8.8347(3)	18.2876(14)	11.3972(4)
b (Å)	11.3323(3)	11.9344(6)	14.8549(5)
c (Å)	18.2059(6)	21.1483(14)	14.9080(6)
α (°)	89.936(2)	90	65.749(3)
β (°)	81.625(3)	114.786(9)	68.359(3)
γ (°)	79.007(2)	90	79.656(3)
V (Å^3)	1769.54(10)	4190.5(5)	2137.73(15)
Z	2	4	2
D_{calc}, (g/m^3)	1.117	1.115	1.167
μ (mm^{-1})	0.328	0.288	0.288
F(000)	648	1528	808
Crystal size (mm)	0.21×0.17×0.16	0.19×0.14×0.08	0.12×0.09×0.08
2θ range (°)	1.831-31.789	2.009-30.764	1.587-30.832
reflns collected	31745	23852	34781
Indep reflns/R_{int}	9908/0.0546	9866/0.0522	10814/0.0628
param	339	412	548
GOF on F^2	1.127	1.034	1.052
R_1,[a] wR_2[b] [$I>2\sigma(I)$]	0.0820, 0.2191	0.0586, 0.1324	0.0561, 0.1404
R_1,[a] wR_2[b] (all data)	0.1016, 0.2274	0.1003, 0.1435	0.0934, 0.1537

[a] $R_1 = \Sigma \, ||Fo| - |Fc|| \, / \, \Sigma \, |Fo|$, [b] $wR_2 = [\Sigma \, [w(Fo^2 - Fc^2)^2 / \Sigma \, w(Fo^2)^2]]^{1/2}$

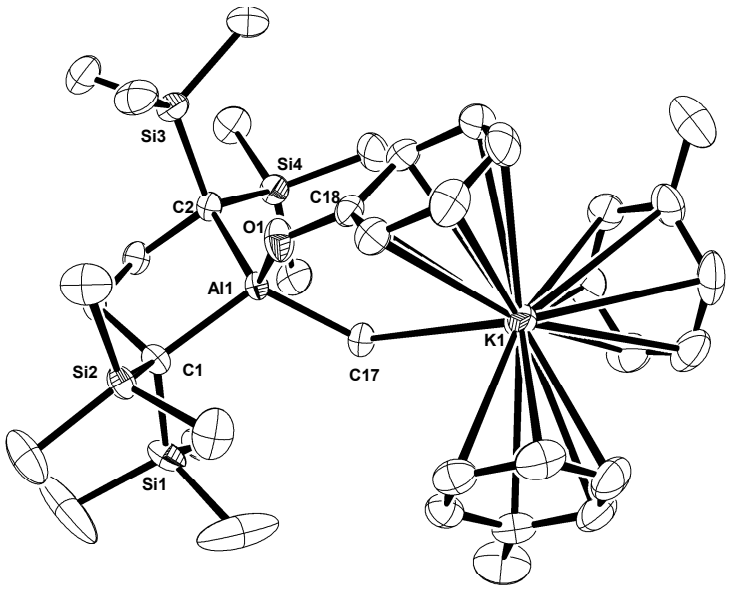

Figure S11. Crystal structure of **18** with thermal ellipsoids at 50% probability; hydrogen atoms have been omitted for clarity.

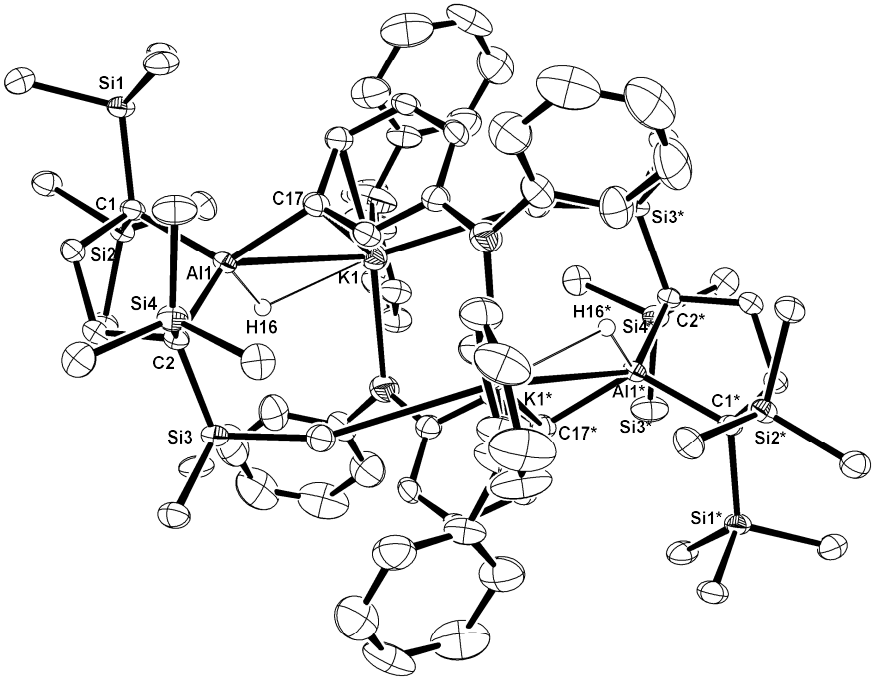

Figure S12. Crystal structure of **19** with thermal ellipsoids at 50% probability; hydrogen atoms except H16 have been omitted for clarity; asterisks denote atoms generated by symmetry operations.

Computational Methods

Part of the computations were performed using workstation at Research Center for Computational Science, National Institutes of Natural Sciences, Okazaki, Japan. The theoretical approach is based on the framework of density functional theory (DFT). The artificial force induced reaction (AFIR) method implemented in the GRRM17 program was used for searching the reaction pathways initially. The structure optimization and vibrational frequency calculation were performed by using Gaussian 16 (revision B.01[25] or C.021) program, with the PBE0 functional[23] using def2-SVP basis set[26] (PBE0 functional was selected based on the comparison with other functionals). All local minima and saddle points were confirmed by their vibrational frequency calculations (with zero and one imaginary frequencies, respectively). The saddle points found were confirmed to be the correct ones by IRC. The single point calculation was performed by using Gaussian 16 (revision C.01)[27] program with the M06-HF functional[28] using def2-SVP basis set,[26] and PCM correction using SMD method[29] (toluene) was adopted. All the values of free-energy change are at 298.15 K. Natural bond orbital (NBO) analysis for some stationary points was performed by using Gaussian NBO 3.1.

3-4. Reference

1. Hicks, J.; Vasko, P.; Goicoechea, J. M.; Aldridge, S. *Nature* **2018**, *557*, 92-95.
2. Hicks, J.; Mansikkamäki, A.; Vasko, P.; Goicoechea, M. J.; Aldridge, S. *Nat. Chem.* **2019**, *11*, 237.
3. Liu, H-Y.; Schwamm, J. L.; Hill, S. M.; Mahon, F. M.; McMullin, L. C.; Rajabi, A. N. *Angew. Chem. Int, Ed.* **2021**, *60*, 14390-14393.
4. Sugita, K.; Yamashita, M. *Chem. Eur. J.* **2020,** *26,* 4520-4523.
5. Koshino, K.; Kinjo, R. *J. Am. Chem. Soc.* **2020**, *142*, 9057-9062.
6. Harder, S.; Grams, S.; Eyselein, J.; Langer, J.; Färber, C. *Angew. Chem. Int. Ed.* **2020**, *59*, 15982-15986.
7. a) Buchner, E.; Feldmann, L. *ChemischeBerichte,* **1903**, *36,* 3509. b) Simmons, H. E.; Smith, R. D. *J. Am. Chem. Soc.* **1958**, *80*, 5323.
8. Boudjouk, P. Black, E,; Kumarathasan, R. *Organometallics* **1991**, *10*, 2095.
9. Hicks, J.; Vasko, P.; Goicoechea, J. M.; Aldridge, S. *J. Am. Chem. Soc.* **2019**, *141*, 11000-1100.
10. Schwamm, R. J.; Anker, M. D.; Lein, M.; Coles, M. P. *Angew. Chem. Int. Ed.* **2019**, *58*, 1489-1493.
11. Sugita, K.; Nakano, R.; Yamashita, M. *Chem. Eur. J.* **2020,** *26,* 2174-2177.
12. Hicks, J.; Heilmann, A.; Vasko, P.; Goicoechea, M. J.;Aldridge, S., Aldridge, S. *Angew. Chem. Int. Ed.* **2019**, *58*, 1849.
13. a) Anker, D. M.; Coles, P. M. *Angew. Chem. Int. Ed.* **2019**, *58*, 13452-13455. b) Anker, D. M.; Coles, P. M. *Angew. Chem. Int. Ed.* **2019**, *58*, 18429-18433. c) Evans, J. M.; Anker, D. M.; Rajabi, A. N.; Coles, P. M. *Angew. Chem. Int. Ed.* **2021**, *60*, 2673-2676. d) Evans, J. M.; Anker, D. M.; Coles, P. M. *Angew. Chem. Int. Ed.* **2021**, *60*, 4772-4778. e) Koshino, K.; Kinjo, R. *Organometalics* **2020**, *39*, 4183-4186.
14. Sugita, K.; Yamashita, M. *Organometallics* **2020**, *39*, 2125-2129.
15. Shatunov, V.V.; Korlyukov, A.A.; Lebedev, V. A.; Sheludyakov, D. V.; Kozyrkin, I. B.; Yu. D. *J. Organomet. Chem.* **2011**, *696*, 2238-2251.
16. Rçsch, B.; Gentner, T.X.; Elsen, E.; Fischer, C. A.; Langer, J.; Wiesinger, M.; Harder, S. *Angew. Chem. Int. Ed.* **2019**, *58*, 5396–5401.
17. Hicks, J.; Vasko, P.; Heilmann, A.; Goicoechea, M. J.; Aldridge, S. *Angew. Chem. Int. Ed.* **2020**, *59*, 20376-20380.
18. Ohsato, T.; Okuno, Y.; Ishida, S.; Iwamoto, T.; Lee, K.-H.; Lin, Z.; Yamashita, M.; Nozaki, K. *Angew. Chem. Int. Ed.* **2016,** *55*, 11426-11430.
19. Dettenrieder, N.; Aramaki, Y;. Wolf, B.; Maichle-Mo¨ssmer, C.; Zhao, X.; Yamashita, M.; Nozaki, K.; Anwander, R. *Angew. Chem. Int. Ed.* **2014**, *53,* 6259-6262.
20. a) Bryce-Smith, D.; Gold, V.; Satchell, D. P. N. *J. Chem. Soc.* **1954**, 2743 – 2747. b) Bryce-Smith, D.; Turner, E. E. *J. Chem. Soc.* **1953**, 861 – 867.
21. Schlosser, M.; Jung, H. C.; Takagishi, S. *Tetrahedron* **1990**, *46*, 5633 – 5648.
22. CrysAlisPRO *CrysAlisPRO*, Oxford Diffraction/Agilent Technologies UK Ltd: Yarnton, England, 2015.
23. Kabuto, C.; Akine, S.; Kwon, E. Release of Software (Yadokari-XG 2009) for Crystal Structure Analyses. *J. Cryst. Soc. Jpn.* **2009,** *51*, 218-224.
24. Burla, M. C.; Caliandro, R.; Carrozzini, B.; Cascarano, G. L.; Cuocci, C.; Giacovazzo, C.; Mallamo, M.; Mazzone, A.; Polidori, G. Crystal structure determination and refinement via SIR2014. *J. Appl. Crystallogr.* **2015,** *48*, 306-

309.

25. Sheldrick, G. Crystal structure refinement with SHELXL. *Act. Cryst. Sec. C* **2015,** *71*, 3-8.
26. Adamo, C.; Barone, V. Toward reliable density functional methods without adjustable parameters: The PBE0 model. *J. Chem. Phys.* **1999,** *110*, 6158-6170.
27. Frisch, M. J.; Trucks, G. W.; Schlegel, H. B.; Scuseria, G. E.; Robb, M. A.; Cheeseman, J. R.; Scalmani, G.; Barone, V.; Petersson, G. A.; Nakatsuji, H.; Li, X.; Caricato, M.; Marenich, A. V.; Bloino, J.; Janesko, B. G.; Gomperts, R.; Mennucci, B.; Hratchian, H. P.; Ortiz, J. V.; Izmaylov, A. F.; Sonnenberg, J. L.; Williams; Ding, F.; Lipparini, F.; Egidi, F.; Goings, J.; Peng, B.; Petrone, A.; Henderson, T.; Ranasinghe, D.; Zakrzewski, V. G.; Gao, J.; Rega, N.; Zheng, G.; Liang, W.; Hada, M.; Ehara, M.; Toyota, K.; Fukuda, R.; Hasegawa, J.; Ishida, M.; Nakajima, T.; Honda, Y.; Kitao, O.; Nakai, H.; Vreven, T.; Throssell, K.; Montgomery Jr., J. A.; Peralta, J. E.; Ogliaro, F.; Bearpark, M. J.; Heyd, J. J.; Brothers, E. N.; Kudin, K. N.; Staroverov, V. N.; Keith, T. A.; Kobayashi, R.; Normand, J.; Raghavachari, K.; Rendell, A. P.; Burant, J. C.; Iyengar, S. S.; Tomasi, J.; Cossi, M.; Millam, J. M.; Klene, M.; Adamo, C.; Cammi, R.; Ochterski, J. W.; Martin, R. L.; Morokuma, K.; Farkas, O.; Foresman, J. B.; Fox, D. J. *Gaussian 16, Revision C.01*, Wallingford, CT, 2016.
28. (a) Zhao, Y.; Truhlar, D. G. *J. Phys. Chem. A* **2006,** *110*, 5121-5129; (b) Zhao, Y.; Truhlar, D. G. *J. Phys. Chem. A* **2006,** *110*, 13126-13130.
29. (a) Foster, J. P.; Weinhold, F. *J. Am. Chem. Soc.* **1980,** *102*, 7211-7218; (b) Reed, A. E.; Weinhold, F. *J. Chem. Phys.* **1983,** *78*, 4066-4073; (c) Reed, A. E.; Weinhold, F. *J. Chem. Phys.* **1985,** *83*, 1736-1740; (d) Reed, A. E.; Weinstock, R. B.; Weinhold, F. *J. Chem. Phys.* **1985,** *83*, 735-746; (e) Reed, A. E.; Curtiss, L. A.; Weinhold, F. *Chem. Rev.* **1988,** *88*, 899-926.

Chapter 4:

Synthesis and Properties of (Dialkyl)(Diaryl)Alumaborane Possessing Electronically Non-Stabilized Al-B σ-Bond

4-1. Introduction

Neutral tricoordinate boron and aluminum compounds are widely used for organic synthesis as Lewis acid catalysts. Their Lewis acidity due to a vacant p-orbital is generally weakened by substitution with π-electron donating group(s), coordination of Lewis base, or formation of a 3-center-2-electron bond to satisfy octet rule. Therefore, carbon-substituted boron and aluminum compounds without such stabilizing effects should exhibit their unperturbed Lewis acidity. It is widely known to enhance Lewis acidity of carbon-substituted boron and aluminum compounds by introducing electron-withdrawing group(s) to the carbon substituents as $B(C_6F_5)_3$ behaves as a strong Lewis acid. In contrast, an enhancement of the Lewis acidity of the boron atoms in pinB–$BMes_2$ (pin = pinacol, Mes = 2,4,6-$Me_3C_6H_2$) by overlapping two vacant p-orbitals of two boron atoms has been reported.[1] This concept could be expanded to all carbon-substituted diborane(4) (**K**, Figure 4-1-1), a B–B bonded homodinuclear species, that exhibits even higher Lewis acidity than those of the corresponding triarylborane and pinB–$BMes_2$.[1-2] Similar carbon-substituted homodinuclear B–B or Al–Al species **L**-**O** and **6** also have been synthesized,[3-6] although the Lewis acidity of them has not been mentioned. In contrast to that these electronically non-stabilized homodinuclear group 13 element compounds have been investigated, all reported heterodinuclear alumaboranes **P**-**S**[7-9] were electronically stabilized by π-electron donating group(s), coordination of Lewis base, and/or formation of a 3-center-2-electron bond. Thus, electronically unperturbed heterodinuclear B–Al species has never been reported.

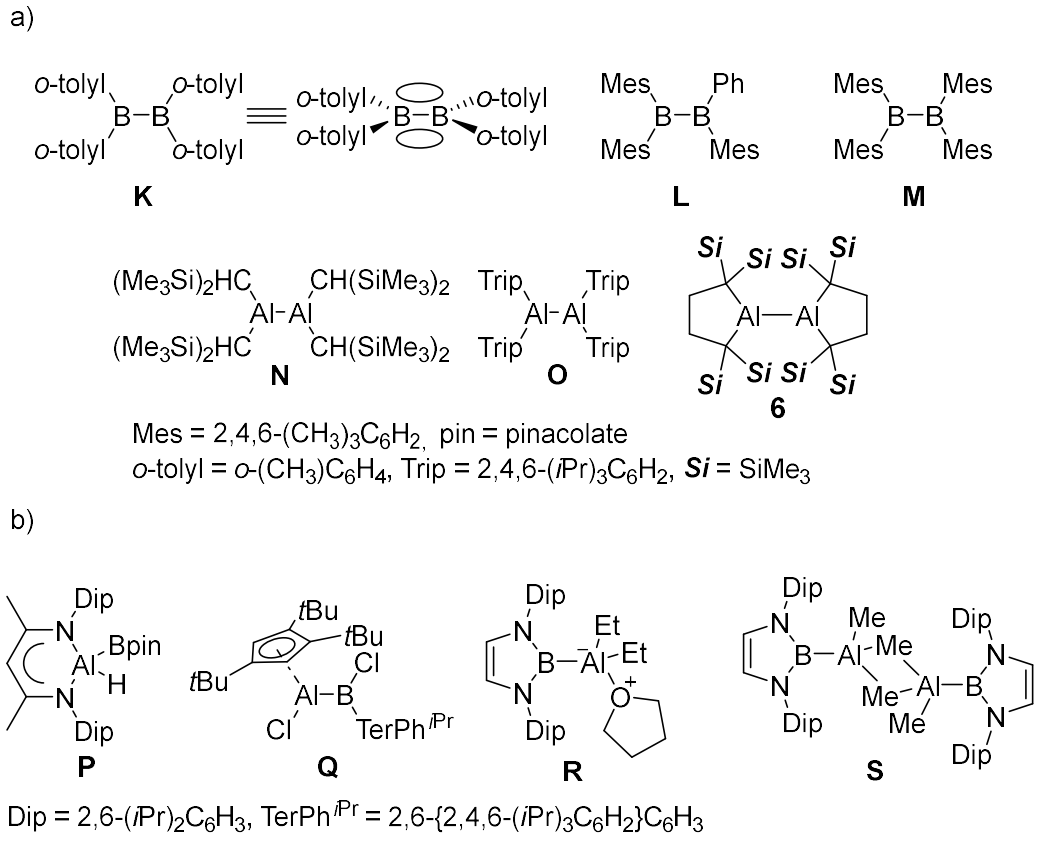

Figure 4-1-1. Reported (a) homodinuclear group 13 element compounds having electronically non-stabilized homodinuclear structure, and (b) dinuclear group 13 element compounds having electronically stabilized heterodinuclear structure.

Boron and aluminum compounds have Lewis acidic vacant 2p- or 3p-orbital, and their strength are characterized by different factors. Boron compounds have a high electron-affinity due to the lower energy level of 2p-orbital on boron atom than that of 3p-orbital on aluminum. Whereases vacant 3p-orbital in aluminum compounds are sterically not easily affected due to its larger orbital size than that of 2p-orbital. As a computational method for evaluating Lewis acidity, fluoride ion affinity (FIA)[10] is broadly adopted. The reported FIA, 59.2 kcal/mol for BMe_3 and 88.1 kcal/mol for $AlMe_3$, indicates $AlMe_3$ behaves as stronger Lewis acid toward fluoride ion than BMe_3. Here, it is thought that electropositive Al atom strongly interacts with negatively charged fluoride ion. That is, Coulomb interaction can also be a factor in determining Lewis acidity. From these things, it is interesting to know which of aluminum and boron in alumaborane is more Lewis acidic.

In this chapter, the synthesis of an electronically non-stabilized alumaborane **21,** by using dilalklaluminum nucleophile and diaryl boron electrophile, will be described (Scheme 4-1-1).

Scheme 4-1-1. Strategy for synthesis of electronically non-stabilized alumaborane.

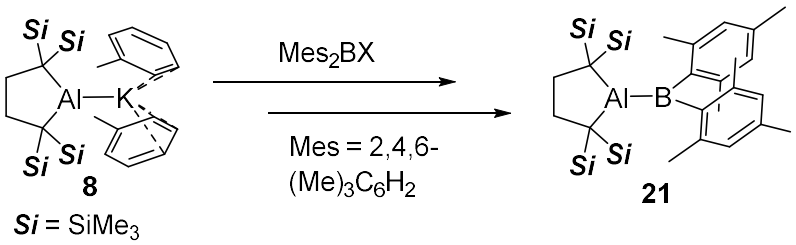

4-2. Synthesis and properties of (dialkyl)(diaryl)alumaborane

The electronically non-stabilized alumaborane **21** was synthesized as illustrated in Scheme 4-2-1. Reaction of **8** with dimesitylfluoroborane gave borylfluoroaluminate **20** as red crystals through the migration of fluoride from the boron to the aluminum atom. Subsequently, **20** was treated with trimetylsilyl triflate for removal of fluoride to afford yellow crystalline alumaborane **21**. Although the reactions of **8** with other boron electrophiles were also performed, the desired Al-B bond formation did not proceeded. In the case of treating **8** with Ar_2BX (Ar = Ph, *o*-tolyl, X = Cl, Br) or 9-BBN chloride gave corresponding (*m*-tolyl)alumane **22** and hydroborane through a hydride reduction of haloboranes by **15,** which is generated by the intermolecular C-H cleavage in **8**. The ^{1}H NMR spectrum of **20** indicated its C_s symmetrical structure (unsymmetrical two silyl groups and methylene). Broadening of the ^{19}F NMR signal at 139 ppm ($h_{1/2}$ = 251 Hz) and a low-field ^{11}B NMR signal at δ_B 122 ppm support that the fluoride binds to aluminum in solution of **20** as observed in the solid state (vide infra). In contrast, the ^{1}H NMR spectrum of **21** exhibited a C_{2v} symmetrical pattern (symmetrical for silyl groups and two methylene) and the ^{11}B NMR signal of **21** resonated at δ_B 109 ppm, supporting the existence of the planarized aluminum and boron atoms in solution.

Scheme 4-2-1. Synthesis of (dialkyl)(diaryl)alumaborane **21** in two steps from **8**. And reactions of **8** with other boron nucleophiles.

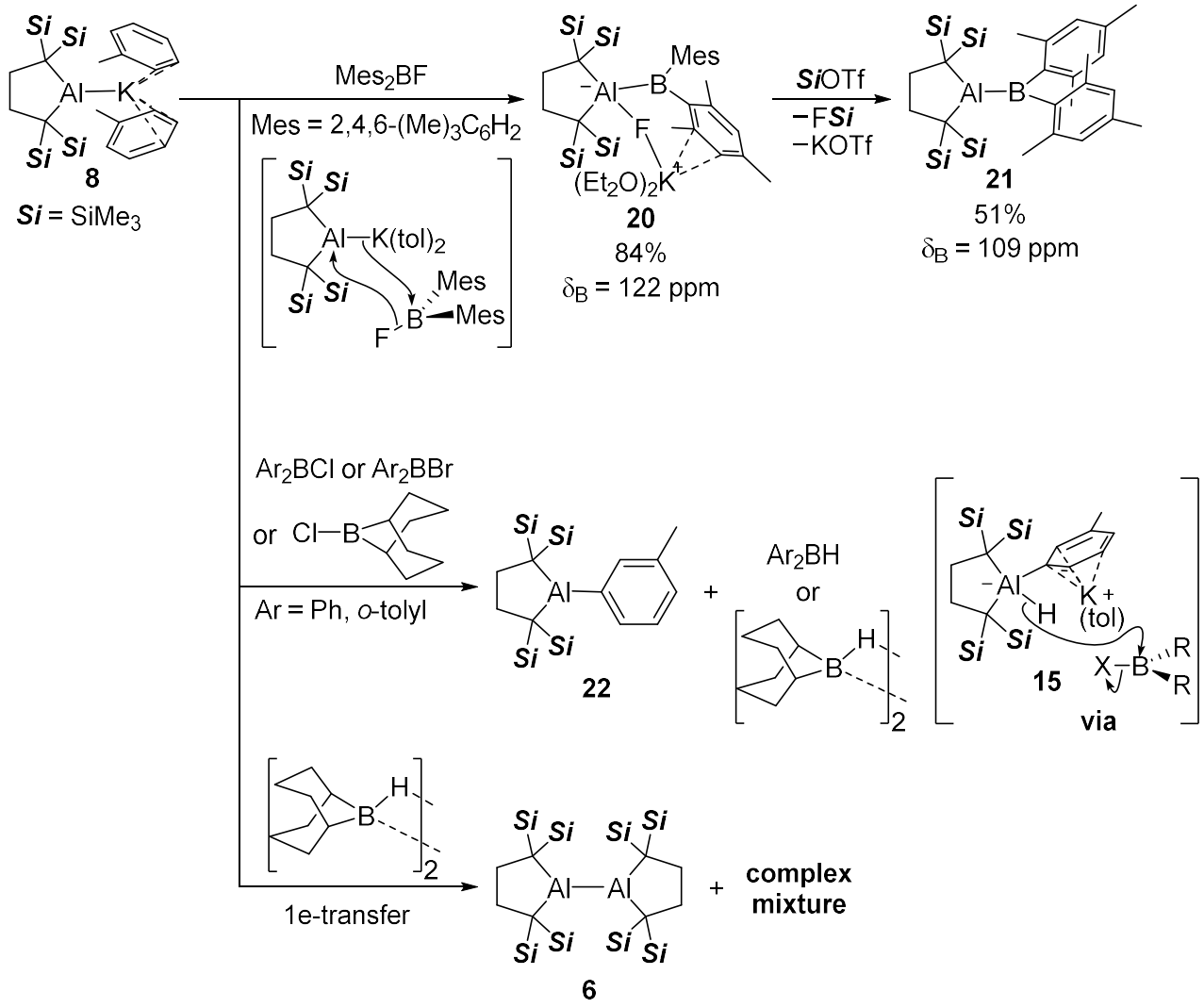

The crystal structures of **20** and **21** are shown in Figure 4-2-1. The Al-B bonds in **20** [2.2805(19) Å] and **21** [2.191(2) Å] are longer than those of all previously reported electronically stabilized alumaboranes **P**-**S** [2.119(3)-2.156(2) Å],[9-11] probably due to the steric repulsion between bulky trimethylsilyl and mesityl groups. The shorter Al–B bond in **21** compared with that of **20** would reflect the change of hybridization at the aluminum atom. In the structure of **21**, planar and trigonal Al and B atoms were disclosed (angles sum around Al and B = 360°), where the two planes of Al and B are twisted (C-Al-B-C = −60.5°).

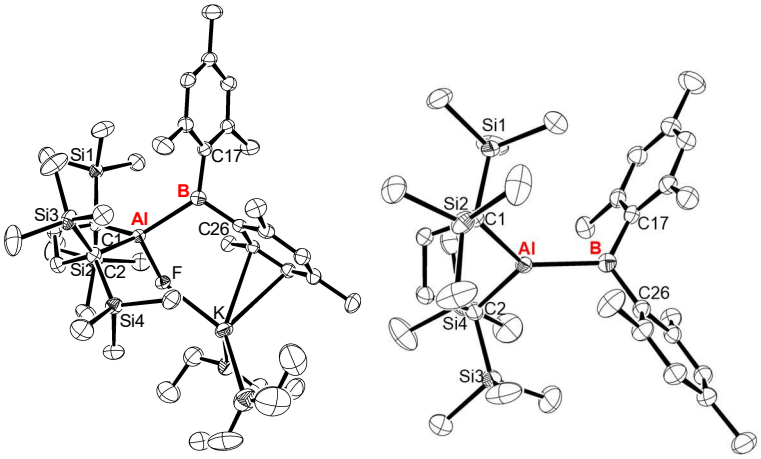

compound	**20**	**21**
Al-B (Å)	2.2805(19)	2.191(2)
C-Al-B-C (°)		−60.5
ΣAl (°)	347	360
ΣB (°)	360	360

Figure 4-2-1. Crystal structures of **20** and **21** and their selected structural parameters.

The electronic character of **21** was estimated by UV-vis absorption spectrum and DFT calculations. Similar to the report for diborane(4) **K** the dependence of the LUMO energy level and the free energy on the C−Al−B−C torsion angle of **21** was estimated by DFT calculations.[2] In the case of diborane(4)s, the LUMO energy level and the free energy were lowered when the torsion angles were increased from −90° to 0°. Although the alumaborane **21** also changed its free energy and the LUMO energy level with torsion angle, its tendency was different from that of diborane(4)s as follows (Figure 4-2-2). Reflecting the crystal structure, a conformer with a torsion angle of 60° corresponds to the bottom of the energy profile. The LUMO energy level was lowered upon rotation of Al–B bond an the lowest LUMO energy level of −1.36 eV was observed at the torsion angle of –20°, which is slightly higher than that of diborane(4) **K**. The maximum energy change was less than +3.1 kcal/mol between the lowest and highest free energy (C-Al-B-C = 30°), indicating the rotation of the Al−B bond should occur rapidly at room temperature. The lowering of the LUMO of **21** upon Al−B bond rotation should be attributed to the overlapping of the two unoccupied 3p and 2p orbitals on the Al and B atoms (Figure 4-2-3). According to the difference in energy between 2p and 3p orbitals, LUMO of the ground state (−61.9°) mainly consists of 2p orbital of the B atom and π*-orbitals of two mesityl rings. In contrast, a large contribution of 3p orbital of the Al atom was found in the LUMO+1. At the torsion angle of −20.0°, LUMO corresponds to two completely merged vacant p-orbitals on Al and B atoms. It should be noted that the Al–B bond significantly contributes to HOMO in both cases, indicating the high reactivity of the

Al–B bond should retain regardless of the torsion angle. On the other hand, it was reported that tetra(*o*-tolyl)diborane **K** has similar electronic structure to that of **21** (B-B σ-bond and π-orbitals of two o-tolyl rings for HOMO, vacant 2p-orbital on boron atom and π*-orbitals of two o-tolyl rings for LUMO). The HOMO energy level of **21** (−6.70 eV, M06-2X/6-31G(d) level of theory) was higher than that of **K** (−7.01 eV), that would arise from the increment effect of electropositive aluminum and more donating Mes substituents in **21**.

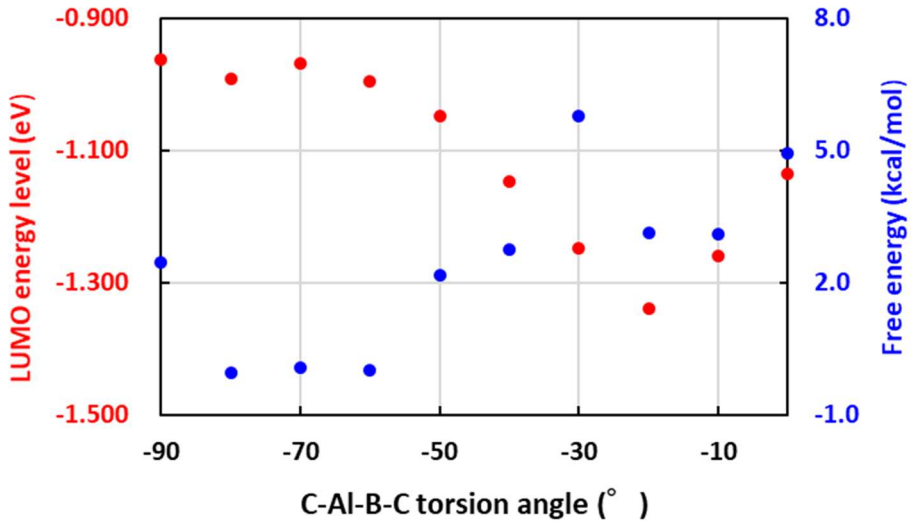

Figure 4-2-2. Dependency of the LUMO energy level (in eV) and the relative stability (in kcal/mol) of **21** on the torsion angle of the C−Al−B−C moiety.

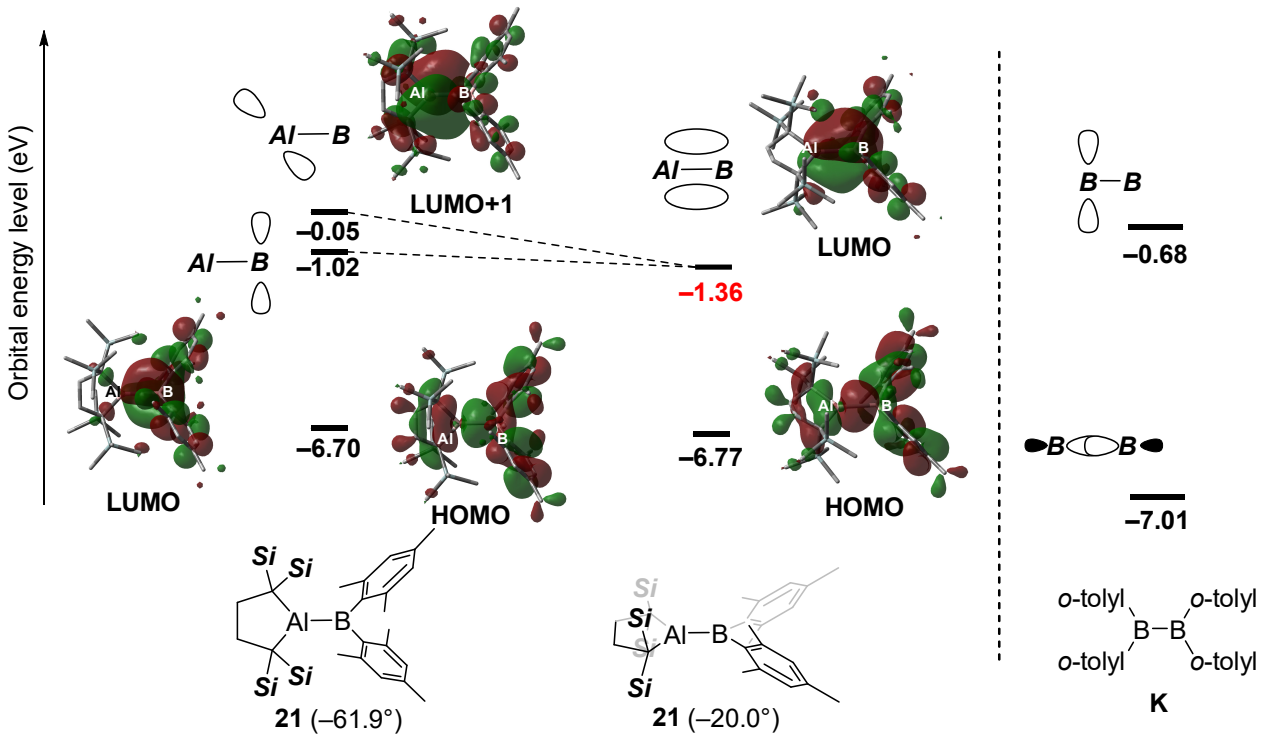

Figure 4-2-3. Frontier orbitals of the rotational isomers of **21** at C−Al−B−C = −61.9° and C−B−B−C = −20.0°.

A detailed property of electronically non-perturbed alumaborane **21** was estimated by NBO (natural bond orbital) analysis (Figure 4-2-4). NPA charges of +1.82 on Al and +0.14 on B suggested the polarized nature as Al(δ^+)–B(δ^-) due to the difference in electronegativity of Al and B atoms. The second-order perturbation energy analysis provided information about the weak interaction of four Si–C σ bonds donate electrons to the vacant 3p-orbital of the Al atom via negative hyperconjugation (0.78-19.38 kcal/mol) and π-orbitals of two Mes substituents donate electrons to the vacant 2p-orbital of B atom (1.59-8.47 kcal/mol). Considering the strong FIA of $AlMe_3$ (88.1 kcal/mol), these interaction only weakly stabilized this alumaborane **21**. That is, one can say that alumaborane **21** has almost non-perturbed vacant 2p and 3p orbitals on boron and aluminum atoms, respectively. The UV-Vis spectrum of **21** in hexane exhibited absorption maximum at 452 nm (ε = 3370), and reflecting the yellow color of **21** (Figure 4-2-5). TD-DFT calculations indicated that a transition from the HOMO to the LUMO (445 nm) reproduces the characteristic absorptions observed in the UV-vis spectrum. This is contrasting result from that the reported electronically stabilized alumaboranes **P-S** are colorless.[7-9] .

a)

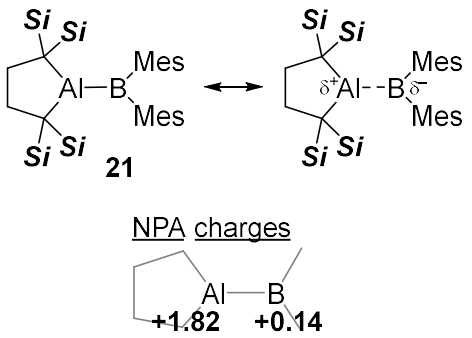

b)

Donor NBO (i)	Acceptor NBO (j)	E(2) [kcal/mol]	E(j)-E(i) [a.u.]	F(i,j) [a.u.]
BD (1)C 2 – Si 10	LP*(1)Al 1	19.08	0.74	0.109
BD (1)C 2 – Si 10	LP*(2)Al 1	19.38	0.74	0.109
BD (1)C 2 – Si 10	LP*(3)Al 1	0.78	0.66	0.020
BD (1)C 2 – Si 11	LP*(1)Al 1	13.60	0.74	0.092
BD (1)C 2 – Si 11	LP*(2)Al 1	15.52	0.74	0.098
BD (1)C 2 – Si 11	LP*(3)Al 1	7.65	0.66	0.064
BD (1)C 3 – Si 12	LP*(1)Al 1	19.08	0.74	0.109
BD (1)C 3 – Si 12	LP*(2)Al 1	19.38	0.74	0.109
BD (1)C 3 – Si 12	LP*(3)Al 1	0.78	0.66	0.020
BD (1)C 3 – Si 13	LP*(1)Al 1	13.60	0.74	0.092
BD (1)C 3 – Si 13	LP*(2)Al 1	15.52	0.74	0.098
BD (1)C 3 – Si 13	LP*(3)Al 1	7.65	0.66	0.064
BD (1)C 63 – C 64	LP*(11)B 62	8.47	0.30	0.048
BD (1)C 63 – C 65	LP*(1)B 62	1.59	0.77	0.032
BD (1)C 83 – C 84	LP*(1)B 62	8.47	0.30	0.048
BD (1)C 83 – C 85	LP*(1)B 62	1.59	0.77	0.032

Figure 4-2-4. Results of NBO analysis calculated at M062X/6-31G(d) level theory. Selected (a) NPA charges and (b) donor-acceptor interactions.

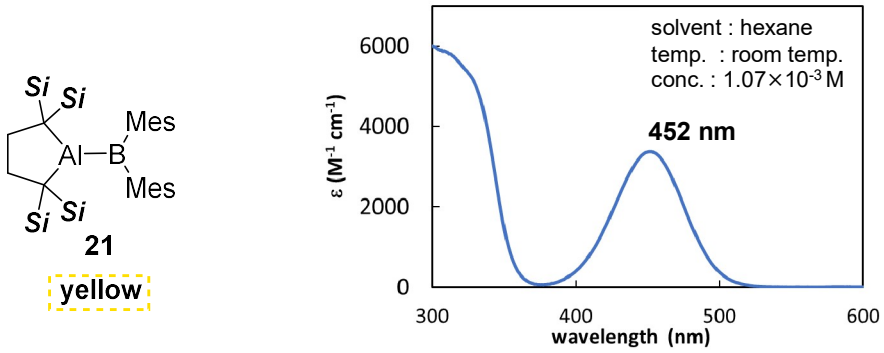

cf. Color of the reported stabilized alumaborane

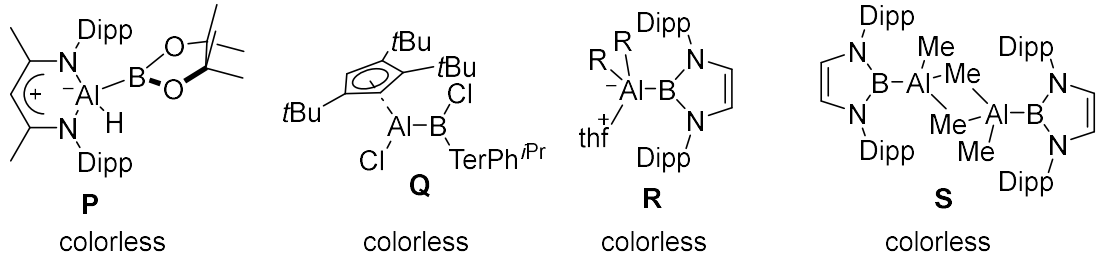

Figure 4-2-5. Optical absorption of alumaborane **21** (in hexane, λ_{max}= 452 nm, ε = 3370), and related electronically stabilized alumaboranes **P-S**.

4-3. Reactivity of (dialkyl)(diaryl)alumaborane

Subsequently, the reactivity of alumaborane **21** were examined (Scheme 4-3-1). The reaction of **21** with DMSO (dimethylsulfoxide) led to a deoxygenation to afford boroxtalumane **23**, in the same manner of the reaction of dialumane **J** with DMSO.[11] The ^{1}H NMR spectrum of **21** exhibited a C_{2v} symmetrical pattern and the ^{11}B NMR signal of **21** resonated at relatively low-field of δ_B 48 ppm, supporting the existence of the B-O bond in **21**. On the other hand, the reaction of **21** with CO afforded **24** in which the C≡O triple bond and the benzylic C-H bond of the Mes group were cleaved. Four Ar-Me signals and two low-field broad signals which are attributable to methine and methylene protons in the ^{1}H NMR spectrum of **24** indicate that -H cleavage of one Me group took place during this reaction. Moreover, a high-field ^{11}B NMR signal at δ_B 51 ppm supports that the oxygen atom binds to the boron atom as observed in the solid state.

Scheme 4-3-1. Reactivity of **21** toward CO and DMSO.

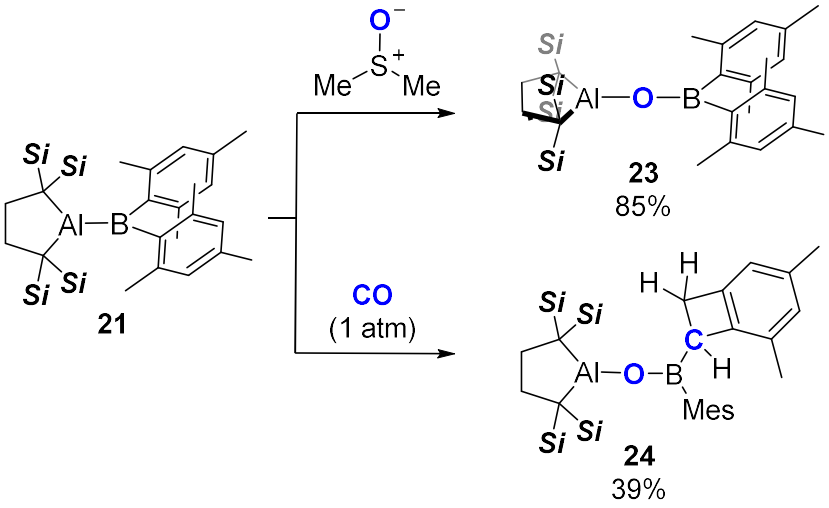

DFT calculations at the M06-2X/6-31+G(d)/PCM (SMD, Benzene)//M06-2X/6-31G(d) level of theory were used to shed light on the details of the mechanism by which **23** is produced from **21** and Me_2S^+–O^-. A schematic illustration of the mechanism and its energy profile are provided in Figure4-3-1. Two possible intermediates, **Int_25** and **Int_26**, were found, in which the negatively charged oxygen atom of Me_2S^+–O^- binds to Al and B atoms to form a four-coordinate aluminate or borate structure. The subsequent 1,2-B-shift from **Int_25** and 1,2-Al-shift from **Int_26** afford the same product (**23**) via $\mathbf{TS_{25\text{-}23}}$ and $\mathbf{TS_{26\text{-}23}}$, in which the migrating boryl or alumanyl group nucleophilically attacks the O atom with concomitant elimination of dimethyl sulfide. The pathway via **Int_25** and $\mathbf{TS_{25\text{-}23}}$ has a lower activation energy than that via **Int_26** and $\mathbf{TS_{26\text{-}23}}$. These results suggest that the Coulomb interaction between the electropositive Al atom and the negatively charged O atom can be expected to contribute to the energetically lower pathway, which is consistent with the preference of the fluoride for the Al atom rather than the B atom in **20**.

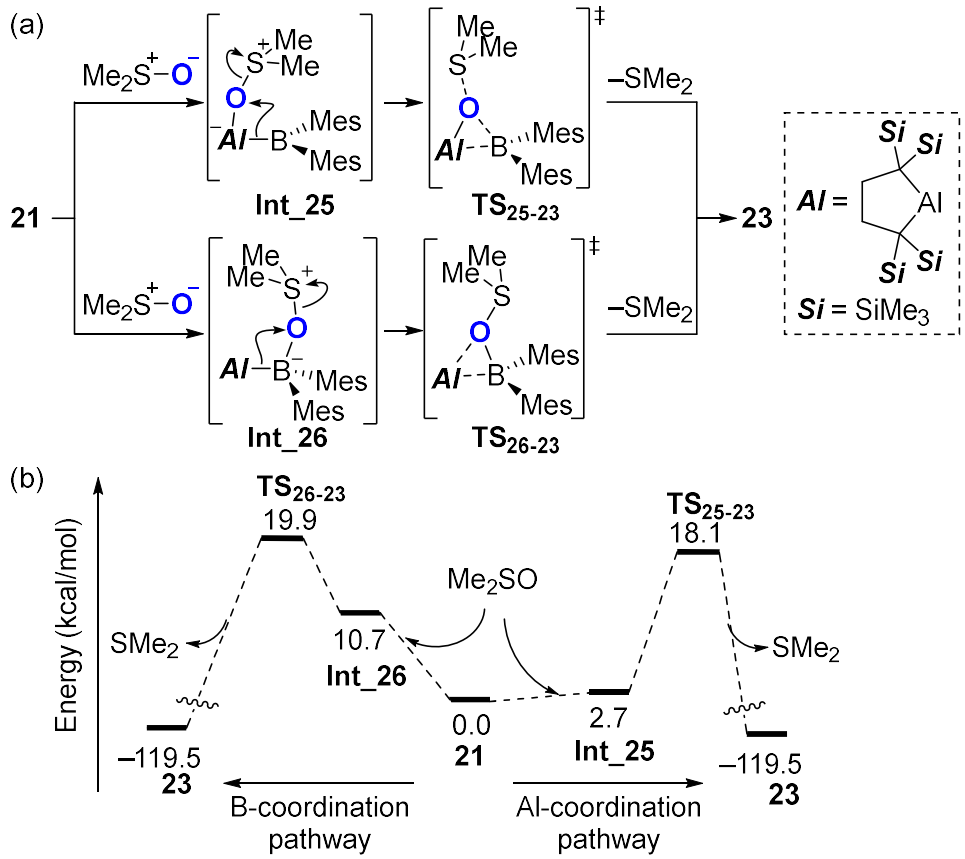

Figure 4-3-1. (a) Schematic illustration of the DFT-based reaction mechanism for the formation of **24** from **21**; (b) energy profile.

A schematic representation of the DFT-based mechanism and its energy profile for the reaction of **21** with CO to form **23** is summarized in Figure 4-3-2. Coordination of CO to **21** generates four-coordinate borate intermediate **Int_27**, in which the carbon atom of CO binds to the B atom. A subsequent 1,2-shift of the R_2Al moiety to the C atom of CO furnishes the second intermediate, O--Al interacting (alumanyl)(boryl)ketone **Int_28** via $\mathbf{TS_{27\text{-}28}}$ with an activation energy of 4.3 kcal/mol. It is feasible to assume another pathway via four-coordinate aluminate intermediate **Int_30** and O--B interacting (alumanyl)(boryl)ketone intermediate **Int_31**. However, these intermediates are less stable than **Int_27** and **Int_28**. These results stand in stark contrast to the reaction of **21** with Me_2S^+–$O^–$, which is initiated by O--Al interaction (Figure 4-3-1). These results indicate two characteristics: (i) The relative stability between **Int_27** and **Int_28** is controlled by orbital interactions. i.e., the lone pair on the C atom of CO interacts with the vacant 2p orbital on the B atom in **Int_27** more strongly than with the 3p orbital on the Al atom in **Int_30**. (ii) The Coulomb interactions control the relative stability between **Int_28** and **Int_31**), i.e., the electronegative O atom of the carbonyl group interacts with the electropositive Al atom in **Int_28** more strongly than with the B atom in **Int_31**. The strained structure of **Int_28** induces the cleavage of the Al–C bond to afford boraoxaallene **Int_29** with a negligible barrier, which further undergoes a 1,2-Mes-shift to furnish boraalkene **Int_32** via $\mathbf{TS_{29\text{-}32}}$. The alumoxy group in **Int_32** migrates to the boron atom with assistance from the π-electrons of the Mes group to give borataallene **Int_33** with concomitant formation of a thermodynamically stable B–O bond. Since **Int_33** can be expected to contain a contribution from (aryl)(boryl)carbene, the C atom of **Int_33** deprotonates the benzylic C–H to generate

ortho-quinodimethane **Int_34** via the highest activation energy in this profile (21.1 kcal/mol). The subsequent aromatizing electrocyclic reaction of **Int_34** results in the formation of **23**. Thus, the distinct characteristic Lewis acidity of the B and Al atoms, with the former preferring orbital interaction and the latter favoring Coulomb interaction, would be responsible for the present characteristic pathway to form **23**.

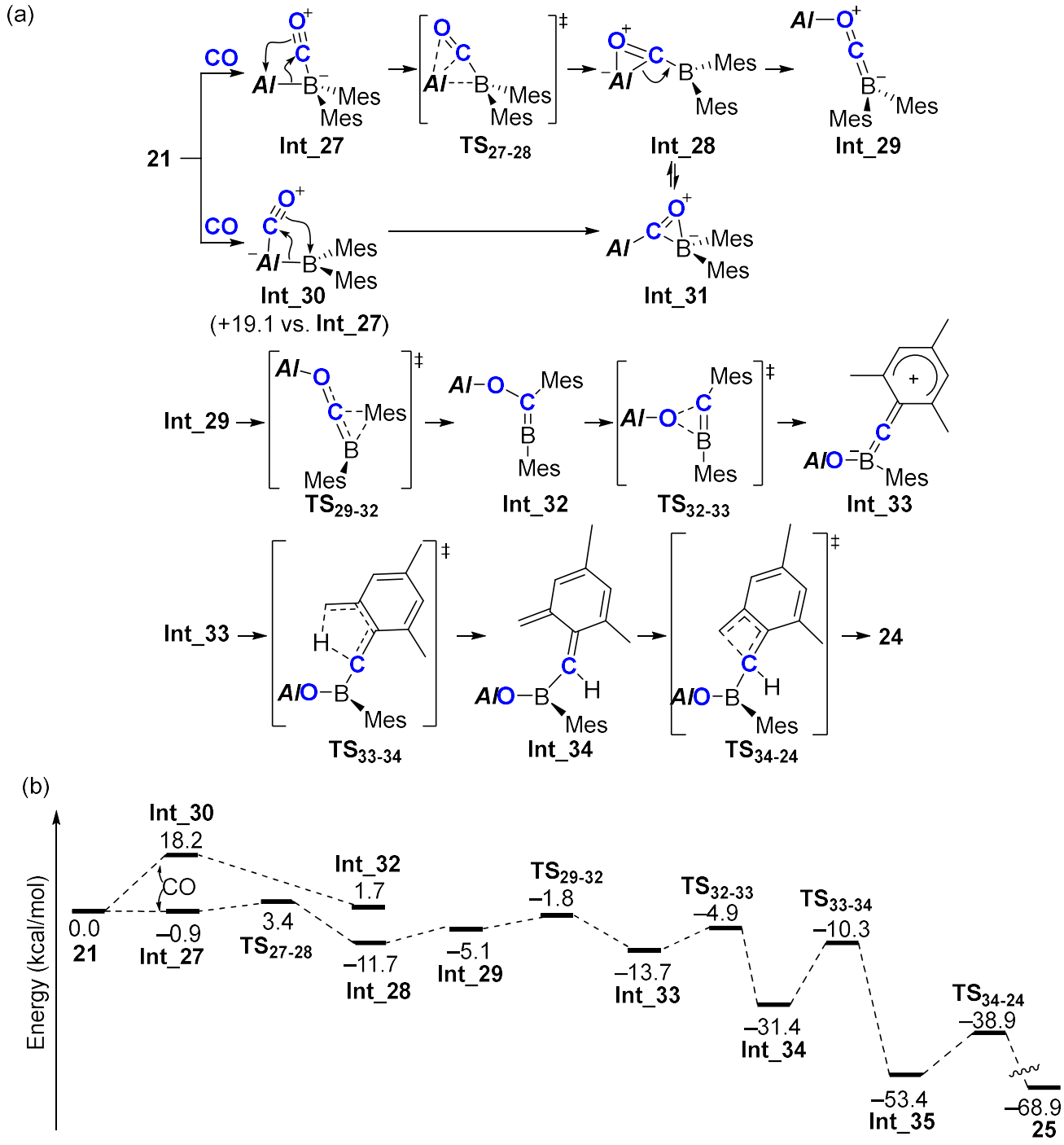

Figure 4-3-2. (a) Schematic illustration of the DFT-based reaction mechanism for the formation of **24** from **21**; (b) energy profile.

In summary, the reaction of the **8** and Mes_2BF Al-B led a formation of Al-B bond and subsequent treatment

of (trimethysilyl)triflate afforded (dialkyl)(diaryl)alumaborane **21**. The character of **21** as electronically non-stabilized A-B bond was revealed by DFT calculations and UV-vis spectrum. the reaction of **21** with DMSO gave deoxygenated compound **23** via formation of four coordinate Al intermediate controlled by orbital interaction. On the other hand, the reaction of **21** with CO gave C≡O triple bond and benzylic C-H bond cleaved compound **24** via formation of four coordinate B intermediate controlled by orbital interaction.

4-4. Supplementally information

Methods

Experimental Section

General

All manipulations involving the air- and moisture-sensitive compounds were carried out under an argon atmosphere using standard Schlenk and glovebox (Korea KIYON) technique. All glassware were dried for 20 min in the 250 °C oven before use. Toluene, hexane, Et_2O, and THF was purified by passing through a solvent purification system (Grass Contour). C_6D_6 were dried by distillation over sodium-benzophenone followed by vacuum transfer. Benzene and pentane were purchased from Kanto chemical (dehydrated) and used in the glovebox without further purification. The nuclear magnetic resonance (NMR) spectra were recorded on JEOL ECS-400 (400 MHz for ^1H, 101 MHz for ^{13}C) or ECZ-600 (600 MHz for ^1H, 151 MHz for ^{13}C). Chemical shifts are reported in ppm relative to the residual protiated solvent for ^1H, deuterated solvent for ^{13}C used as references. The absolute values of the coupling constants are given in Hertz (Hz). Multiplicities are abbreviated as singlet (s), doublet (d), triplet (t), quartet (q), multiplet (m), and broad (br). Melting points were determined on Optimelt (SRS) and were uncorrected. Elemental analyses were performed on a Perkin Elmer 2400 series II CHN analyzer.

Synthesis of 20

In a glovebox, a pre-cooled (–35 °C) toluene solution (2 mL) of **8** (50.0 mg, 84.1 μmol) was added to pre-cooled (–35 °C) toluene solution (6 mL) of Mes_2BF (22.7 mg, 84.1 μmol) in 15 mL vial. After stirring the reaction mixture for several minutes at –35 °C, the reaction mixture was evaporated under reduce pressure. The residue was recrystallized from Et_2O to afford red crystals of **20** (34.4 mg, 70.6 μmol, 84%). ^1H NMR (Figure 4-3-1, 400 MHz, C_6D_6) 0.25(s, 18H, CH_3 of $SiMe_3$), 0.43 (s, 18H, CH_3 of $SiMe_3$), 1.12 (t, 12H, CH_3 of Et_2O), 2.06 (s, 6H, CH_3 of Mes), 2.33 (br, 4H, CH_2), 2.38 (s, 12H, CH_3 of Mes), 3.26 (t, 8H, CH_2 of Et_2O), 6.54 (s, 4H, ArH of Mes), ^{11}B NMR (Figure 4-4-2, 160.5 MHz, C_6D_6) δ 124 (brs), ^{19}F NMR (Figure 4-4-3, 376 MHz, C_6D_6) δ –139 (s); ^{13}C NMR (Figure 4-4-4, 126 MHz, C_6D_6) δ 5.08 ($SiMe_3$), 5.25 ($SiMe_3$), 10.15 (br, 4°), 14.16 (CH_3 of Et_2O), 20.51 (CH_3 of Mes), 26.54 (CH_2), 35.26 (CH_3 of Mes), 65.59 (CH_2 of Et_2O), 128.04 (Ar), 135.47 (Ar, 4°), 135.84 (Ar, 4°), 152.49 (Ar, 4°); mp 141.7-142.2°C (decomp.); Anal. Calcd for $C_{34}H_{62}AlBSi_4FK \cdot 0.5$ (Et_2O) [calculated from ^1H NMR spectrum of vacuumed solid for a long time]: C, 60.37; H, 9.43; Found: C, 60.14; H, 9.50.

Synthesis of 21

In a glovebox, Et_2O solution (2.5 mL) of trimethylsilyl triflate (5.4 mg 24.2 μmol) was added to Et_2O solution (2.5 mL) of **20** (20.0 mg 24.2 μmol) in 3 mL vial. After stirring the reaction mixture for several minutes, the reaction mixture was evaporated under reduce pressure. The residue was recrystallized from hexane to afford yellow crystals of **21** (7.7 mg, 47.5 μmol, 84%). ^1H NMR (Figure 4-4-5, 400 MHz, C_6D_6) 0.17 (s, 36H, CH_3 of $SiMe_3$), 2.13 (s, 6H, CH_3 of Mes), 2.20 (s, 4H, CH_2), 2.29 (s, 12H, CH_3 of Mes), 6.71 (s, 4H, ArH of Mes), ^{11}B NMR (Figure 4-4-6, 376 MHz, C_6D_6) δ 109 (br); ^{13}C NMR (Figure 4-4-7, 126 MHz, C_6D_6) δ 3.33 ($SiMe_3$), 20.19 (br, 4°), 20.62 (CH_3 of Mes), 25.00 (CH_2), 33.49 (CH_3 of Mes), 127.91 (Ar), 135.87 (Ar, 4°), 138.46 (Ar, 4°), 146.90 (Ar, 4°); mp 151.5-

152.0°C (decomp.); HRMS (APCI, negative) Calcd. for $C_{34}H_{62}AlBSi_4$ $[M-H]^-$: 619.3760. Found: 619.3773.

Synthesis of 23

In a glovebox, 10 μL of 0.161 M dimethylsulfoxide in benzene was added to benzene solution (1.6 mL) of **21** (10.0 mg, 16.1 μmol) in 3 mL vial. After stirring the reaction mixture for several minutes, the reaction mixture was evaporated under reduce pressure. The residue was recrystallized from hexane to afford colorless crystals of **23** (8.7 mg, 13.6 μmol, 85%). ^{1}H NMR (Figure 4-4-8, 400 MHz, C_6D_6) 0.17 (s, 36H, CH_3 of $SiMe_3$), 2.13 (s, 6H, CH_3 of Mes), 2.20 (s, 4H, CH_2), 2.29 (s, 12H, CH_3 of Mes), 6.71 (s, 4H, ArH of Mes), ^{11}B NMR (Figure 4-4-9, 160.5 MHz, C_6D_6) δ 48.44 (br); ^{13}C NMR (Figure 4-4-10, 126 MHz, C_6D_6) δ 3.33 ($SiMe_3$), 20.19 (br, 4°), 20.62 (CH_3 of Mes), 25.00 (CH_2), 33.49 (CH_3 of M es), 127.91 (Ar), 135.87 (Ar, 4°), 138.46 (Ar, 4°), 146.90 (Ar, 4°) HRMS (APCI, negative) Calcd. for $C_{34}H_{62}AlBOSi_4$ $[M-H]^-$: 635.3721. Found: 635.3722.

Synthesis of 24

In a glovebox, a benzene solution (1.6 mL) of **21** (10.0 mg, 16.1 μmol) in a 10 mL J-Young tube was brought out from the glovebox, the J-Young tube was degassed by three of freeze (–78 °C)-pump-thaw cycles. Then, gaseous carbon monoxide (1 bar) was backfilled to the J-Young tube. After the reaction mixture was stirred at room temperature for several minutes, volatiles were removed from the resulting solution under reduced pressure. Purification of the residue by recrystallization with hexane afforded colorless crystals of **24** (4.1 mg, 6.3 μmol, 39%).^{1}H NMR (Figure 4-4-11, 400 MHz, C_6D_6) 0.15(s, 18H, CH_3 of $SiMe_3$), 0.20 (s, 18H, CH_3 of $SiMe_3$), 1.73 (s, 3H, CH_3 of Mes), 1.73-1.93 (m, 4H, CH_2), 2.03 (s, 3H, CH_3 of Mes), 2.15 (s, 3H, CH_3 of Mes), 2.22 (s, 3H, CH_3 of Mes), 2.42 (s, 3H, CH_3 of Mes), 3.43 (br, 2H, CH_2 of benzyl), 3.43 (br, 1H, CH), 6.61 (s, 1H, ArH), 6.69 (s, 1H, ArH), 6.61 (s, 2H, ArH of Mes) ^{11}B NMR (Figure 4-3-12, 160.5 MHz, C_6D_6) δ 51.74 (br); ^{13}C NMR (Figure 4-4-13, 126 MHz, C_6D_6) δ 3.33 ($SiMe_3$), 20.19 (br, 4°), 20.62 (CH_3 of Mes), 25.00 (CH_2), 33.49 (CH_3 of M es), 127.91 (Ar), 135.87 (Ar, 4°), 138.46 (Ar, 4°), 146.90 (Ar, 4°); mp 74.4-76.4°C (decomp.); Anal. Calcd for $C_{35}H_{62}AlBOSi_4$: C, 64.77; H, 9.63; Found: C, 64.78; H, 9.93.

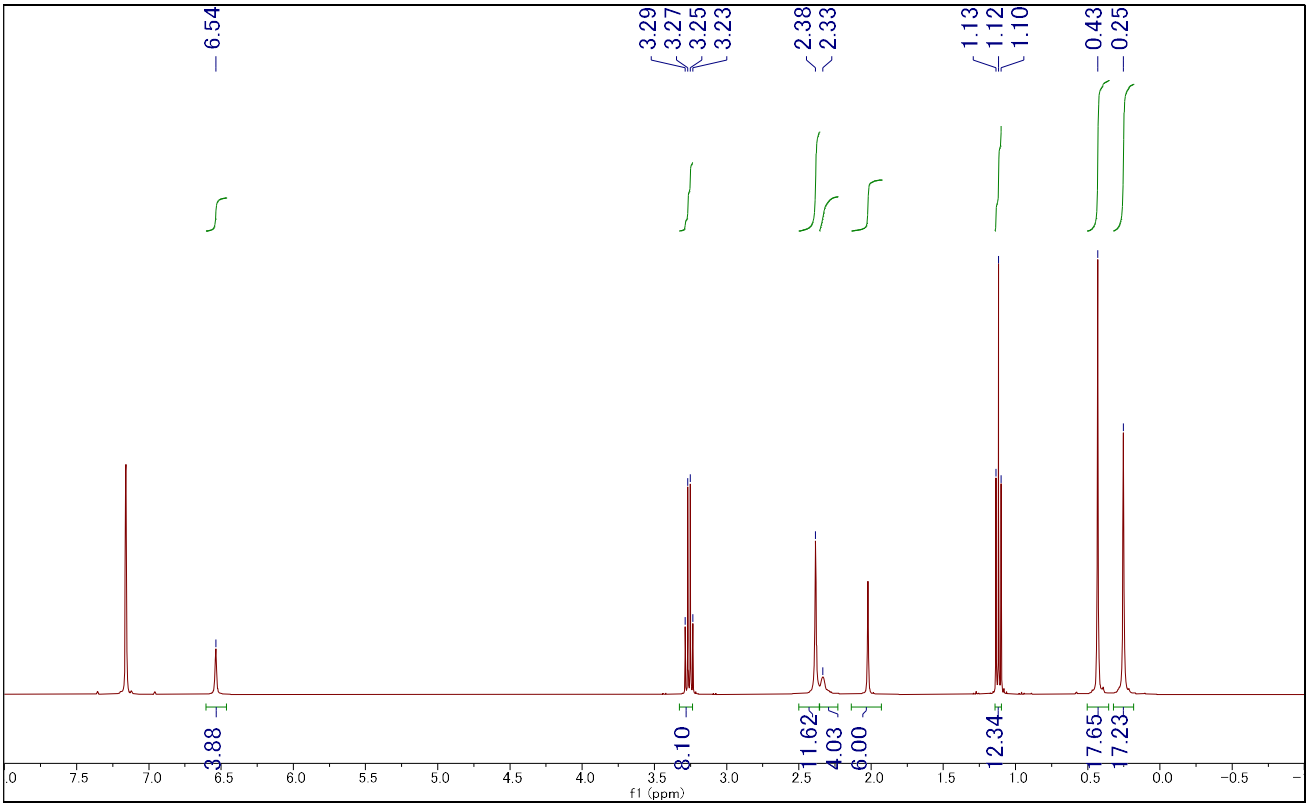

Figure 4-4-1. ^{1}H NMR spectrum of (boryl)(fluoro)aluminate **20**.

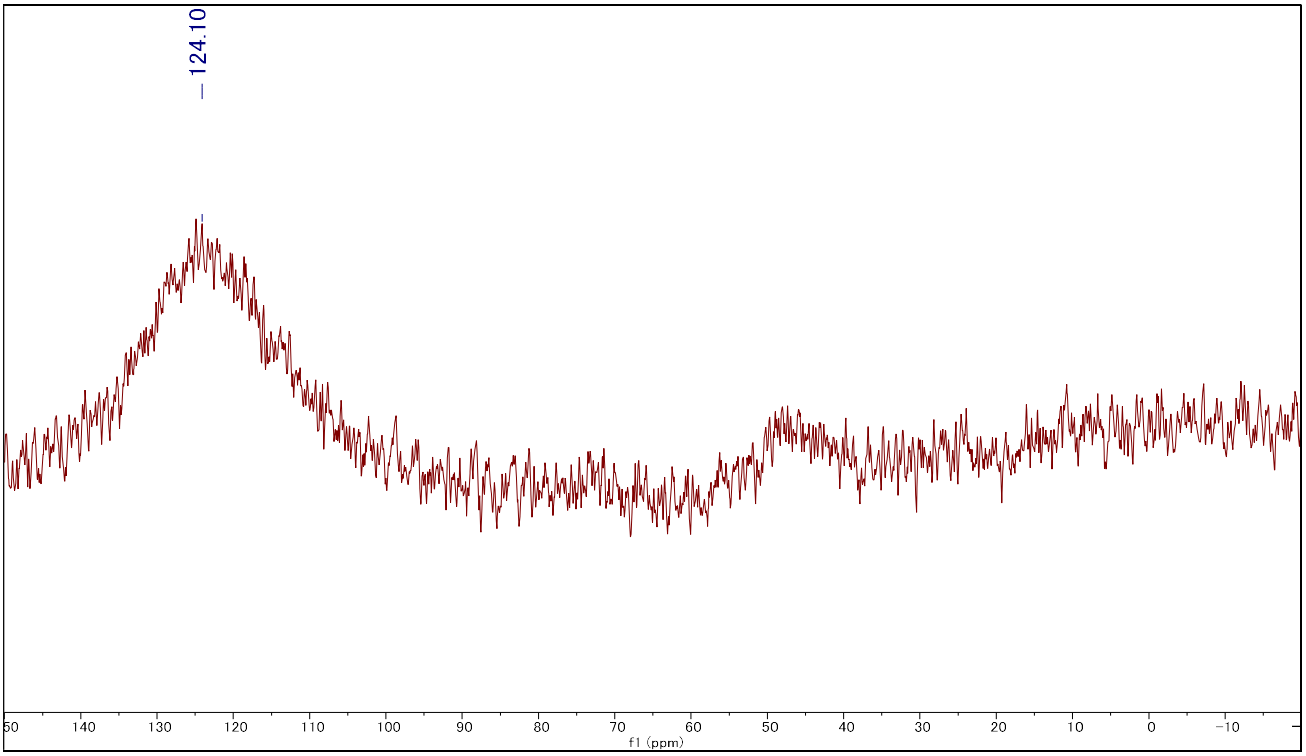

Figure 4-4-2. ^{11}B NMR spectrum of (boryl)(fluoro)aluminate **20**.

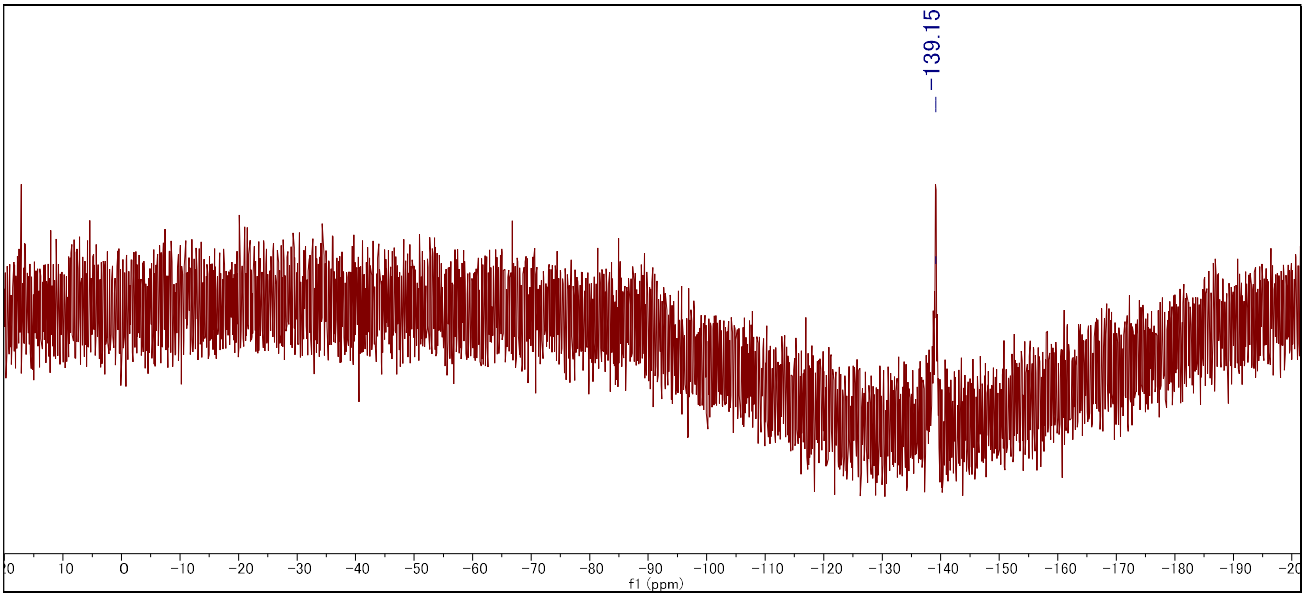

Figure 4-4-3. ^{19}F NMR spectrum of (boryl)(fluoro)aluminate **20**.

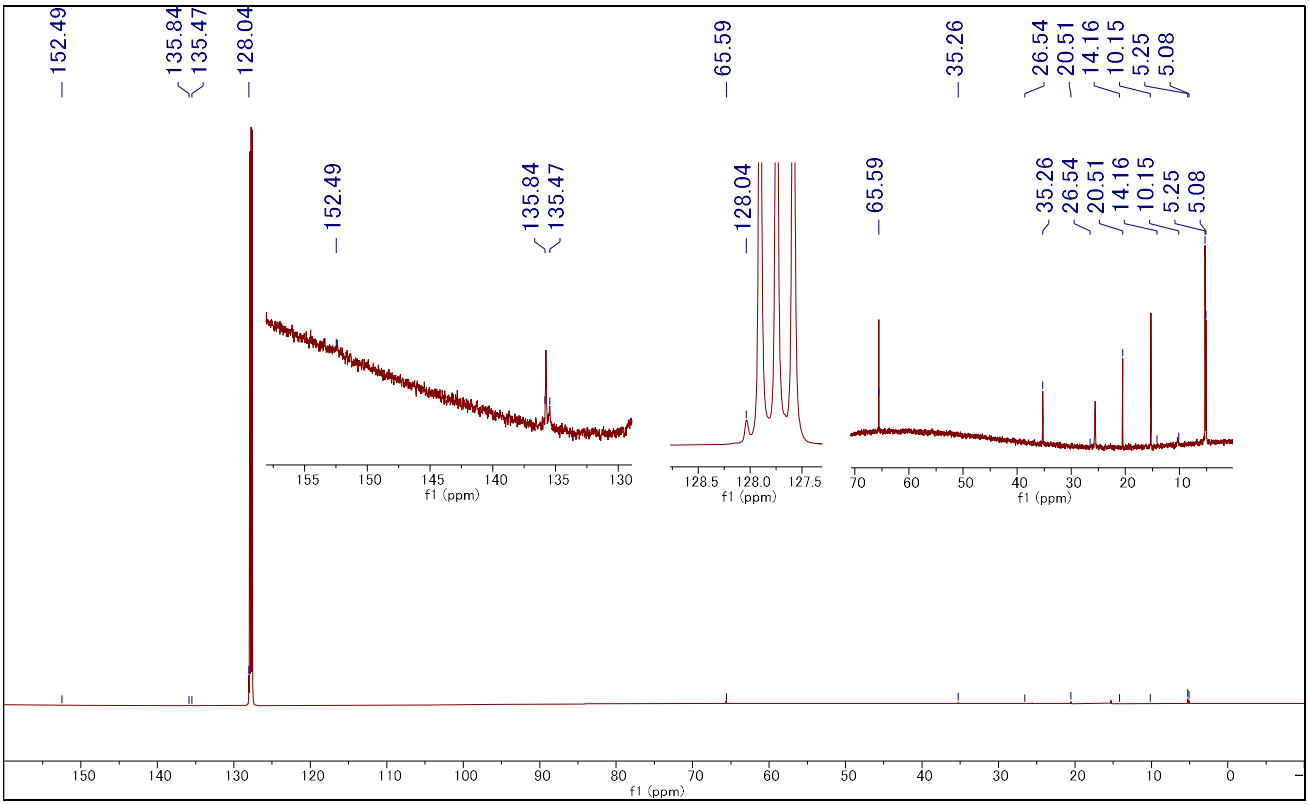

Figure 4-4-4. ^{13}C NMR spectrum of (boryl)(fluoro)aluminate **20**

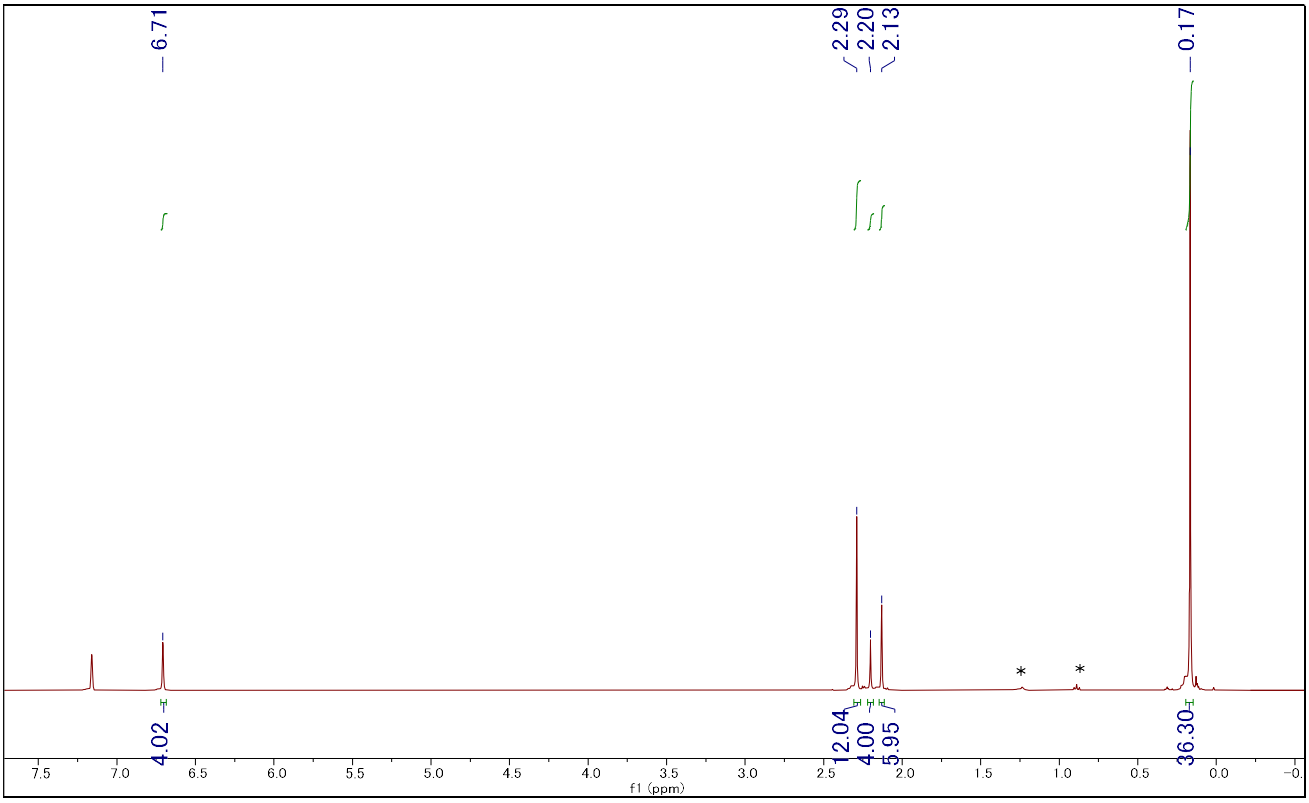

Figure 4-4-5. ^{1}H NMR spectrum of (dialkyl)(diaryl)alumaborane **21**.

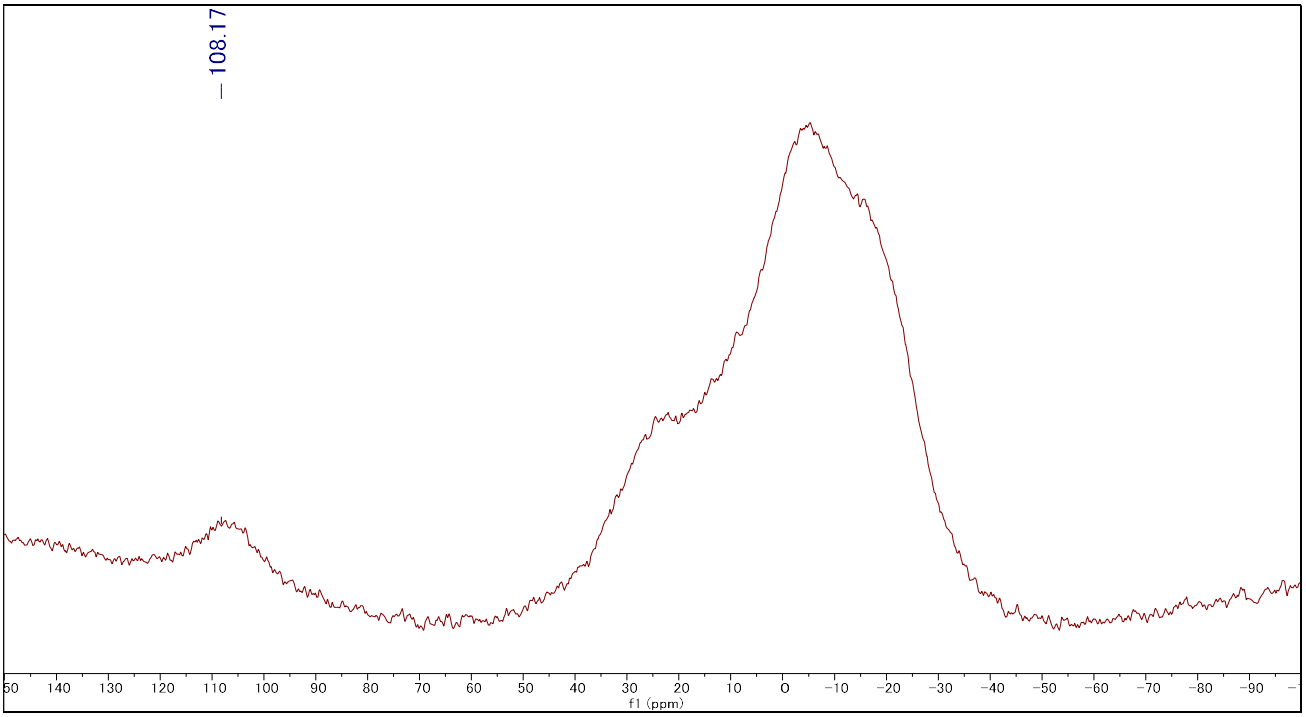

Figure 4-4-6. ^{11}B NMR spectrum of (dialkyl)(diaryl)alumaborane **21**.

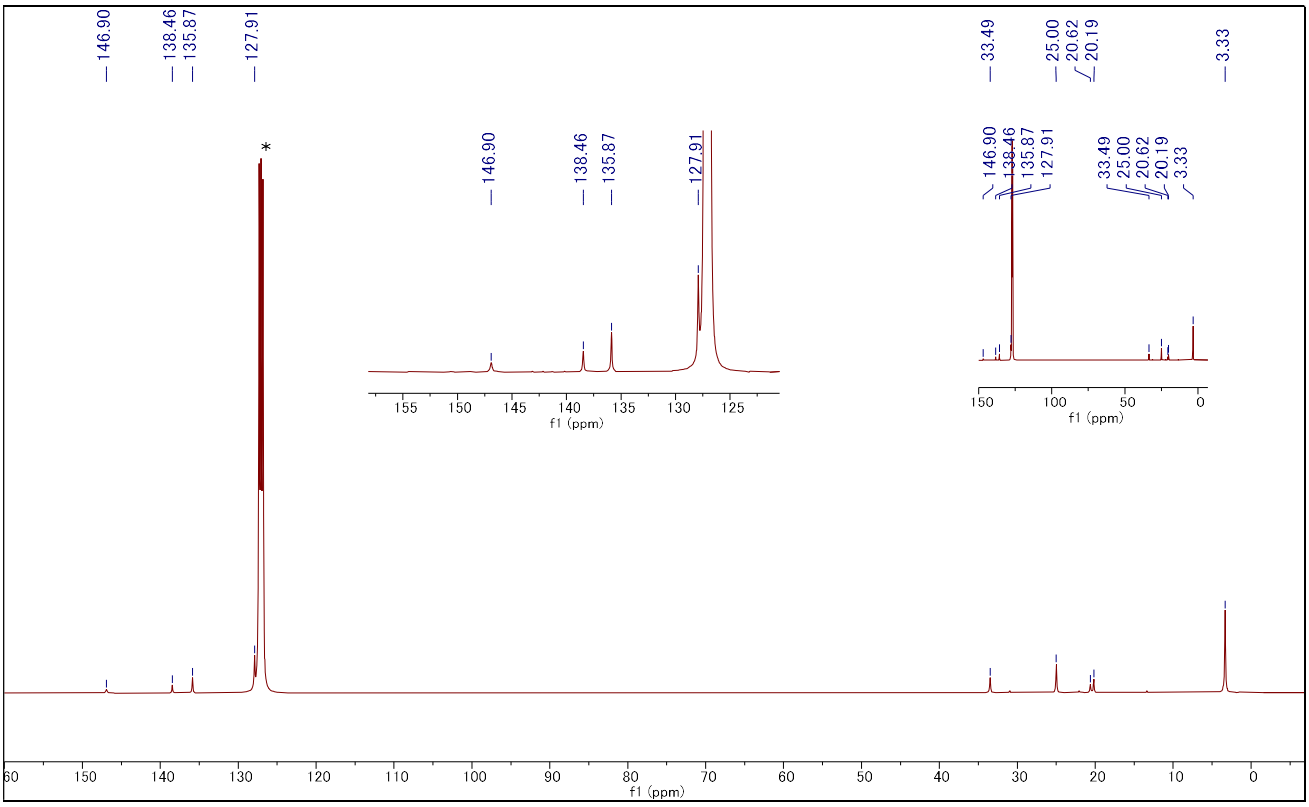

Figure 4-4-7. ^{13}C NMR spectrum of (dialkyl)(diaryl)alumaborane **21**.

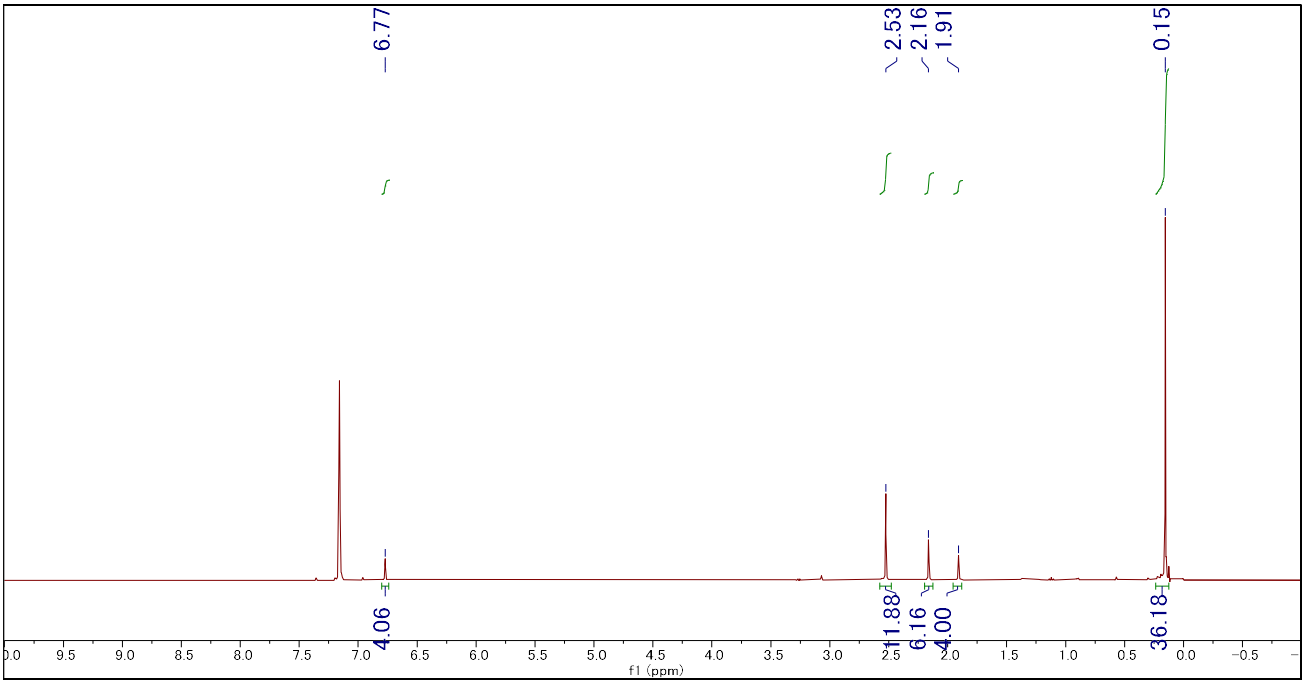

Figure 4-4-8. ^{1}H NMR spectrum of **23**.

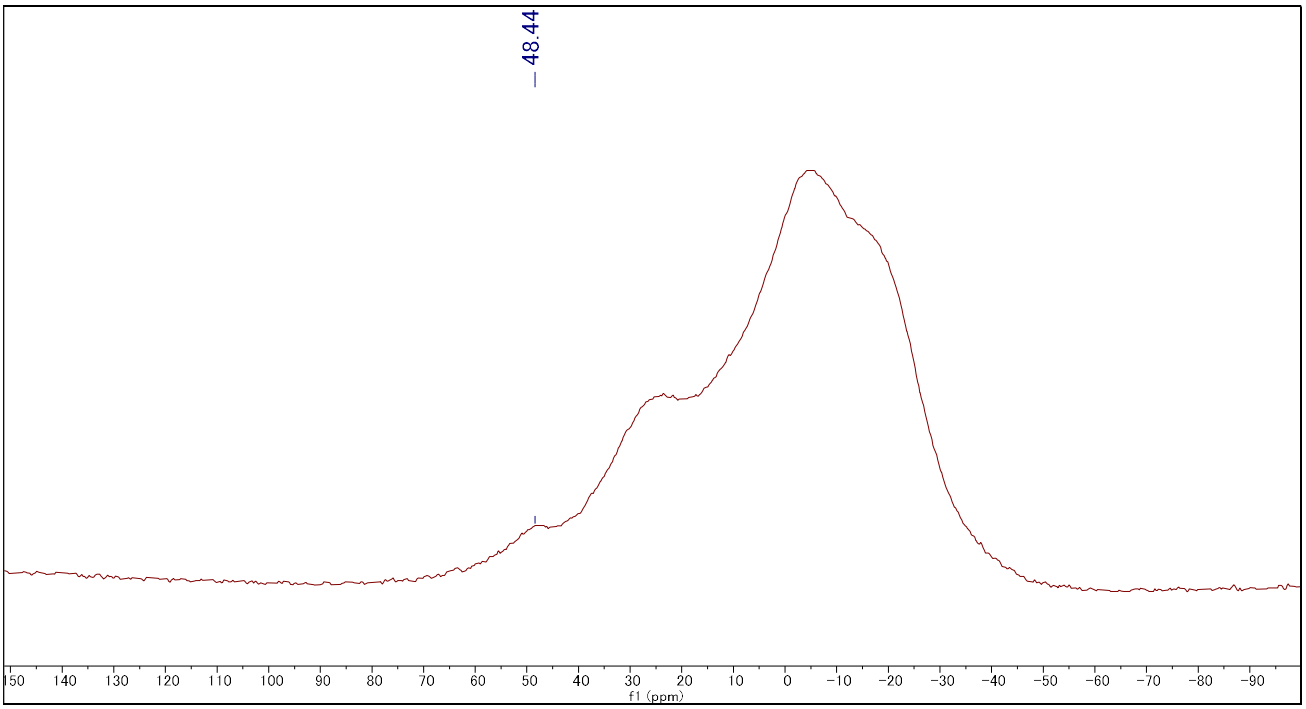

Figure 4-4-9. ^{11}B NMR spectrum of **23**.

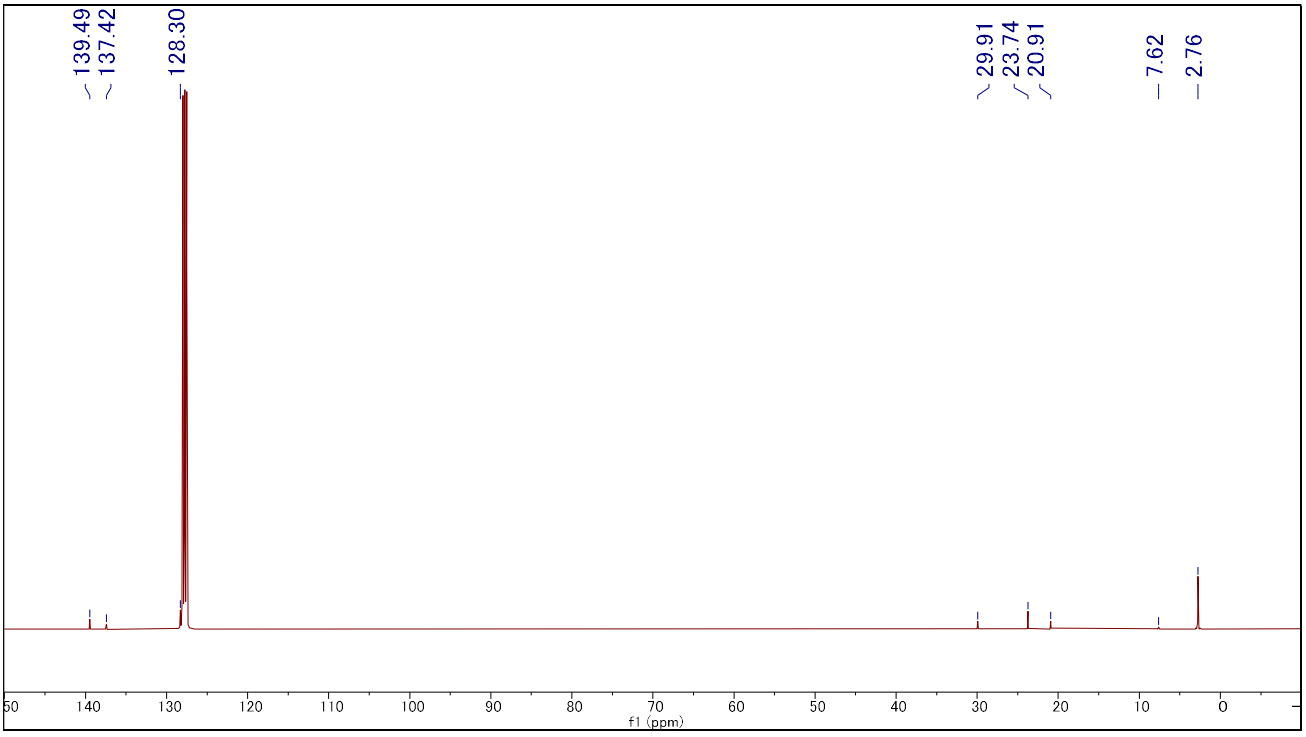

Figure 4-4-10. ^{13}C NMR spectrum of **23**.

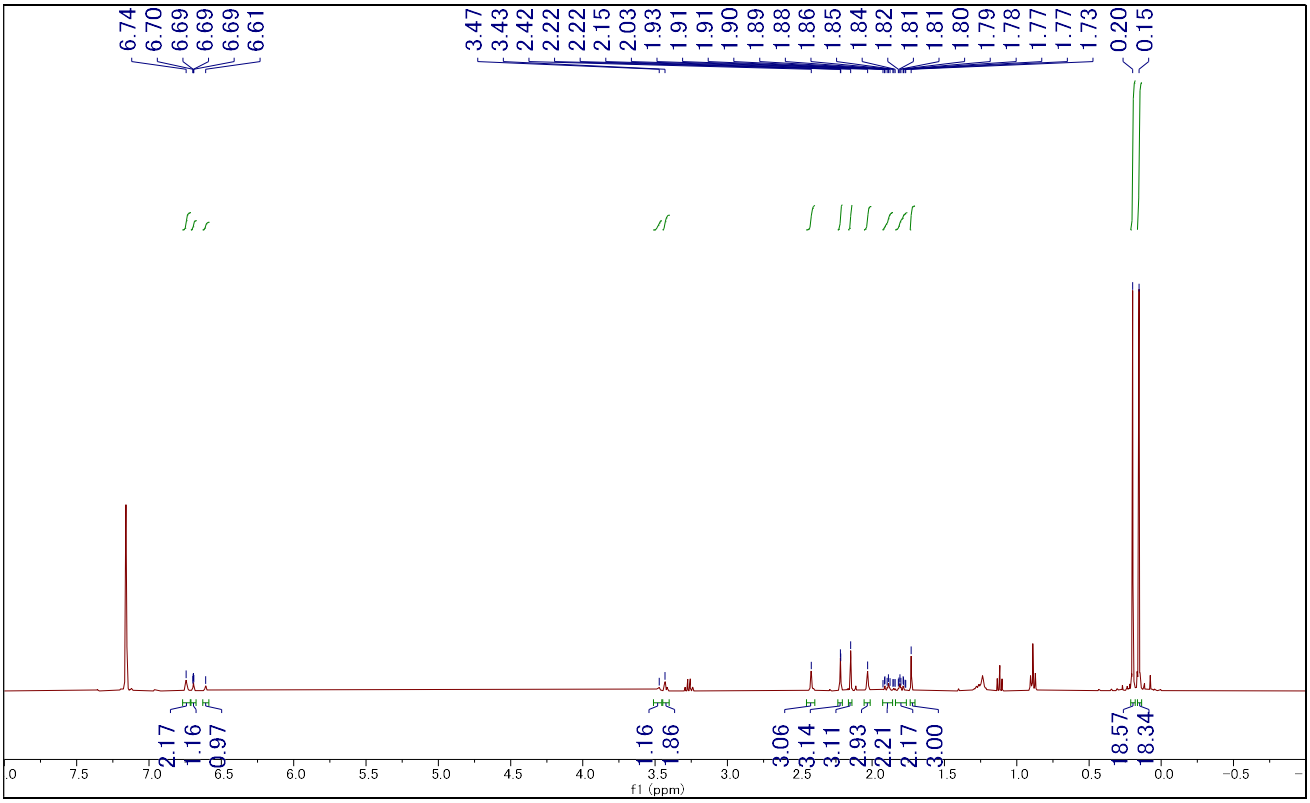

Figure 4-4-11. ^{1}H NMR spectrum of **24**.

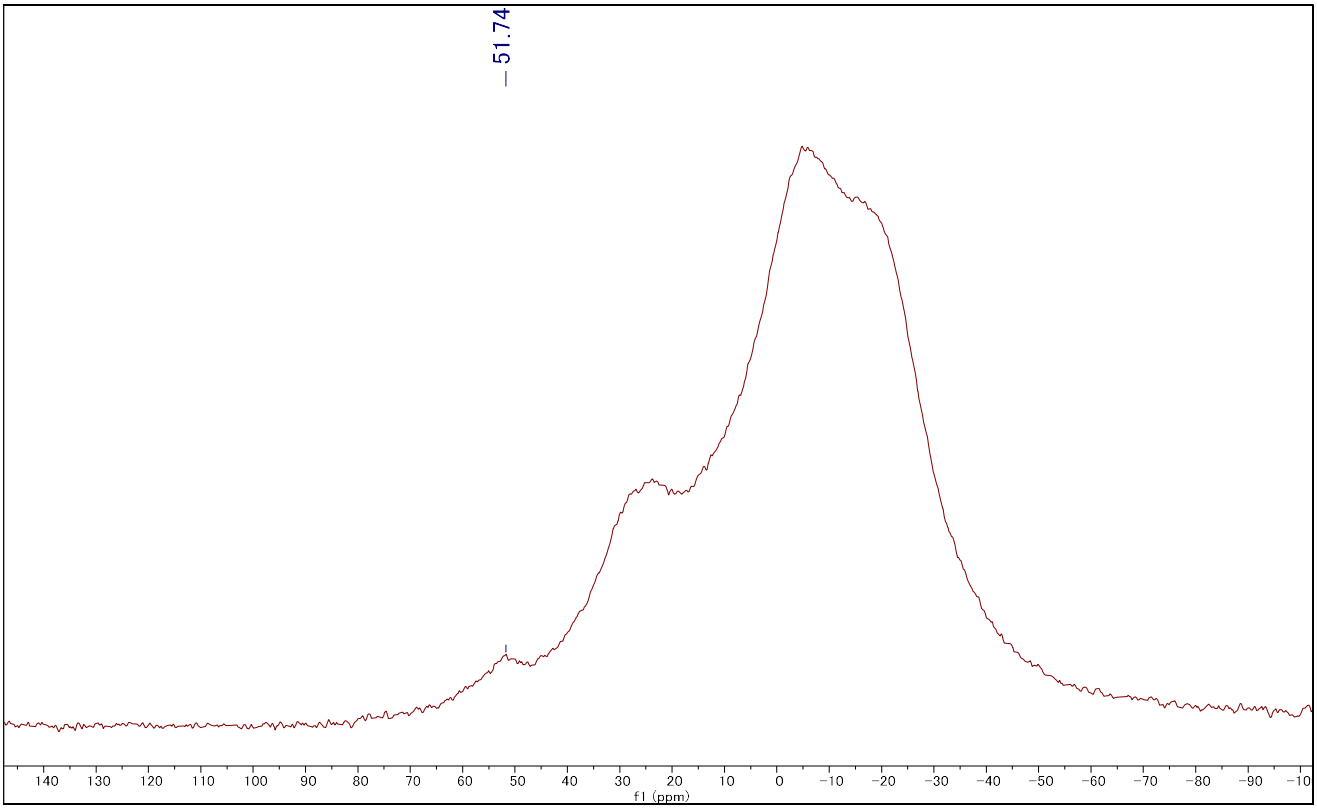

Figure 4-4-12. ^{11}B NMR spectrum of **24**.

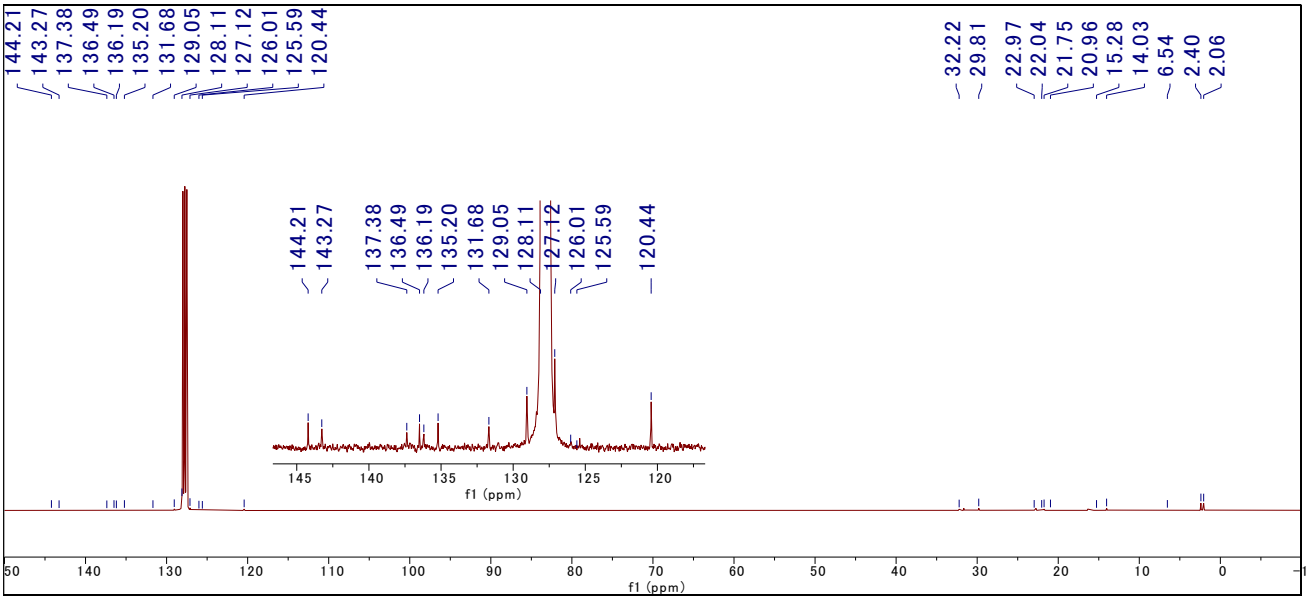

Figure 4-4-13. ^{13}C NMR spectrum of **24**.

Electrochemical measurement

Due to the instability of alumaborane **21** in THF (decomposition product was not identified), all electrochemical measurement was performed in CH_2Cl_2 solvent. As the cyclic voltammogram in Figure 4-4-14 shows irreversible reduction wave, the one-electron reduction seems to form unstable radical anion species under the present condition. Therefore, the reduction potentials of **K** and **21** in CH_2Cl_2 were estimated by differential pulse voltammetry (Figure 4-4-15).

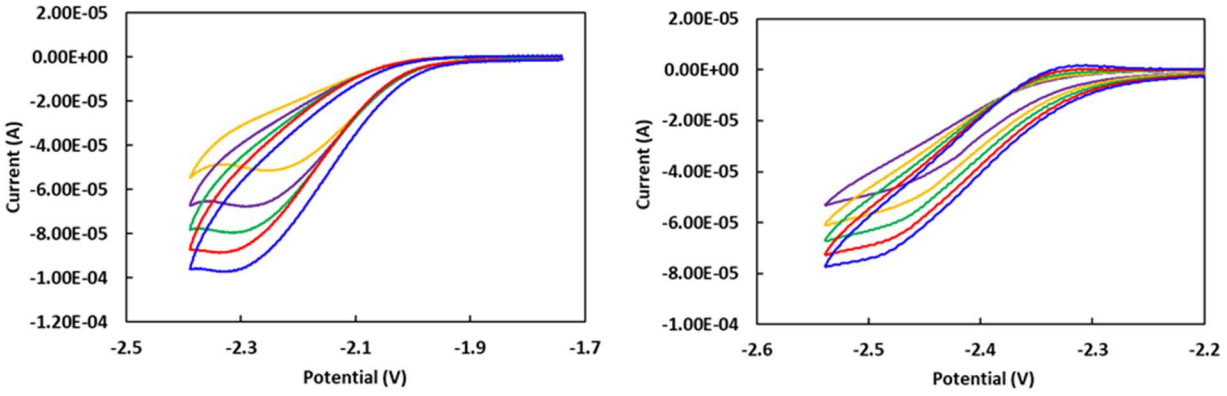

Figure 4-4-14. Cyclic voltammetry of **K** (left) and **21** (right) in CH_2Cl_2 (electrolyte: 100 mM [nBu$_4$N][PF$_6$], working: glassy carbon, reference: Ag/Ag$^+$, counter: Pt wire, potentials were compensated with Cp_2Fe/Cp_2Fe^+ redox couple; yellow: 100 mV/s, purple: 200 mV/s, green: 300 mV/s, red: 400 mV/s, blue: 500 mV/s).

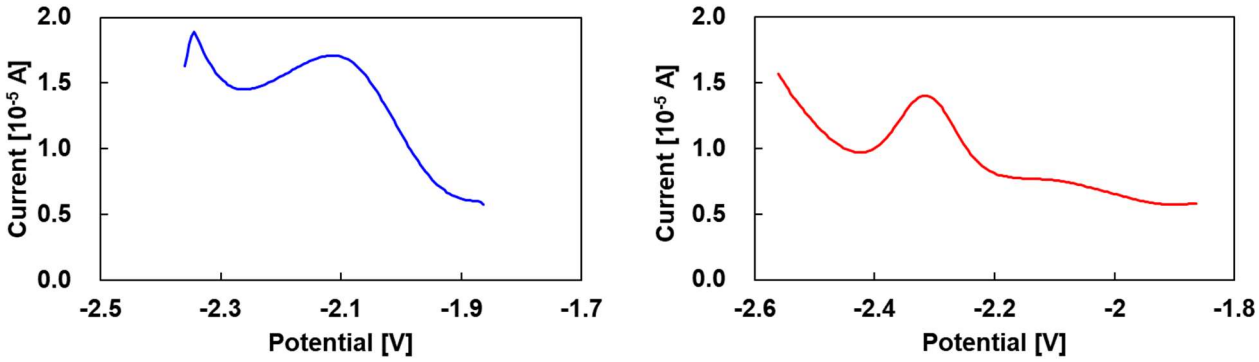

Figure 4-4-15. Differential pulse voltammetry of **K** (left) and **21** (right) in CH_2Cl_2 (electrolyte: 100 mM [*n*Bu_4N][PF_6], working: glassy carbon, reference: Ag/Ag^+, counter: Pt wire, potentials were compensated with Cp_2Fe/Cp_2Fe^+ redox couple).

Details for X-ray crystallography

Crystallographic data for **20**,**21, 23** and **24** are summarized in Table 4-4-1. The crystals were coated with immersion oil and put on a MicroMountTM (MiTeGen, LLC), and then mounted on diffractometer. Diffraction data were collected on a Rigaku Saturn CCD or a Bruker Photon detectors using MoKa radiation. The Bragg spots were integrated using CrysAlisPro program package. Absorption corrections were applied. All the following procedure for analysis, Yadokari-XG 2009 was used as a graphical interface. The structure was solved by a direct method with programs of SIR2014 and refined by a full matrix least squares method with the program of SHELXL-2018. Anisotropic temperature factors were applied to all non-hydrogen atoms. The hydrogen atoms were put at calculated positions, and refined applying riding models. The detailed crystallographic data have been deposited with the Cambridge Crystallographic Data Centre: Deposition code CCDC 2150710-2150713. A combined CIF file for the data of **2-5** can be obtained free of charge via http://www.ccdc.cam.ac.uk/products/csd/request.

Table S1. Crystallographic data and structure refinement details for **20**,**21, 23** and **24**.

Compound #	**20**	**21**	**23**	**24**
CCDC deposit #	2150710	2150711	2150712	2150713
Empirical formula	$C_{42}H_{82}AlBFKO_2Si_4$	$C_{34}H_{62}AlBSi_4$	$C_{34}H_{62}AlBOSi_4$	$C_{35}H_{62}AlBOSi_4$
Formula weight	827.32	620.98	636.98	648.99
T(K)	93(2)	93(2)	93(2)	93(2)
λ (Å)	0.71073	0.71073	0.71073	0.71073
Crystal system	*Monoclinic*	*Monoclinic*	*orthorhombic*	*triclinic*
Space group	$P2_1/n$	$P2_1/n$	*Pbcn*	*P-1*
a (Å)	15.8257(3)	18.6697(3)	20.2943(5)	11.3759(8)
b (Å)	15.7429(3)	13.8780(3)	10.8089(3)	17.1548(12)
c (Å)	20.4670(5)	29.5679(7)	17.6889(6)	20.7830(15)
α (°)	90	90	90	101.190(6)
β (°)	98.088(2)	94.637(2)	90	97.256(6)
γ (°)	90	90	90	90.382(6)
V(Å^3)	5048.48(19)	7635.9(3)	3880.2(2)	3944.8(5)
Z	4	8	4	4
D_{calc}, (g/m^3)	1.088	1.080	1.090	1.093

μ (mm^{-1})	0.252	0.200	0.200	0.198
F(000)	1808	2720	1392	1416
Crystal size (mm)	0.41 × 0.39 × 0.38	0.32 × 0.16 × 0.09	0.10 × 0.09 × 0.08	0.24 × 0.16 × 0.08
2θ range (°)	1.6260-30.8030	2.2320-32.5260	2.1180-30.5820	2.1360-30.5770
reflns collected	13034/	19587	4362	16387
Indep reflns/R_{int}	10013/0.0420	14404/0.0592	3737/0.0446	13811/0.0446
param	491	757	196	791
GOF on F^2	1.027	1.034	1.058	1.088
R_1,[a] wR_2[b] [I>2σ(I)]	0.0469, 0.1221	0.0430, 0.1087	0.0443, 0.1293	0.1195, 0.2904
R_1,[a] wR_2[b] (all data)	0.0666, 0.1338	0.676, 0.1227	0.0561, 0.1381	0.1386, 0.3050

[a] $R_1 = \Sigma \, ||Fo| - |Fc|| \, / \, \Sigma \, |Fo|$, [b] $wR_2 = [\Sigma \, [w(Fo^2 - Fc^2)^2 / \Sigma \, w(Fo^2)^2]]^{1/2}$

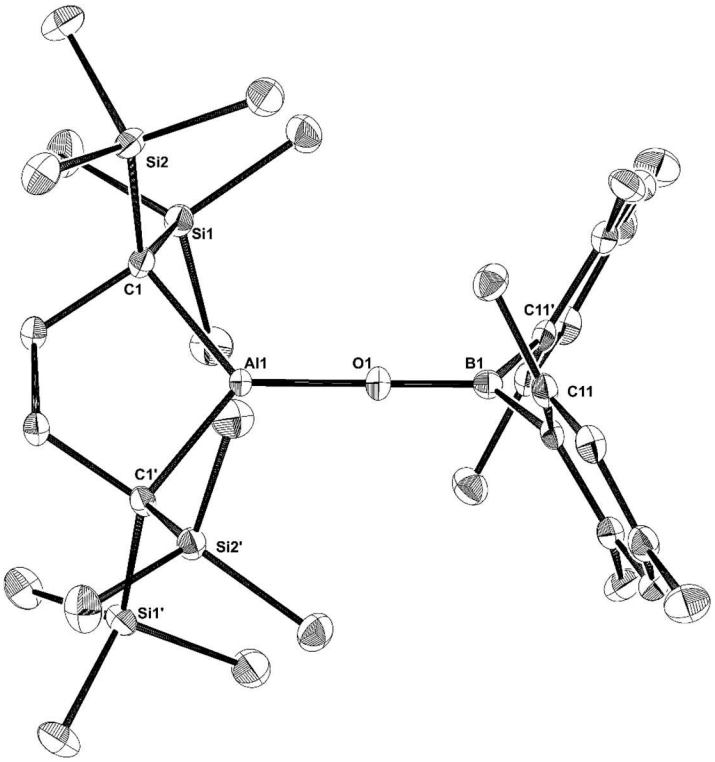

Figure 4-4-16 Crystal structure of **23** with thermal ellipsoids at 50% probability; hydrogen atoms have been omitted for clarity.

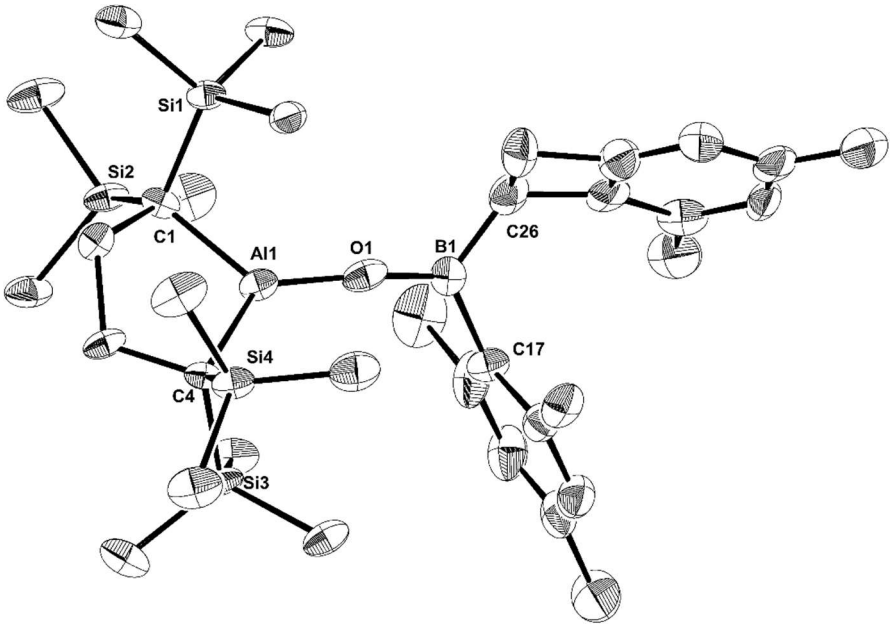

Figure 4-4-17 Crystal structure of **24** with thermal ellipsoids at 50% probability; hydrogen atoms have been omitted for clarity.

4-4. Reference

1. Tsukahara, N.; Asakawa, H.; Lee, K.-H.; Lin, Z.; Yamashita, M.,. *J. Am. Chem. Soc.* **2017**, *139*, 2593-2596.
2. Asakawa, H.; Lee, K.-H.; Lin, Z.; Yamashita, M., *Nat. Commun.* **2014**, *5*, 4245.
3. Moezzi, A.; Olmstead, M. M.; Bartlett, R. A.; Power, P. P. *Organometallics* **1992**, *11*, 2383–2388.
4. Shoji, Y.; Tanaka, N.; Ikabata, Y.; Sakai, H.; Hasobe, T.; Koch, N.; Nakai, H.; Fukushima, T., *Angew. Chem. Int. Ed*. **2022**, *In Press*.
5. Uhl, W. *Naturfor*, **1988**, *43b*, 1113–1118.
6. Wehmschulte, R. J.; Ruhlandt-Senge, K.; Olmstead, M. M.; Hope, H.; Sturgeon, B. E.; Power, P. P. *Inorg. Chem.* **1993**, *32*, 2983–2984.
7. Chu, T.; Korobkov, I.; Nikonov, G. I., *J. Am. Chem. Soc.* **2014**, *136*, 9195-9202.
8. Hofmann, A.; Pranckevicius, C.; Tröster, T.; Braunschweig, H., *Angew. Chem. Int. Ed.* **2019**, *58*, 3625-3629.
9. (a) Dettenrieder, N.; Dietrich, H. M.; Schädle, C.; Maichle-Mössmer, C.; Törnroos, K. W.; Anwander, R., *Angew. Chem. Int. Ed.* **2012**, *51*, 4461-4465; (b) Dettenrieder, N.; Schädle, C.; Maichle-Mössmer, C.; Anwander, R., R *Dalton Trans.* **2014**, *43*, 15760-15770.
10. Erdmann,P.; Leitner, J.; Schwarz, J.; Greb, L., *ChemPhysChem* **2020**, *21*, 987-994.
11. Uhl, W.; Koch, M.; Hiller, W.; Heckel, M. *Angew. Chem. Int. Ed*. **1995**, *34*, 989–990.

Chapter 5:
Conclusion

I developed the chemistry of alkyl-substituted alumanyl anion. In chapter 2, the alkyl-substituted alumanyl anion **8** was synthesized from bissilylethylene **3** in 4 steps. Moreover, the electronic structure of **8** possessing unperturbed lone-pair and vacant 3p-orbital on aluminum atom was revealed by combination of DFT calculations and UV-vis spectrum. In chapter 3, the reactivities of **8** were examined. Nucleophilic substitution was performed in the reaction with MeOTf. On the other hand, the reaction of **8** with C_6F_6 gave 1,4-dialuminated compound **12**. In this reaction, it was considered that the aluminuidyl moiety, which is introduced by the first C-F oxidative addition, accelerates the second oxidative addition. Furthermore, the reaction of **8** with benzene or toluene afforded C-H cleaved compounds. The kinetic study and DFT calculations revealed the mechanism as hydride-eliminating S_NAr reaction of **8**. In chapter 4, the synthesis of (dialkyl)(diaryl)alumaborane **21** via nucleophilic Al-B bond formation of **8** was performed. DFT calculations revealed the electronic structure of **21** possessing overlapped vacant 3p- and 2p-orbital. The reaction of **21** with CO gave C≡O triple bond and benzylic C-H bond cleaved compound **23** via formation of four coordinate boron intermediate controlled by orbital interaction, whereases the reaction of **21** with DMSO gave deoxygenated compound **24** via formation of four coordinate Al intermediate controlled by orbital interaction.

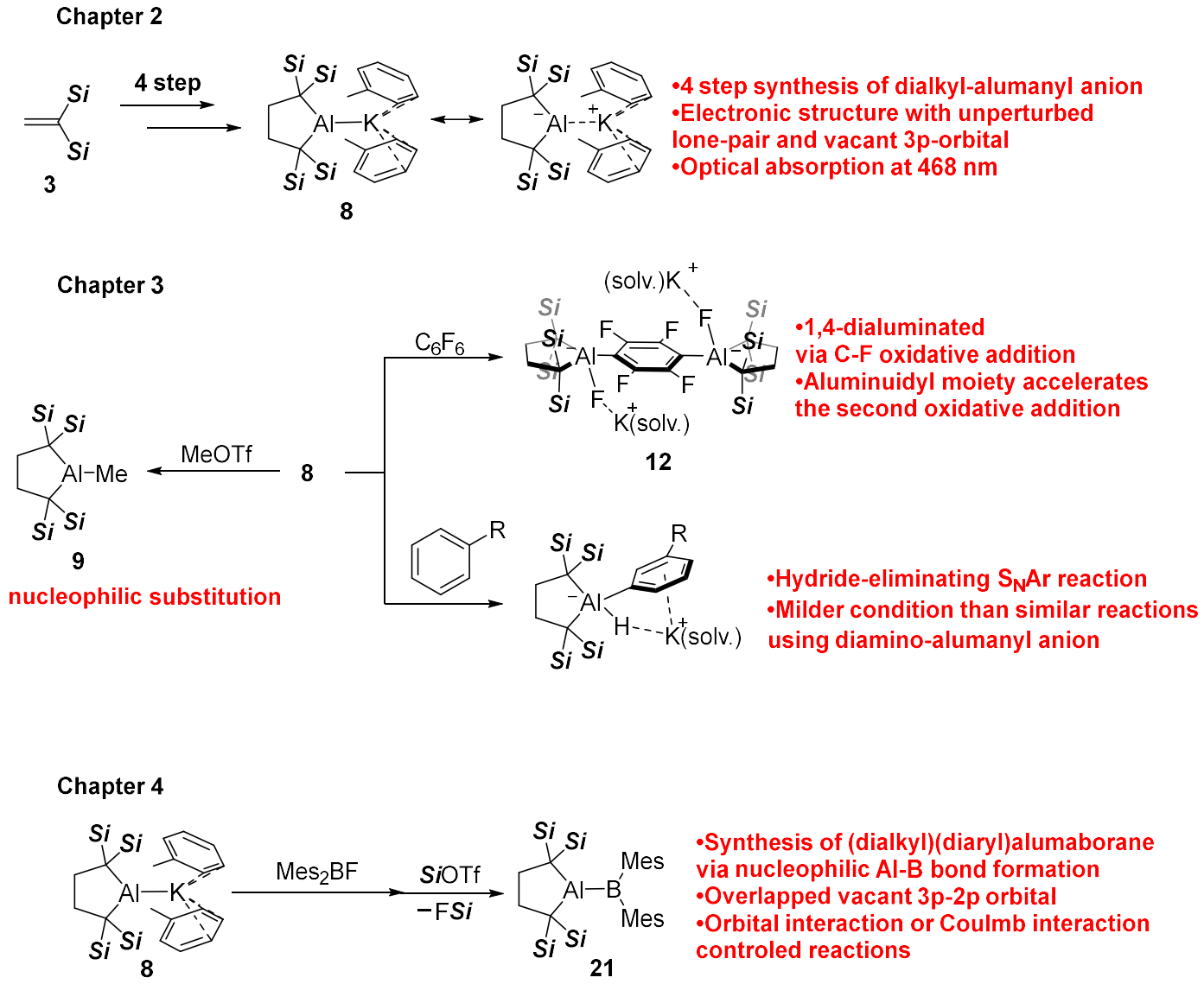

Figure 5-1. Conclusion of this doctoral thesis.

Publication List

1. Kurumada, S.; Takamori, S.; Yamashita, M. An Alkyl-Substituted Aluminium Anion with Strong Basicity and Nucleophilicity. *Nat. Chem.* **2020**, *12*, 36–39.

2. Kurumada, S.; Sugita, K.; Nakano, R.; Yamashita, M. A Meta-Selective C−H Alumination of Mono-Substituted Benzene by Using An Alkyl-Substituted Al Anion through Hydride-Eliminating SNAr Reaction. *Angew. Chem. Int. Ed.* **2020**, *59*, 20381–20384.

3. Kurumada, S.; Yamashita, M. A Tetraorganyl-Alumaborane with An Al–B σ-Bond and Two Adjacent Lewis-Acidic Centers. *J. Am. Chem. Soc.* **2022**, *144*, 4327–4332.

Acknowledgement

All the works have been performed under supervision of Prof. Makoto Yamashita. from 2016 to 2017 in Chuo university, and from 2017 to 2022 in Nagoya university. I gratefully appreciate for his persistent discussion, finding, and encouragement.

I am very grateful to my Ph.D. dissertation committee Prof. Hiroshi Shinokubo, Prof. Takeaki Iwamoto, and Prof. Hajime Ito. I would like to thank both for their valuable suggestions for my work.

I would like to thank Dr. Kengo Sugita, who developed the chemistry of alkyl-substituted alumanyl anion together, and Mr. Shuhei Takamori, who firstly confirmed the generation of alkylene dianion in Et_2O solution.

I would like to thank Dr. Jun-ichi Ito, Dr, Ryo Nakano, and Dr, Katsunori Suzuki for the usual discussion and encouragement.

I would like to thank Dr. Koji Kubota (Hokkaido university, ICReDD), and Dr. Hideto Ito for the technical support of mechanochemistry.

I would like to thank Dr. Shintaro Ishida (Tohoku university) for ^{27}Al NMR measurement, and Dr. Yoshitaka Aramaki for supporting measurement of NMR spectra and single-crystal X-ray structural analysis.

I would like to thank all awesome of Yamashita group members: Dr. Feng Genfeng, Mr. Ding Tao, Ms. Tomomi Kato, Mr. Shinnosuke Takegasa. Mr, Ryotaro Yamanashi, Mr. Takaya Kaneiwa, Mr. Yoshiki Sugano, Mr. Kei Tokuhiro, Mr. Kota Matsubara, Mr. Masahiro Yamamoto, Mr. Takayoshi Yoda, Mr. Naoto Uno, Mr. Hiroki Tanaka, Mr. Ryunosuke Fujita, Mr. Noriyuki Funasoko, and all alumni members.

Finally, I appereciates Hiroshi Kurumada, Namie Kurumada, Nana Kurumada and Saki Moro-oka for kind assistance and financial for a long student life.

March 2022

Satoshi Kurumada